R-06-59

Very deep hole concept

Thermal effects on groundwater flow

Niko Marsic, Bertil Grundfelt, Marie Wiborgh
Kemakta Konsult AB

September 2006

Svensk Kärnbränslehantering AB
Swedish Nuclear Fuel
and Waste Management Co
Box 5864
SE-102 40 Stockholm Sweden
Tel 08-459 84 00
+46 8 459 84 00
Fax 08-661 57 19
+46 8 661 57 19

ISSN 1402-3091
SKB Rapport R-06-59

Very deep hole concept

Thermal effects on groundwater flow

Niko Marsic, Bertil Grundfelt, Marie Wiborgh
Kemakta Konsult AB

September 2006

Summary

The purpose of the present study is to investigate the stability of deep groundwater conditions in a repository for spent nuclear fuel based on the Very Deep Hole concept. The study is based on a repository design originally set up in the PASS study. In this design, canisters containing spent nuclear fuel are assumed to be stacked in the lower 2 km of 4 km deep holes and surrounded by a slurry consisting of bentonite and water. The canisters are separated by “cushions” consisting of 1 m long compacted bentonite blocks. The upper 2 km of the borehole is sealed with bentonite, asphalt and concrete. In all 45 disposal holes, each hosting 300 canisters, is required for the disposal of the spent fuel from operating the Swedish nuclear reactors 40 years.

In each disposal hole, a heat source with a decaying power corresponding to the time behaviour of the radioactive decay of the spent disposed nuclear fuel was introduced. The salinity of the groundwater was varied over depth in accordance with the distribution generalised from data available. Correspondingly, the water from the surface down to a depth of 700 m is assumed have a zero salt concentration. In a zone from 700 to 1,500 m depth the salt content of the groundwater increases linearly from zero to 10%. The groundwater below 1,500 m depth is assumed to have a salt content of 10%. The density of the groundwater can be assumed to increase approximately linearly with the salt content such that a groundwater with 10% salt content has a density that is about 10% higher than fresh water. This creates a stable layering of the groundwater system. In order to alter this stability, driving forces have to be applied to the groundwater system.

The Connectflow software created by Serco Assurance was used to carry out the modelling applying a coupled variable density and heat transport solution. A finite element grid was created including the 45 disposal holes. The grid was constituted by 264,003 elements with 540,055 nodes.

The results of the calculations were evaluated using tracking of particle starting in different positions in the deposition holes. The travel times for these particles to the surface were calculated. The particle tracking was performed for individual time steps assuming that the conditions of that time step remained constant throughout the particle travel times. This is of course not true, in particular as the calculated travel times are much longer that the duration of the heat pulse from the deposited spent fuel.

A more refined variant of the grid including 1,245,680 finite elements corresponding to 2,525,744 nodes was tested in order to verify that the discretisation used was adequate. In this case, all elements inside the repository area and those closest to this area were refined by a factor of two in each of the three dimensions. The elements constituting the boreholes were left unchanged. The results of this test show that both the flow pattern and the calculated Darcy velocities are significantly affected by the disretisation while the calculated particle travel times were little influenced. Because of the little difference of travel times and due to the fact that the computational times of the larger grid were hard to manage within a reasonable project schedule, it was decided to use the smaller grid for the calculations.

A large number of calculations were performed in which the sensitivity of the results with respect to different combinations of surface hydraulic gradients, heat output from the deposited spent fuel and fracture zone orientations was tested. In general, the calculated travel times for the particles are extremely long, in the order of 1–100 Myrs.

The thermal output from the spent fuel is insufficient to alter the stability of the near-stagnant saline groundwater present at depth in the rock. However, the performed sensitivity analysis showed effects on the Darcy velocities, flow field and calculated hypothetical travel times, but the differences do not have a practical effect on the performance of the repository.

There are several scenarios that have not been analysed in the present study. One of the most obvious is the effect of future glaciations. At the time when the present study was performed, the glaciation was being analysed by another group in the context of the KBS-3 concept. Therefore, it was decided await the results of that study.

Contents

1 Background 7

2 Model set-up and specifications 9
2.1 Modelling methodology 9
2.2 Finite element grid 9
2.3 Material properties 14
2.4 Boundary and initial conditions 14
2.5 Heat source 15
2.6 Fracture zones using the Implicit Fracture Zone method 17
2.7 Transport performance measures 21

3 Sensitivity study 23
3.1 Summary of calculated variants 23
3.2 Sensitivity to top boundary condition and rock properties 28
3.2.1 Case 1. Base Case 28
3.2.2 Case 2. Head gradient 32
3.2.3 Case 3. Homogeneous rock properties 32
3.3 Sensitivity to structural model 33
3.3.1 Case 4. Single fracture zone (slope +60°) 33
3.3.2 Case 5. Single fracture zone (slope –60°) 35
3.3.3 Case 6. Connected regional fracture zones 38
3.3.4 Case 7. Disconnected regional fracture zones 38
3.3.5 Case 8. HCD model Laxemar v1.2 41
3.3.6 Case 9. Extended HCD model Laxemar v1.2 42
3.4 Sensitivity to borehole properties 46
3.4.1 Case 10. Increased borehole permeability at Z = 0 to –500 m 46
3.4.2 Case 11. Increased borehole permeability at Z = –500 to –2,000 m 46
3.4.3 Case 12. Increased borehole permeability at Z = 0 to –2,000 m 48
3.4.4 Case 13. Increased borehole permeability 48
3.5 Sensitivity to heat and salt IC 51
3.5.1 Case 14. No heat source in boreholes 51
3.5.2 Case 15. Freshwater IC with single fracture zone (slope –60°) 52
3.5.3 Case 16. Freshwater IC with fracture zone (slope –60°) and no heat generation in boreholes 54
3.5.4 Case 17. Freshwater filled boreholes 54
3.5.5 Case 18. Freshwater filled boreholes with increased permeability 56
3.5.6 Case 19. Freshwater filled boreholes with connected regional fractures 60
3.5.7 Case 20. Freshwater filled boreholes and nearby rock 60
3.6 Sensitivity to borehole depth 65
3.6.1 Case 21. Shallower boreholes 65
3.6.2 Case 22. Shallower boreholes with connected regional fractures 66
3.7 Additional cases 66
3.7.1 Case 23. Combined case 1 68
3.7.2 Case 24. Combined case 2 69
3.7.3 Case 25. Refined model grid 71

4 Discussion 73

5 Acknowledgement 77

6 References 79

1 Background

The purpose of the present study is to analyse a repository for spent nuclear fuel based on the Very Deep Hole concept with respect to the influence of the repository on the assumed natural groundwater conditions. in the basic safety feature of this concept is that the groundwater at great depth is assumed to be virtually stagnant due primarily to the higher salinity and consequent higher density of this groundwater compared to the more superficial groundwater. This stability of the groundwater system can potentially be negatively affected by the natural geothermal gradient and by the heat output from the deposited spent fuel.

The study is based on a repository design originally set up in the PASS study /SKB 1992/. In this design, canisters containing spent nuclear fuel are assumed to be stacked in the lower 2 km of 4 km deep holes and surrounded by a slurry consisting of bentonite and water. The canisters are separated by “cushions” consisting of 1 m long compacted bentonite blocks. The upper 2 km of the borehole is sealed using a combination of bentonite, asphalt and concrete. In all 45 disposal holes, each hosting 300 canisters, is required for the disposal of the spent fuel from operating the Swedish nuclear reactors 40 years. A schematic of the design of a borehole is shown in Figure 1-1.

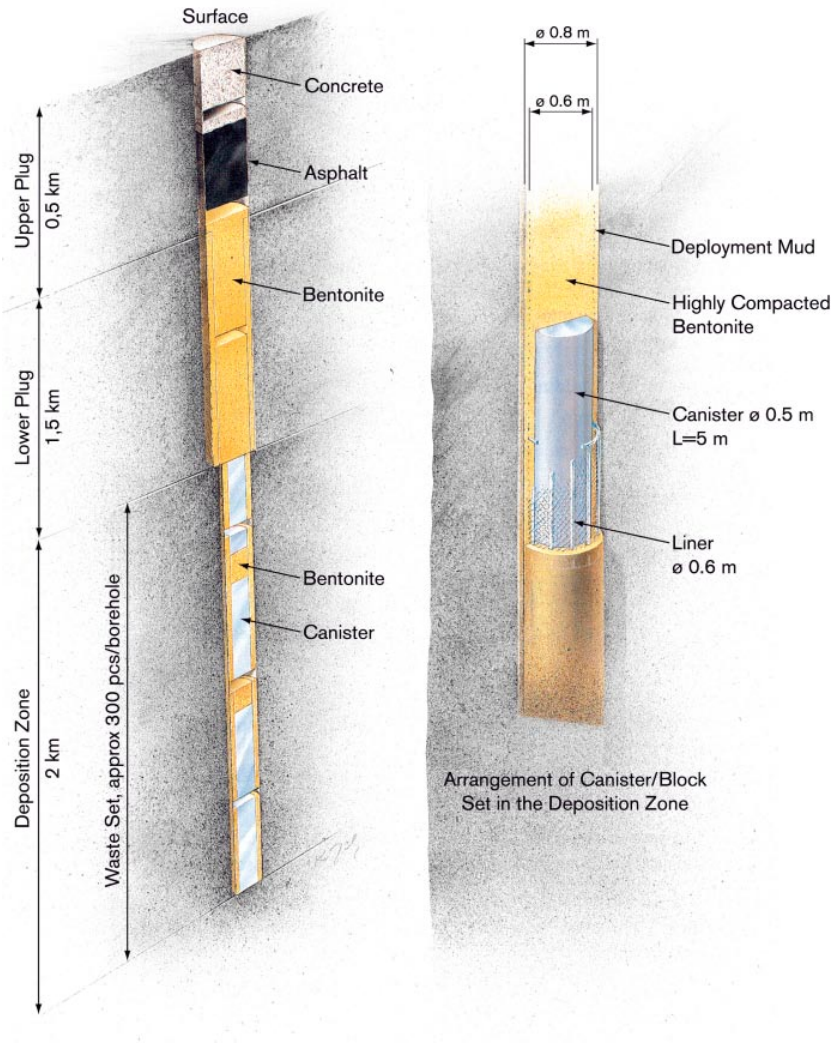

Figure 1-1. *Conceptual design of a disposal borehole in the VDH concept.*

The available geo-scientific knowledge about the conditions at great depth has been reviewed by /Juhlin et al. 1989/. This review was later complemented with a review of more recent data updated by /Smellie 2004/. The knowledge is based on observations in very few boreholes. These have been drilled in locations that geologically or hydrogeologically are not necessarily compatible with sites that would be used for a Swedish VDH repository. The observations available confirm the general view that the groundwater salinity, the temperature and the rock stresses increase with depth whereas the hydraulic conductivity decreases. It should be noted, however, that although the conductivity decreases, connected and conductive fractures are observed in the rock also at the depth of several km.

The prerequisites for drilling in crystalline rock 4 km deep disposal holes with a diameter of 80 cm in the lower 2 km and subsequently to dispose of spent fuel canisters in these holes was studied by /Harrison 2000/. As pointed out in that study, the high rock stresses at great depths in crystalline rocks cause deformation and fracturing of the borehole and the surrounding rock. Hence, it must be assumed that the borehole is surrounded by a disturbed zone with an increased fracture frequency and a higher permeability than the intact rock.

During drilling a drilling fluid consisting of a stiff foam is used /Harrison 2000/. Before the emplacement of canisters, the foam must be displaced with a disposal slurry consisting of bentonite dispersed in fresh water. The canisters are then pushed through the disposal slurry. The canisters are assumed to prior to disposal be arranged in packages consisting of two canisters with a cushion of highly compacted bentonite between. The hydraulic properties of the material in the borehole will be a function of the composition of the deposition slurry, the bentonite cushions and the confining pressure in the hole.

Spent nuclear fuel generates heat because of the radioactive decay. Although the rate of heat generation initially drops quite rapidly, the heat output remains potentially significant for some hundreds of years.

The heat will increase the temperature of the rock and groundwater in the vicinity of the repository. This temperature rise will be superimposed on the temperature gradient caused by the natural geothermal flux. This leads to buoyancy forces that tend to create convection cells with flow up through the repository and down at some distance from the repository. This flow will be superimposed on the flow that would otherwise occur. The modification of the flow will potentially alter the groundwater flow pattern from the repository during the period when the buoyancy forces are significant. In addition, the increased temperature in the vicinity of the repository will alter the groundwater density and viscosity there thus influencing the hydraulic conductivity.

The main objective of the present study is to investigate if the thermal output from spent nuclear fuel would create sufficient buoyancy forces to jeopardise the stability of the groundwater system created by the high salinity expected in the deep groundwater as mentioned above. The possible flow paths along the borehole as well in the disturbed zone and in the material in the borehole (“buffer”) is investigated. In addition, the effects of introducing sub-vertical and sub-horizontal zones is analysed. In order to allow conclusions regarding principal effects of various model features, a generic model is used that is not related to any particular site.

2 Model set-up and specifications

This chapter describes the main concepts used in the calculations and the assumed properties in the bedrock and the repository.

2.1 Modelling methodology

The Connectflow software created by Serco Assurance was used to carry out the modelling as it allows a fully coupled variable density and heat transport solution. GeoVisage, a 3D visualisation tool developed by Serco Assurance, was used to visualise the model results.

The finite element models of the bedrock and the repository generated in this study have been used to calculate the transport of groundwater, salt and heat in the rock. The main mechanism for heat transport in the rocks of interest is conduction. Advective transport of heat by flowing groundwater is less important since both the water content of the rock and the flow velocities are low. Advective heat flow has therefore been neglected.

Based on these models, the flow-field at chosen times has been used to track particles released from the buffer material inside the boreholes to the model boundary.

2.2 Finite element grid

A finite element grid was created including the 45 disposal holes required for disposal of the spent nuclear fuel from operating the Swedish reactors for 40 years. A regular grid is built from 42 element layers vertically (Z) and 67 elements in each horizontal direction (X and Y). This makes a total of 188,538 cuboid, eight-node finite elements (type CB81), prior to including the boreholes. The model is symmetric in the horizontal plane and the dimensions are 19,050×19,050 m. In the vertical dimension, the model extends down to 7,000 m depth. The discretisation of the grid is illustrated with horizontal sections in Figure 2-1. The top picture shows the entire model domain and the bottom picture is a close-up view over the central part of the grid containing the 45 boreholes (red markers). The boreholes are placed in a regular grid of 7×7 boreholes with the corner positions removed. Each borehole is placed in the centre of a 50×50 m patch. The borehole patches are in turn separated in the horizontal plane by four 112.5 m square elements. This gives a distance between the borehole centres of 500 m and forms a square repository area of 3,000×3,000 m. Outside of the repository area, the element sizes gradually increase from 250 m to 500 m. Note, the diagonal lines displayed in each element are an artefact of the visualisation software used.

In Figure 2-2, a vertical section through the centre of the model illustrates the discretisation of the entire model grid. Figure 2-3 shows a close-up view of the repository in the centre of the model. The row of seven boreholes, indicated as red lines, propagate vertically through the model. The discretisation of the grid is finer at the top of the model using 50 m thick elements in the top 100 m and gradually becomes coarser down to 500 m depth where the thickness is 125 m. Between 500 and 2,000 m depth, the element thickness is 250 m. In the section containing the canisters, i.e. 2,000 to 4,000 m depth, the element thickness is 100 m. Beneath this level the thickness again increases to 250 m. At the bottom of the model two layers of 500 m elements are used.

In Figure 2-4 a vertical cross-section through the bottom of one borehole is presented. The top row shows the full width of the borehole patch measuring 50 m horizontally. The canisters (yellow) have a diameter of 50 cm and are surrounded by 15 cm of buffer material (orange).

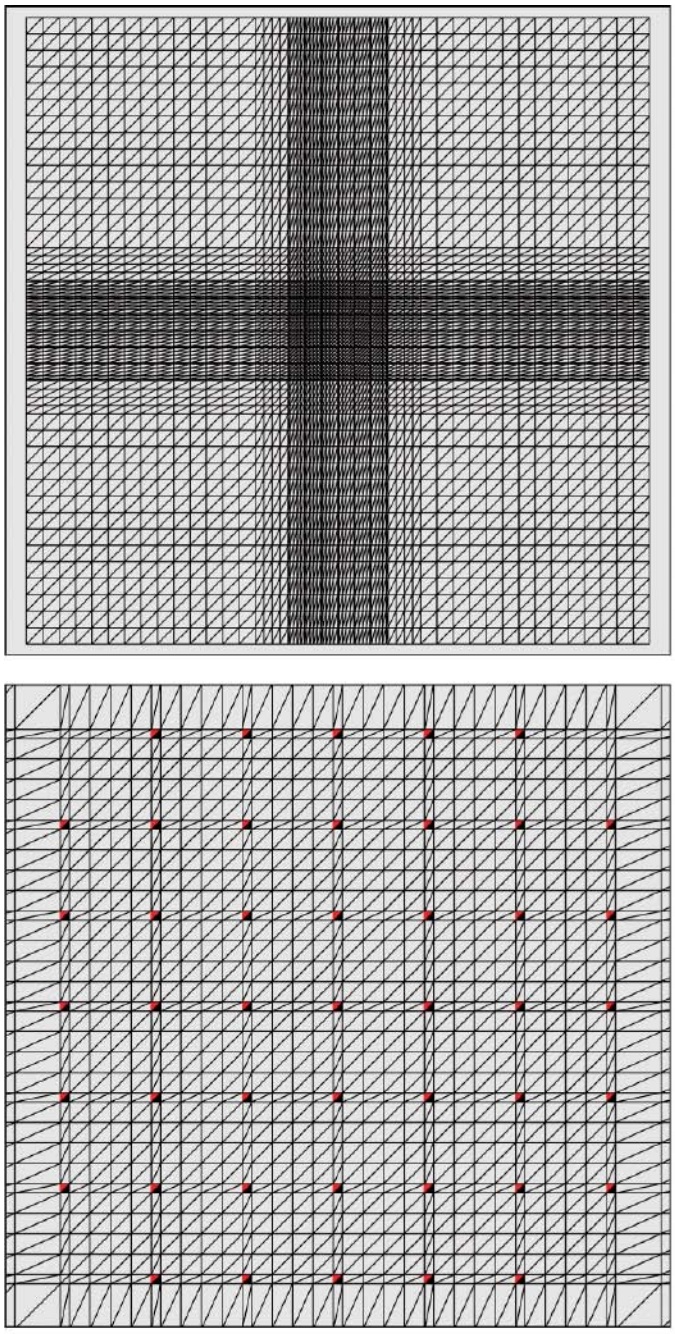

Figure 2-1. *Horizontal sections showing the discretisation of the model grid. The top picture shows the entire model domain and the bottom picture is a close-up view over the central part of the grid containing the 45 boreholes (red markers). (The triangles are an artefact of the program used to plot the grid.)*

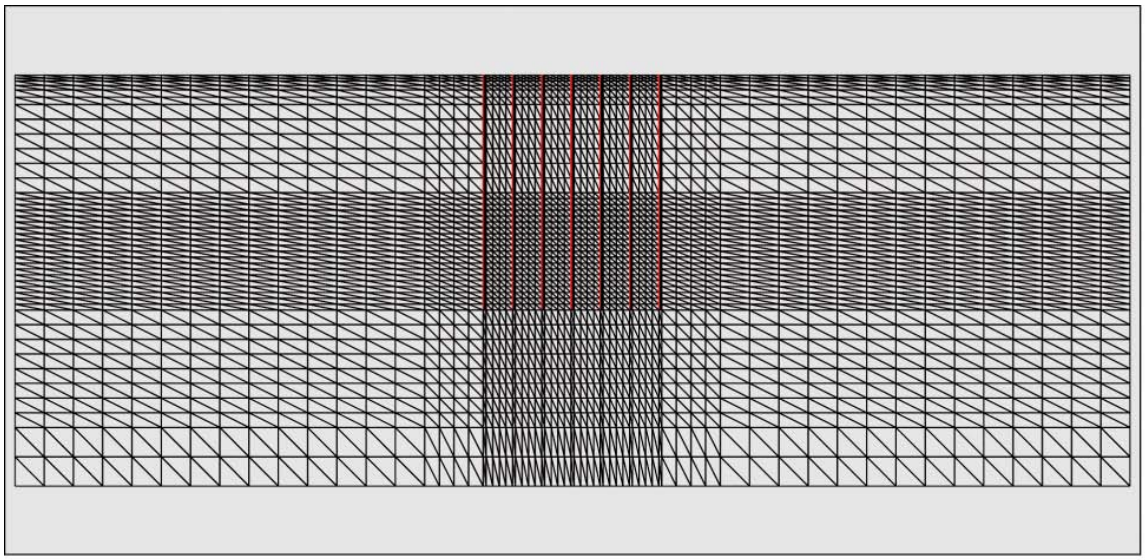

Figure 2-2. *Vertical section showing the discretisation of the entire model grid. (The triangles are an artefact of the program used to plot the grid.)*

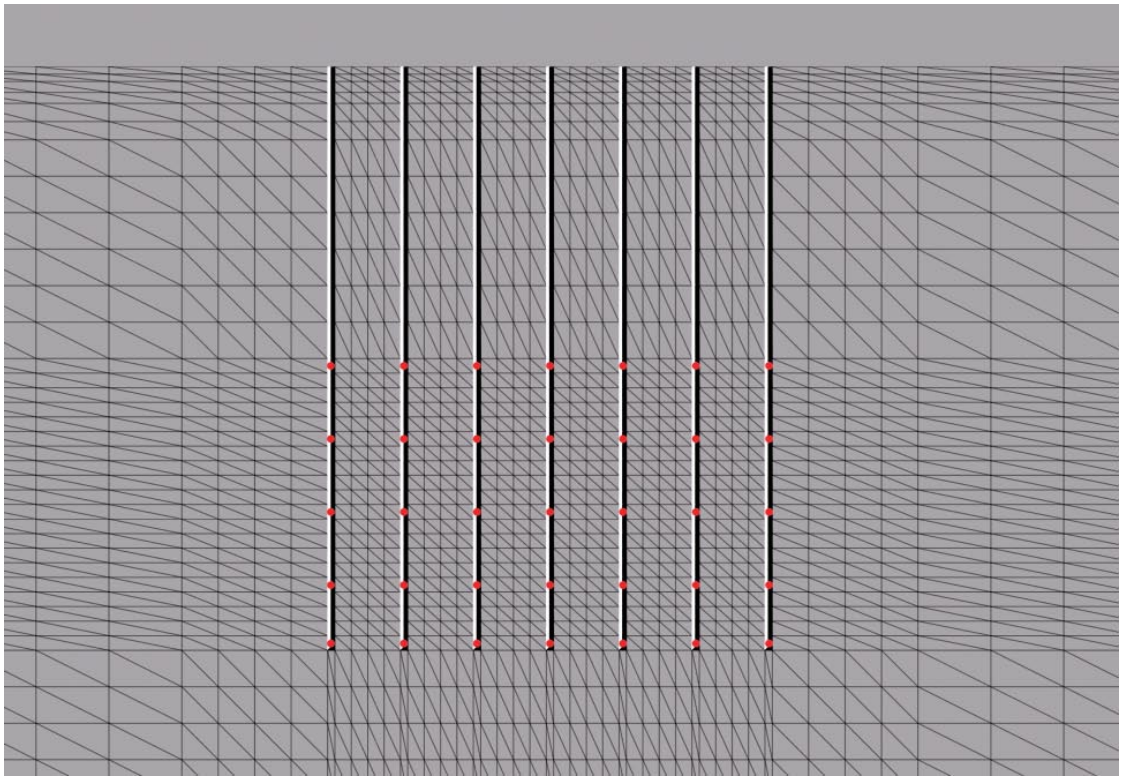

Figure 2-3. *Close-up view of the boreholes in the repository. Starting positions for the released particles are shown as red markers. (The triangles are an artefact of the program used to plot the grid.)*

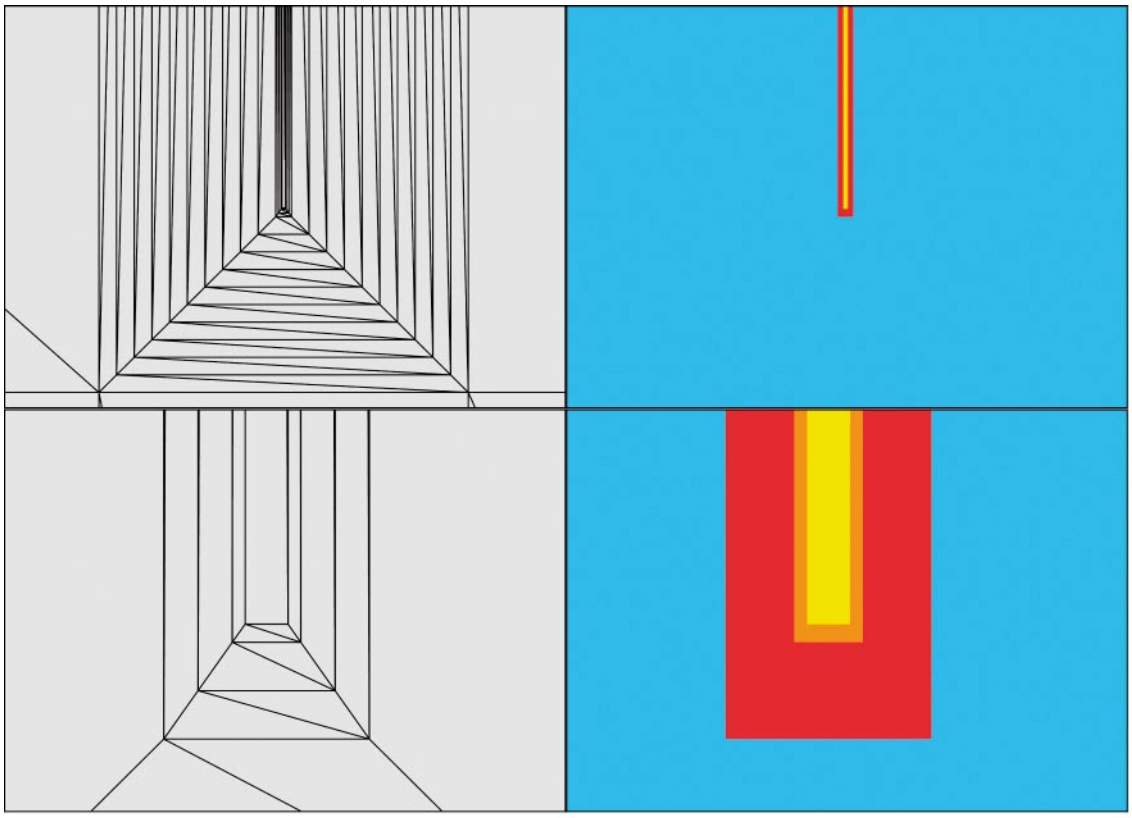

Figure 2-4. *Close-up view of a vertical section through one single borehole showing the radial discretisation and materials: yellow-canister, orange-buffer, red-excavation damaged zone and blue-rock. (The triangles are an artefact of the program used to plot the grid.)*

The canister and the buffer are represented by one element each in the radial direction. The DZ (Damaged Zone around the boreholes) (red) is assumed to have a radius of 80 cm surrounding the buffer and is represented by two elements in the radial direction. The remaining space in the borehole patch consists of rock (blue), i.e. from 1.2 m to 25.0 m radius, and is radially discretised into 10 elements. The grid refinement was designed represent to the temperature and groundwater flow in the immediate vicinity of the boreholes with reasonable accuracy. This was checked using initial scoping calculations.

Figure 2-5 illustrates one single borehole on a horizontal section through the borehole. The top picture shows the full width of the borehole patch and again it can be seen that the rock inside the patch is radially discretised into 10 elements. The azimuthal discretisation (perpendicular to the radius) around the canisters is four elements. This applied for all materials, except the canisters, inside the borehole patch. Thus, in total the boreholes are discretised into 53 elements horizontally for each vertical element layer.

Adding the borehole patches to the grid results in a finite element grid containing 264,003 elements, or 540,055 nodes. A more refined variant of the grid presented above was tested in Case 25 (see Section 3.7.3), in order to verify that the discretisation used is adequate. In this case, all elements inside the repository area and those closest to this area were refined by a factor of two in each of the three dimensions. The elements containing the borehole patches were left unchanged. This resulted in a grid containing 1,245,680 finite elements of CB81 type, corresponding 2,525,744 nodes.

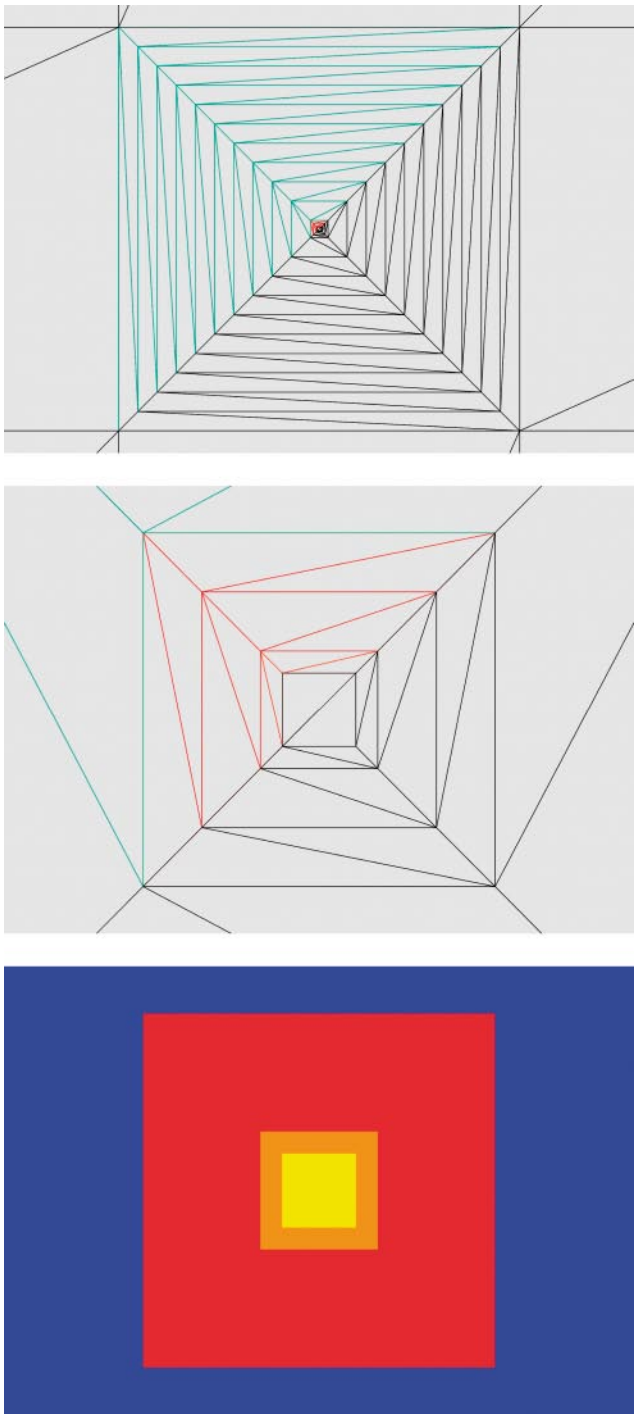

Figure 2-5. *Close-up view of a horizontal section through one single borehole showing the azimuthal discretisation, borehole materials and rock type. (The triangles are an artefact of the program used to plot the grid.)*

2.3 Material properties

In this study, the material properties of different parts of the rock and in the buffer have been varied, in order to investigate the sensitivity of the groundwater flow pattern to different assumptions and uncertainties. In this section, the material properties of the Base Case are presented.

The rock has been divided into three depth intervals and one disturbed zone, DZ, around the boreholes with different hydraulic conductivities and porosities:

1. The upper 100 m of the ambient rock has been assigned a conductivity of 10^{-7} m/s.
2. In the depth interval –100 to –500 m the hydraulic conductivity was given the value 10^{-9} m/s.
3. The hydraulic conductivity below –500 m has been set to 5×10^{-11} m/s.
4. The hydraulic conductivity of the DZ was given the value 5×10^{-9} m/s.

The porosity of the ambient rock has been set to 10^{-4} and that of the DZ to10^{-3}.

The buffer around the canisters in the lower 2 km of the borehole was given a hydraulic conductivity of 10^{-9} m/s and a porosity of 0.3 based on the estimates made in the PASS-study /Birgersson et al. 1992/. The underlying assumptions are that the deposition mud has an initial density of 1,600 kg/m^3 and the bentonite cushions between the canisters a density of 2,200 kg/m^3. The average density of the “buffer” in the deposition zone then becomes 1,900 kg/m^3.

The bentonite in the lower part of the sealing section of the borehole was assigned a hydraulic conductivity value of 5×10^{-11} m/s and a porosity of 0.3. The concrete plug in the upper part of the sealing section was given the same hydraulic conductivity value as the ambient rock in this depth interval, i.e. 5×10^{-11} m/s, but the porosity of the concrete was set to 0.1. Also the asphalt seal was given the conductivity 5×10^{-11} m/s but with a porosity of 10^{-6}.

The main mechanism for dispersion of the heat from the spent fuel into the rock is by heat conduction. The heat conductivity of the rock was given the value of 2.6 W/m,K and that of the buffer 1.0 W/m,K. For the specific heat of the rock a value of 780 J/kg,K was used and for the buffer 1,300 J/kg,K.

2.4 Boundary and initial conditions

On the vertical sides of the model, the boundary condition was set no flux (Neumann type of condition). This boundary condition applies to flow, solutes (salt) and heat transport through the lateral boundaries.

On the bottom boundary, a no flux boundary condition for water was used. For the salt (or Brine), a specified constant concentration corresponding to 10% salinity was used. Salt is allowed to pass the bottom boundary into the model by diffusion only. Figure 2-6 shows the initial salinity profile in the model. The values presented are the fraction of the water that is brine (10% salt content). Hence, we see that the concentration of brine at the bottom of the model equals one whereas at the top, where the water is fresh, the brine concentration equals zero.

At the top boundary, a specified head (Dirichlet type) boundary condition was used. For specified head, the model is assumed to be fully saturated and the datum is set at 0 m. Hence, the head is equal to the elevation of the topographic surface. There are two variants used for the top boundary condition. In the first variant a uniform, constant head equal to zero was used. The second variant is a 1% linearly varying head gradient (decreasing from west to east in the model). The salt concentration is assigned a constant value of zero at the top surface.

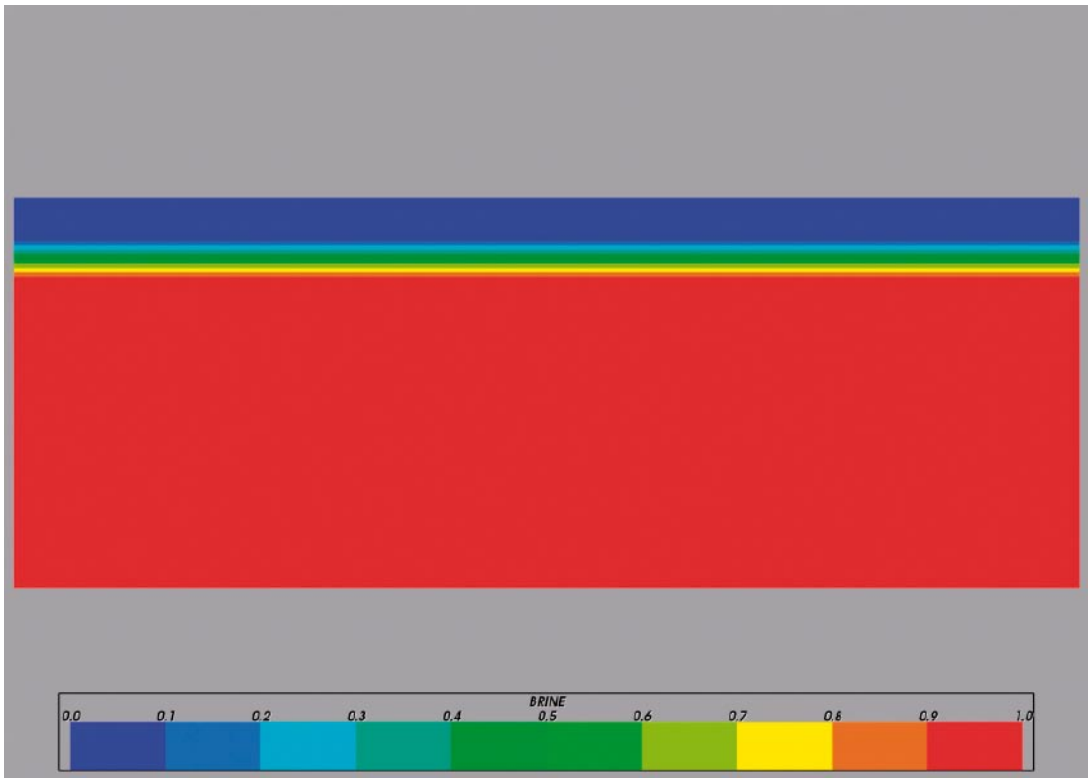

Figure 2-6. *Vertical section showing the initial distribution of Brine (10% salt content).*

The initial condition for salt was set to pure freshwater from the surface down to Z = –700 m. Then linearly increasing salinity to full Brine (10% salt content) at a depth of 1,500 m, and full Brine below Z = –1,500 m, see Figure 2-6.

For heat transport through the bottom boundary, a specified flux boundary condition was used with the value set to –41.8 mW/m^2. This value is consistent with a geothermal gradient of 16°C/km that appears to representative for Swedish bedrock /e.g. Juhlin and Sandstedt 1989, SKB 2000/. At the top boundary a specified value of T = 6°C for the temperature was assigned. Together with the thermal gradient this gives an initial temperature of T = 118°C at the bottom boundary at Z = –7,000 m. The initial condition for heat in the rock and groundwater is shown in Figure 2-7.

2.5 Heat source

The heat output from the spent fuel in the canisters was modelled as a uniform heat source within each of the boreholes at a depth of Z = –2,000 m to Z = –4,000 m. Figure 2-8 presents a graph of the thermal output per metre borehole as a function of time used as input to the model when calculating the heat flux from the source. This data was obtained by taking the total heat output from the spent fuel, as estimated for an operation time of 40 years for the nuclear power plants /Agrenius 2006/ as a basis for calculating the average heat output per canister. The average output per m borehole was then calculated by dividing the heat output from 300 canisters by 2,000 m of borehole length. This was considered to be an appropriate approximation for this sensitivity study and gives the overall temperature and flow distributions on the scale of the repository.

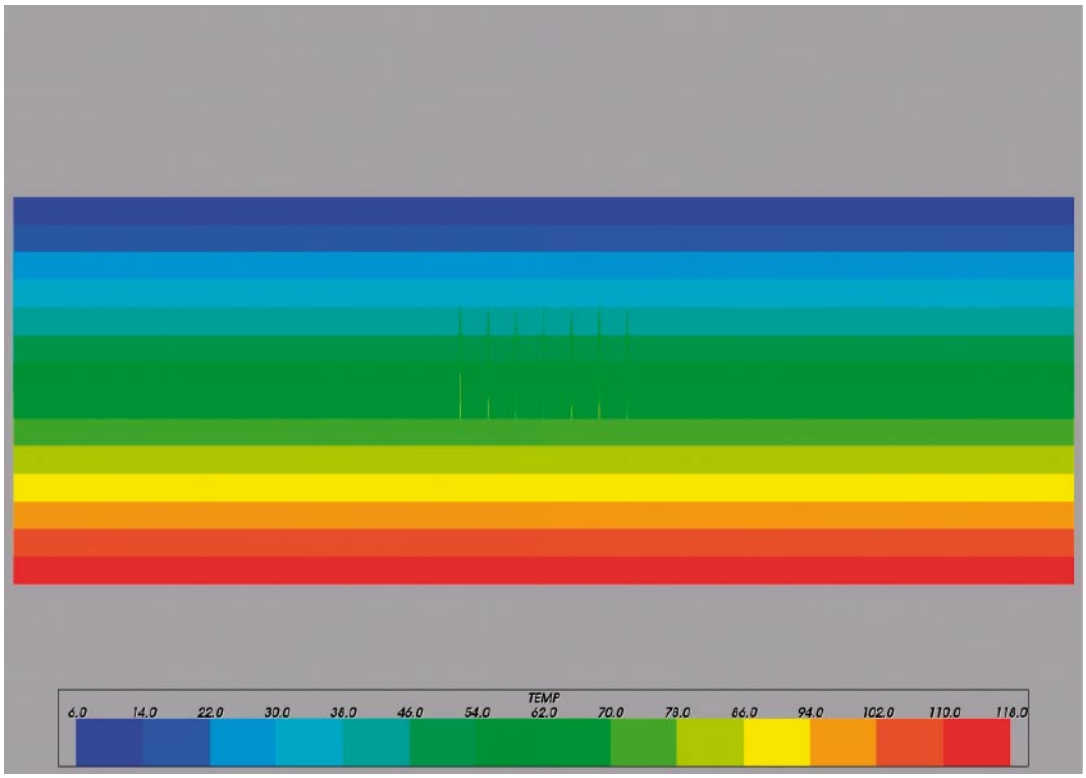

Figure 2-7. *Vertical section showing the initial temperature distribution due to the geothermal gradient. Blue colour indicates lower temperature (T = 6°C on top surface.) and red colour indicates higher temperature. (T = 118°C at Z = –7,000 m.)*

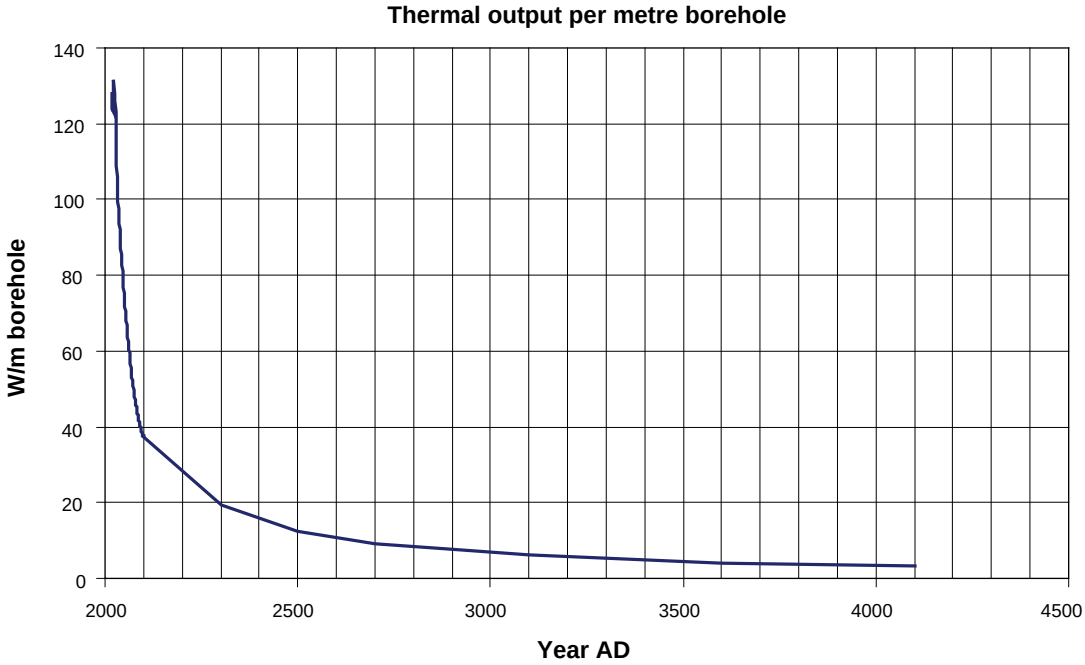

Figure 2-8. *Thermal output calculated per metre borehole as a function of time. Calculated for a total of 40 years of operation of the Swedish nuclear power plants.*

In Figure 2-9, sections through one of the boreholes are showing an early (after 1 year) temperature distribution due to heat generated by the spent fuel. The top picture is showing a vertical section and the bottom picture is showing a horizontal section at Z = –3,000 m. The canisters have an initial temperature of about 80°C. The temperature of the canisters is rapidly decreasing in time and comes down to about 65°C after 100 years. Figure 2-10 and Figure 2-11 show the evolution of the temperature over a horizontal cross section at Z = –3,000 m through one single borehole. The time range is from 1 year to 1,000 years. The rapid decrease in temperature can be seen over the first 100 years or so. After a couple of hundred years, the temperature approaches the background geothermal temperature.

2.6 Fracture zones using the Implicit Fracture Zone method

For some of the variants, the Continuous Porous Medium (CPM) model was modified to incorporate the geometry and properties of a set of large-scale deformation zones using the Implicit Fracture Zone (IFZ) method in Connectflow as described in /Marsic et al. 2001/.

The IFZ downscaling method identifies which elements are crossed by a fracture zone and combines a hydraulic conductivity tensor associated with the fracture zone with a hydraulic conductivity tensor for the background conductivity of the rock. For each element crossed by the fracture zone, the following steps are performed:

- The volume of intersection between the fracture zone and the element is determined.
- The hydraulic conductivity tensor of the background rock is calculated in the coordinate system of the fracture zone.
- The combined conductivity tensor of the background rock and the fracture zone is calculated in the coordinate system of the fracture zone.
- The effective hydraulic conductivity tensor that includes the effect of the fracture zone is determined in the original coordinate system.

The methodology is illustrated diagrammatically in Figure 2-12. In 3D, the resultant hydraulic conductivity is a 6-component symmetric tensor in the Cartesian coordinate system. The tensor can be diagonalised to give the principal components and directions of anisotropy.

Similarly, a combined scalar block-scale porosity is calculated for the element by a weighted combination of the fracture zone porosity and the background block-scale porosity. The weighting is based either on the relative volume or on relative transmissibility (total channel flow capacity, which is transmissivity times flow length [m^3s^{-1}]). The latter weighting can be suitable for transport since it weights the combined porosity toward the fracture zone porosity if this is of a relatively high hydraulic conductivity. The result of this step is to produce a spatial distribution of element properties (hydraulic conductivity tensor and porosity) that represent the combined influence of both the deterministic fractures zones and background rock.

The way this methodology is normally used in the modelling within SKB's site investigations for a KBS-3 repository /e.g. Hartley et al. 2006/ is that the background conductivity is being represented by a stochastic Discrete Fracture Network, DFN, model. The DFN model is then first upscaled to a background conductivity, which is then later combined with the deterministic fracture zones. In this study, because of lack of realistic data, we only include the deterministic fractures into the model as a sensitivity study.

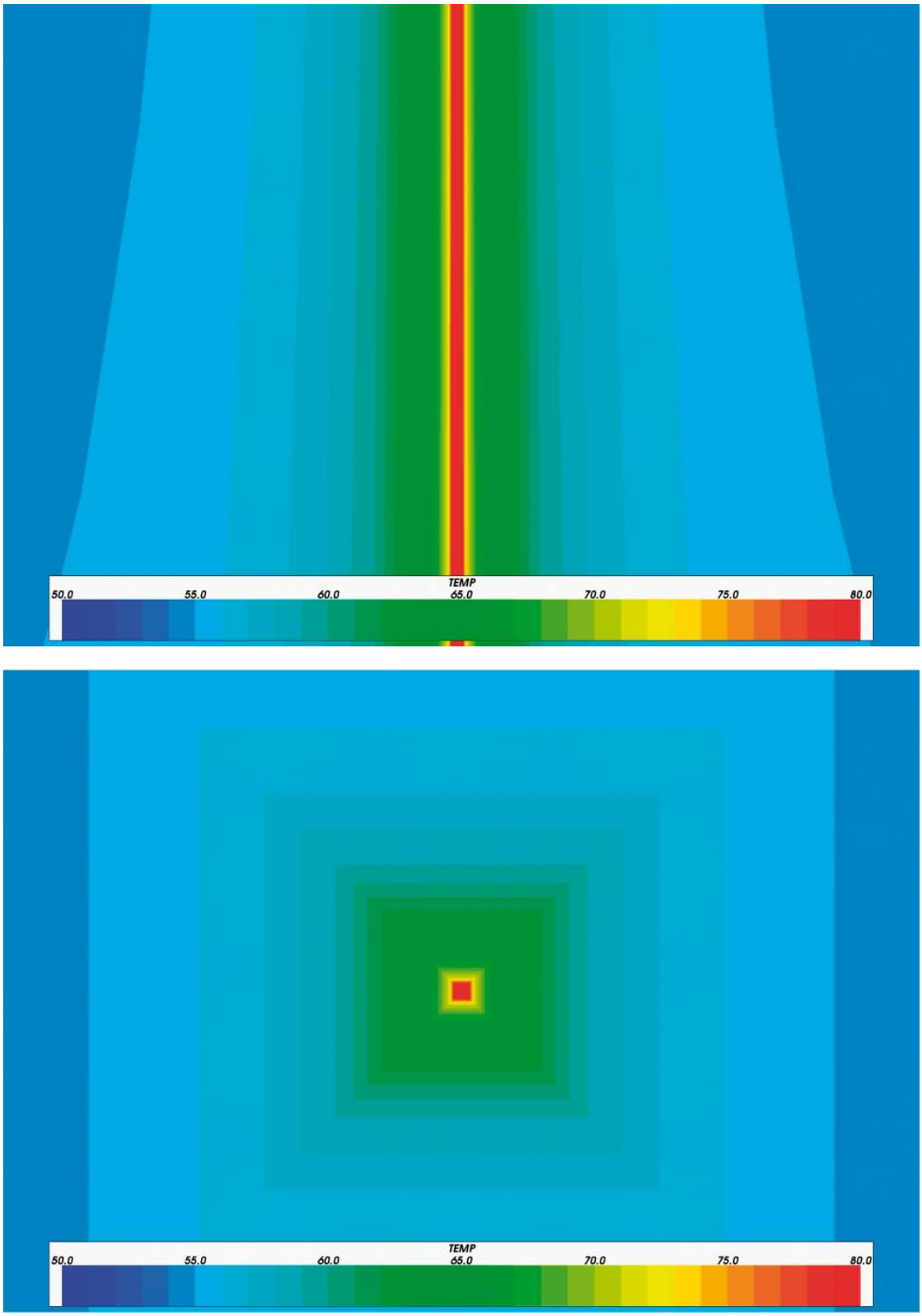

Figure 2-9. *Sections through one borehole showing an early (time = 1 year) temperature distribution due to heat generated by the canisters (top picture showing vertical section, bottom picture showing horizontal section at Z = –3,000 m). Blue colour indicates lower temperature and red colour indicates higher temperature. The canisters have an initial temperature of about 80°C.*

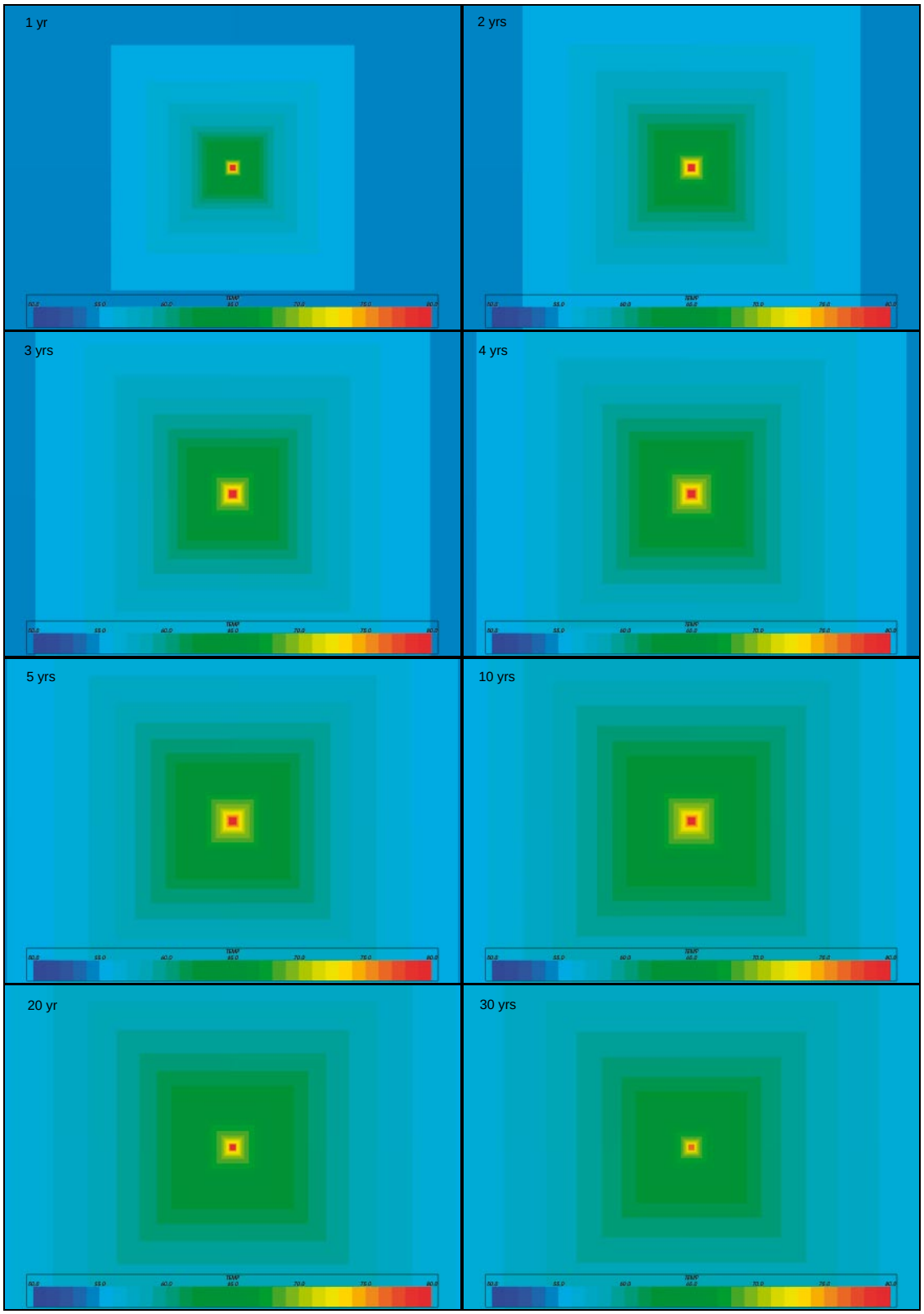

Figure 2-10. *Evolution of the temperature over a horizontal cross section at Z = –3,000 m through one single borehole. Time range: 1 to 30 years.*

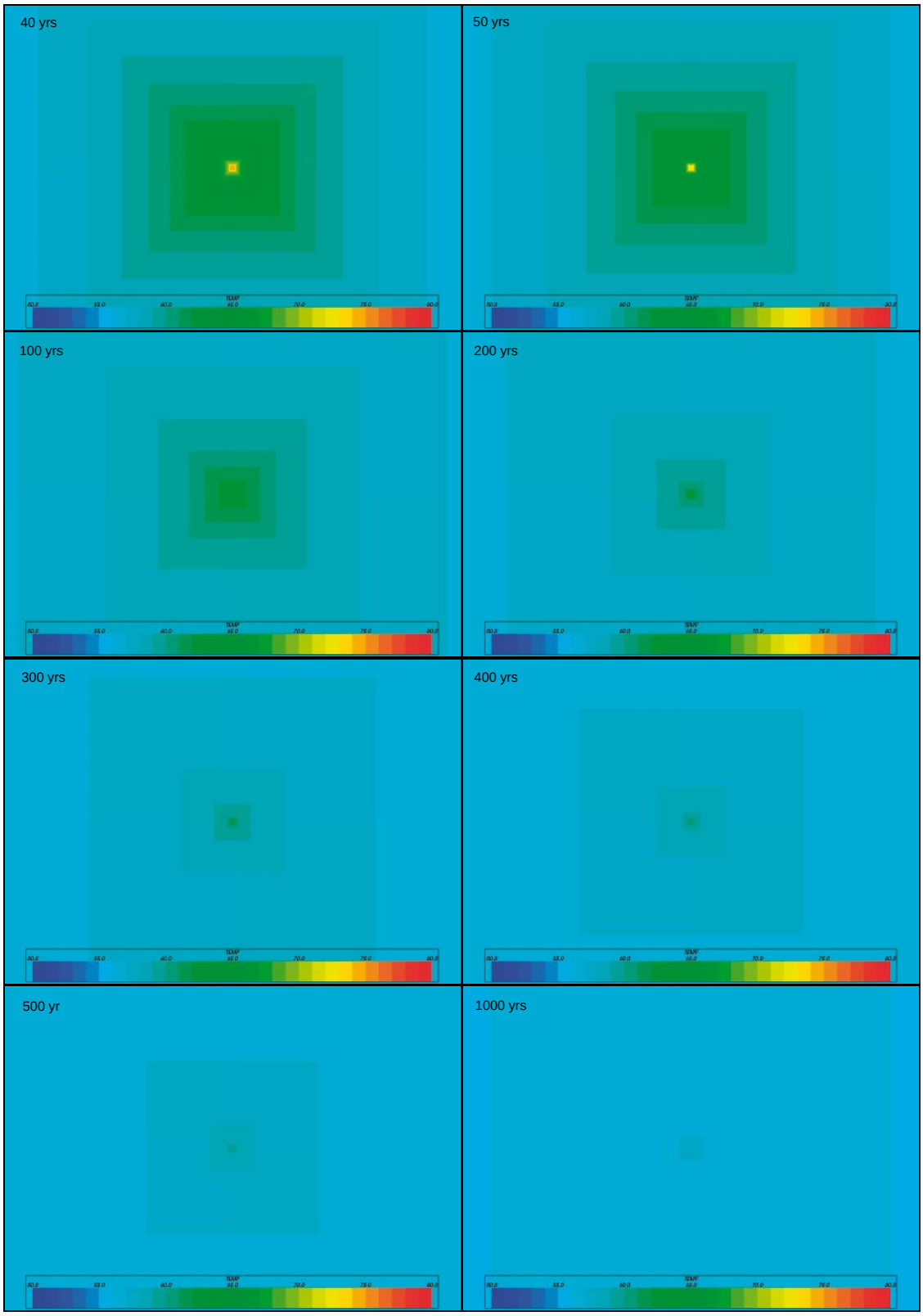

Figure 2-11. *Evolution of the temperature over a horizontal cross section at Z = 3,000 m through one single borehole. Time range: 40 to 1,000 years.*

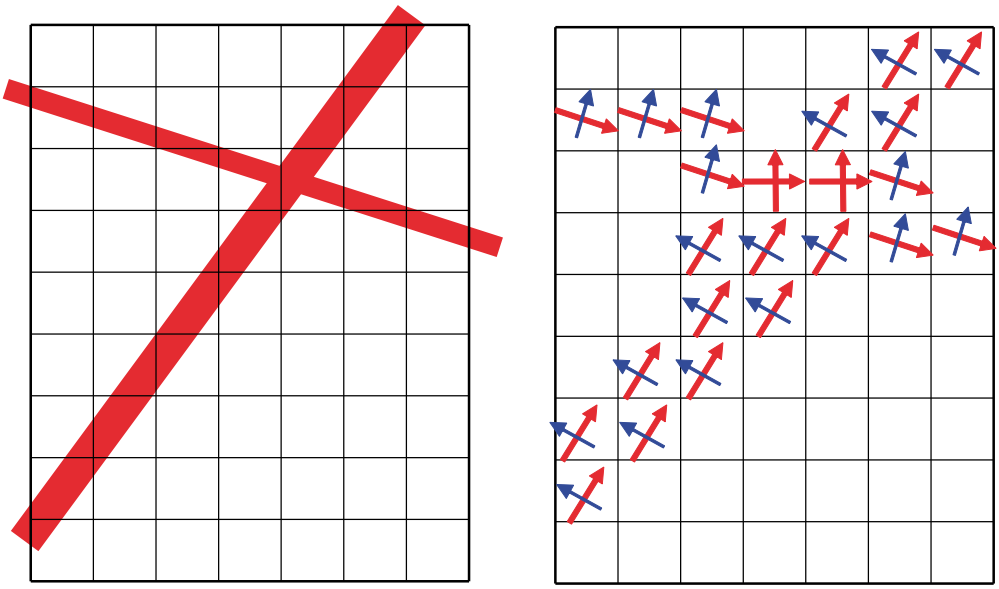

Figure 2-12. *Schematic illustration of the modification of the hydraulic conductivity tensor by the IFZ method. A finite-element grid crossed obliquely by two fracture zones of different thickness (left). The effect on the equivalent porous medium hydraulic conductivity is shown right. Elements with a large IFZ effect are coloured pink. Ones with a lesser effect, where the fracture zone only crosses one corner, are coloured orange. The principal directions of the resultant anisotropic hydraulic conductivity tensor are shown by arrows (red for major component, blue for minor).*

2.7 Transport performance measures

One objective of the presented sensitivity study is to investigate groundwater pathways from repository area to the surface. The approach taken is to track particles moving with the advective flow velocity from a range of release points until they reach the top surface. Although it would be possible in Connectflow to track particles as they move through a velocity field that evolves in time, it is preferred here to use only the velocity field from chosen snap-shots in time.

Particles are released at five different levels evenly distributed along the canister section of the boreholes, i.e. between 2,000 and 4,000 m depth. In Figure 2-3 the starting positions for the released particles are shown as red markers. The particles are released in the buffer material surrounding the canisters, 30 cm out from the centre of the boreholes. No attempt is made to avoid starting particles in deterministic deformation zones. In reality, such features are likely to be avoided during repository construction.

To describe the groundwater flow and the transport of substances dissolved in the groundwater from the repository to the surface, the following concepts are used:

1. Travel-time, $t_r = \sum_l \frac{n_e \delta l}{q}$

Where:

δl is the length of a step in distance along the path;

l denotes steps along a path, for example through one finite-element;

n_e is the kinematic porosity; and

q is the Darcy velocity;

and

2. Path-length, $L_r = \sum_l \delta l$

3 Sensitivity study

3.1 Summary of calculated variants

As mentioned in Chapter 1, the knowledge of the conditions at a depth of several km in crystalline rock is based on very sparse observations. A modelling exercise like the present should therefore be regarded as a generic sensitivity study rather than an attempt to describe actual conditions. In order to carry out such a sensitivity study, a set of topics and uncertainties that would be investigated were identified:

- Buoyancy driven flow in the boreholes together with its sensitivity to the ambient hydraulic gradient and the quality of the borehole sealing.
- The occurrence of fracture zones intersecting the repository.
- The quality of the buffer in the disposal zone (2–4 km depth).
- The salinity distribution and the interaction between the heat source and the salinity.
- The depth of the disposal zone.
- Combinations of the above listed topics created to investigate under what conditions the groundwater flow conditions remain stable and virtually stagnant.

In all, 25 variants have been calculated. A summary of these variants and the properties applied is presented in Table 3-1 below. In order to facilitate the reading of the table, variants addressing similar topics or uncertainties have been coloured with the same colour. The cases within one colour block are then presented below under the same section. Some of the abbreviations and symbols used in the table may require further explanation:

- In the column “model” a reference to the corresponding computer file name is given for traceability.
- BC means boundary condition.
- IC means initial condition.
- FW means fresh water.
- HCD POM L1.2 means Hydraulic Conductor Domain from the Oskarshamn site investigations version Laxemar 1.2.
- FZ means fracture description.

The set-up of each case is further explained in the respective subsection of Section 3.2 below. The results of the base case are presented for two time steps, 10 and 100 years respectively. For most of the other cases the presentations are restricted to one time step, in order to limit the amount of pictures. Only if the differences between time steps are of significance to the conclusions, more time steps are presented.

Table 3-1. Summary of applied variants and properties used.

Case	Model	Description	Heat source	Top BC	Salt IC	Rock domain	Fracture zones	Borehole properties
Case 1	VDH_heat_2_1	Base Case	Included in all boreholes Background thermal gradient in rock	Constant head	Brine fraction linearly increasing from 0 to 1 between Z=-700 and –1,500 m	Increased permeability above Z=-500 m, homogeneous below k=1E–7 m/s; 0 –> –100 m k=1E–9 m/s; –100 m –> –500 m k=5E–11 m/s; –500 m –> –7,000 m ne=1E–4; 0 –> –7,000 m	None	BUFFER k=1E–9 m/s ne = 3E–1 DZ k=5E–9 m/s ne = 1E–3 BENTONITE k=5E–11 m/s ne = 3E–1 CONCRETE k=5E–11 m/s ne = 1E–1 ASPHALT k=5E–11 m/s ne = 1E–6
Case 2	VDH_heat_3_1	Sensitivity to top BC	Same as Base Case	1% head gradient	Same as Base Case	Same as Base Case	None	Same as Base Case
Case 3	VDH_heat_11_1	Sensitivity to rock properties	Same as Base Case	1% head gradient	Same as Base Case	Homogeneous rock permeability k=5E–11 m/s; 0 –> –7,000 m ne=1E–5; 0 –> –7,000 m	None	Same as Base Case but CONCRETE and ASPHALT changed due to homogeneous rock properties
Case 4	VDH_heat_7_1	Sensitivity to structural model	Same as Base Case	1% head gradient	Same as Base Case	Same as Base Case	1 FZ, sloping +60° through repository centre width = 50.0 m k=5E–9 m/s ne=1E–3	Same as Base Case
Case 5	VDH_heat_7_2	Sensitivity to structural model	Same as Base Case	1% head gradient	Same as Base Case	Same as Base Case	1 FZ, sloping –60° through repository centre width = 50.0 m k=5E–9 m/s ne=1E–3	Same as Base Case

Case	Model	Description	Heat source	Top BC	Salt IC	Rock domain	Fracture zones	Borehole properties
Case 6	VDH_heat_10_1	Sensitivity to structural model	Same as Base Case	1% head gradient	Same as Base Case	Same as Base Case	3 connected regional FZs through repository centre width = 100.0 m k=5E–9 m/s ne=1E–3	Same as Base Case
Case 7	VDH_heat_7_4	Sensitivity to structural model	Same as Base Case	1% head gradient	Same as Base Case	Same as Base Case	2 FZs, sloping +60°/–60° through repository centre; width = 50.0 m k=5E–9 m/s ne=1E–3 2 FZs, sloping +30° outside repository; width = 100.0 m k=5E–9 m/s ne=1E–3	Same as Base Case
Case 8	VDH_heat_14_3	Sensitivity to structural model	Same as Base Case	1% head gradient	Same as Base Case	Homogeneous rock permeability	HCD POM L1.2, modified	Same as Base Case
Case 9	VDH_heat_14_4	Sensitivity to structural model	Same as Base Case	1% head gradient	Same as Base Case	Homogeneous rock permeability	HCD POM L1.2, modified and extrapolated down to Z=–5,000 m	Same as Base Case
Case 10	VDH_heat_12_15	Sensitivity to borehole properties	Same as Base Case	1% head gradient	Same as Base Case	Homogeneous rock permeability	None	Same as Base Case but CONCRETE and ASPHALT replaced by BUFFER for Z=0 to –500 m
Case 11	VDH_heat_12_16	Sensitivity to borehole properties	Same as Base Case	1% head gradient	Same as Base Case	Homogeneous rock permeability	None	Same as Base Case but BENTONITE replaced by BUFFER and DZ for Z=–500 to –2,000 m
Case 12	VDH_heat_12_2	Sensitivity to borehole properties	Same as Base Case	1% head gradient	Same as Base Case	Homogeneous rock permeability	None	Same as Base Case but CONCRETE, ASPHALT and BENTONITE replaced by BUFFER and DZ for Z=0 to –2,000 m

Case	Model	Description	Heat source	Top BC	Salt IC	Rock domain	Fracture zones	Borehole properties
Case 13	VDH_heat_12_14	Sensitivity to borehole properties	Same as Base Case	1% head gradient	Same as Base Case	Homogeneous rock permeability	None	Same as Base Case but CONCRETE, ASPHALT and BENTONITE replaced by BUFFER and DZ for Z=0 to –2,000 m k=1E–8 m/s
Case 14	VDH_noheat_ 11_2	Sensitivity to heat source	Excluded	1% head gradient	Same as Base Case	Homogeneous rock permeability	None	Same as Base Case but CONCRETE and ASPHALT changed due to homogeneous rock properties
Case 15	VDH_heat_8_2	Sensitivity to salt IC	Same as Base Case	1% head gradient	Fresh water filled model	Same as Base Case	Same as Case 5	Same as Base Case
Case 16	VDH_noheat_9_2	Sensitivity to heat source/ salt IC	Excluded	1% head gradient	Fresh water filled model	Same as Base Case	Same as Case 5	Same as Base Case
Case 17	VDH_heat_15_1	Sensitivity to salt IC	Same as Base Case	1% head gradient	Boreholes filled with FW to a radius of 2.0 m	Homogeneous rock permeability	None	Same as Base Case but CONCRETE and ASPHALT changed due to homogeneous rock properties
Case 18	VDH_heat_15_2	Sensitivity to salt IC	Same as Base Case	1% head gradient	Boreholes filled with FW to a radius of 2.0 m	Homogeneous rock permeability	None	BUFFER properties assigned to top 2,000 m of boreholes BUFFER and DZ k=1E–8 m/s
Case 19	VDH_heat_15_3	Sensitivity to salt IC	Same as Base Case	1% head gradient	Boreholes filled with FW to a radius of 2.0 m	Homogeneous rock permeability	4 connected regional FZs through repository centre with increased permeability width = 100.0 m k=1E–8 m/s ne=1E–3	BUFFER properties assigned to top 2,000 m of boreholes BUFFER and DZ k=1E–8 m/s
Case 20	VDH_heat_15_4	Sensitivity to salt IC	Same as Base Case	1% head gradient	Boreholes filled with FW to a radius of 50.0 m	Homogeneous rock permeability	None	Same as Base Case but CONCRETE and ASPHALT changed due to homogeneous rock properties

Case	Model	Description	Heat source	Top BC	Salt IC	Rock domain	Fracture zones	Borehole properties
Case 21	VDH_heat_13_1	Sensitivity to borehole depth	Same as Base Case	1% head gradient	Same as Base Case	Homogeneous rock permeability	None	Borehole Z=–1,000 –> –3,000 m, properties same as Base Case
Case 22	VDH_heat_13_4	Sensitivity to borehole depth	Same as Base Case	1% head gradient	Same as Base Case	Homogeneous rock permeability	4 connected regional FZs through repository centre with increased permeability width = 100.0 m k=1E–8 m/s ne=1E–3	Borehole Z=–1,000 –> –3,000 m BUFFER properties assigned to top 1,000 m of boreholes BUFFER and DZ k=1E–8 m/s
Case 23	VDH_heat_16_3	Combined case 1	Same as Base Case	1% head gradient	Boreholes filled with FW to a radius of 2.0 m	Increased depth dependent rock permeability k=1E–8 m/s; 0 –> –100 m k=5E–9 m/s; –100 m –> –250 m k=1E–9 m/s; –250 m –> –7,000 m ne=1E–4; 0 –> –7,000 m	HCD POM L1.2, modified and extrapolated down to Z=–5,000 m	BUFFER properties assigned to top 2,000 m of boreholes BUFFER and DZ k=1E–8 m/s
Case24	VDH_heat_17_1	Combined case 2	Same as Base Case	1% head gradient	Boreholes filled with FW to a radius of 2.0 m	Same as Case 23	HCD POM L1.2, modified and extrapolated down to Z=–5,000 m	Borehole Z=–1,000 –> –3,000 m BUFFER properties assigned to top 1,000 m of boreholes BUFFER and DZ k=1E–8 m/s
Case 25	VDH_heat_18_1	Refined model grid Discretisation increased a factor 2 in X, Y ,Z	Same as Base Case	1% head gradient	Boreholes filled with FW to a radius of 2.0 m	Same as Case 23	HCD POM L1.2, modified and extrapolated down to Z=–5,000 m	Borehole Z=–1,000 –> –3,000 m BUFFER properties assigned to top 1,000 m of boreholes BUFFER and DZ k=1E–8 m/s

3.2 Sensitivity to top boundary condition and rock properties

3.2.1 Case 1. Base Case

The Base Case was set up as a first simple variant to form the basis for comparison for other more complex modelling cases.

At the top surface of the model, a uniform constant head (Dirichlet) boundary condition is applied. The upper 700 m of the model is initially filled with freshwater. Between 700 and 1,500 m depth, the brine content increases from 0 to 100% (corresponding to 10% salinity). Below 1,500 m the model is initially filled with pure brine.

The permeability of the rock decreases with depth in the upper 500 m of the model. Below this level, the permeability is constant. Apart from the depth dependency in the top 500 m, the permeability is homogeneous throughout the model, i.e. no fracture zones or other structures are represented in this variant.

The properties of the upper 2,000 m of the boreholes are assigned the same values as the rock at the same level. Between 2,000 and 4,000 m depth the properties of the boreholes (buffer and the DZ) are assigned values that have been judged reasonable with respect to the assumed density of the bentonite buffer and the rock stress situation around the borehole, see Section 2.3. A more detailed description of used properties is presented in previous sections.

Figure 3-1 and Figure 3-2 show Darcy velocity vectors on a vertical section through the middle of the model after 10 years of simulation. Flow paths for particles released at five different depths in the buffer material of the boreholes are shown in black.

As expected the velocity field is symmetric around the boreholes. When the groundwater is heated by the hot canisters inside the boreholes, buoyancy causes groundwater to rise along the more permeable sections of the boreholes. At a level of –2,000 m, corresponding to the uppermost canisters, the flow between the boreholes changes direction to downward. This is primarily a result of a decrease in temperature of the groundwater higher up in the rock. In the buffer material and the DZ the Darcy velocity reaches up to 10^{-3} m/year. This is still a very low value and it would take about 10^{6} years for a particle to travel from the mid-section of the borehole (Z = –3,000 m) to exit the top of the buffer zone at Z = –2,000 m. This travel time is significantly longer than the duration of the heat input from the spent fuel, hence the calculated flow time is only hypothetical. Above the repository area, the flow is vertical and directed out through the top surface of the model. When the groundwater flow along the vertical sides of the repository reaches above the canisters it bends off in an outward direction from the repository forming a large convection cell around the repository area. However, it should be noted that the flow velocities are very low, typically in the range of 10^{-8}–10^{-10} m/year outside the repository, meaning that the mixing of freshwater and brine and flushing of the system is extremely slow. This is also reflected in the travel times for the released particles, see Figure 3-3, where the calculated range for particles released at 10 years is 10^{6}–10^{8} years. Obviously, such extreme time scales are only hypothetical and not very meaningful since the flow field, due to *inter alia* the decay of the heat source, would have changed completely during the time period. Thus, the conclusion should be that postulating the given boundary conditions, bedrock and repository characteristics, the groundwater situation in and around the repository is stable and the resulting flow velocities very small.

Figure 3-4–Figure 3-6 show results for a snapshot at 100 years of simulation time. The results are similar to the situation at 10 years. The orientation of the flow field is nearly identical as before. The magnitude of the Darcy velocity has increased slightly outside and above the repository area. Between the boreholes, however, the velocities have decreased due to the decrease in canister temperature and hence loss of thermal driving force. The combined effect of this is slightly shorter travel time for some paths but the total range of travel times broadly stays the same.

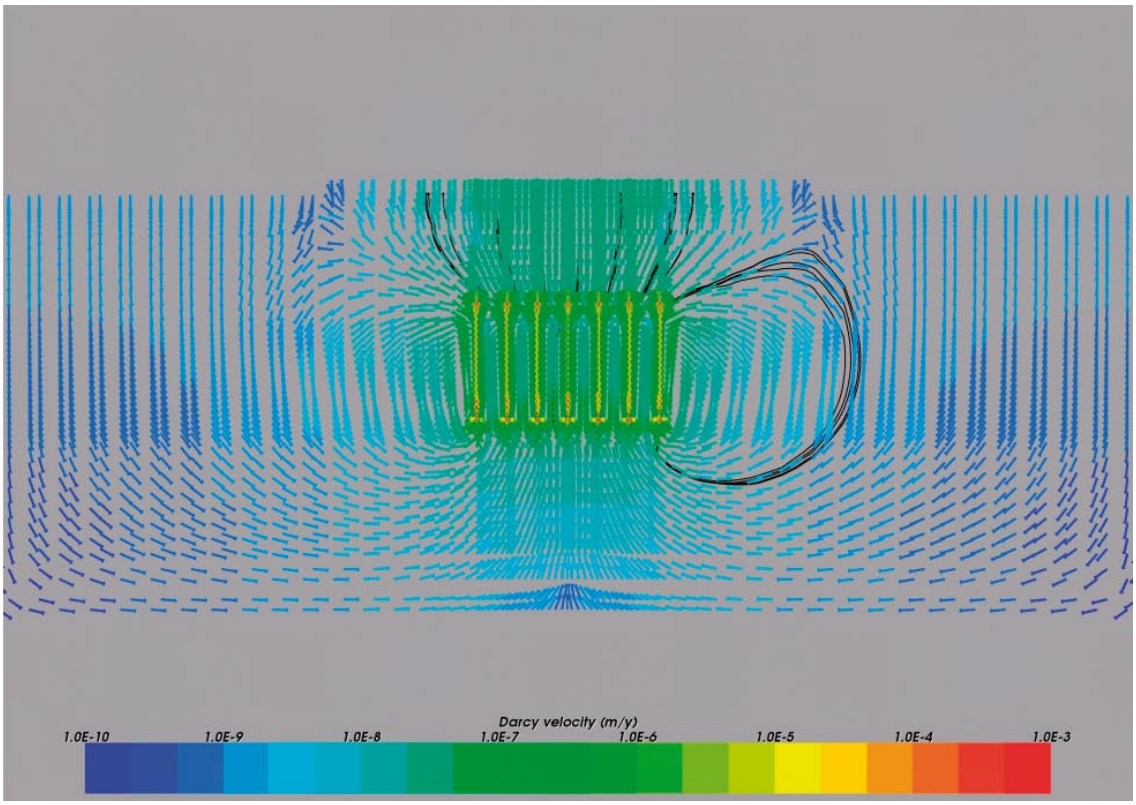

Figure 3-1. *Case 1. Vertical section through the middle of the model showing Darcy velocity vectors. Flow paths are superimposed for illustration. Time = 10 years.*

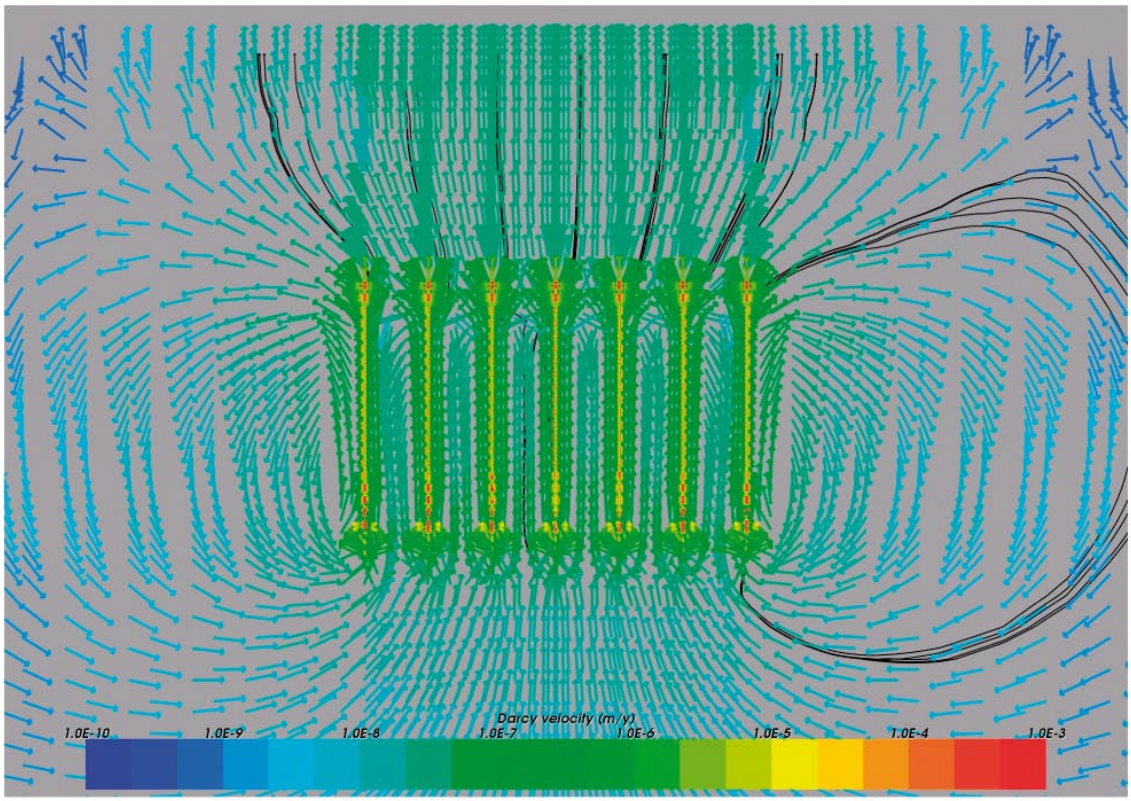

Figure 3-2. *Case 1. Close-up view of a vertical section showing Darcy velocity vectors. Flow paths are superimposed for illustration. Time = 10 years.*

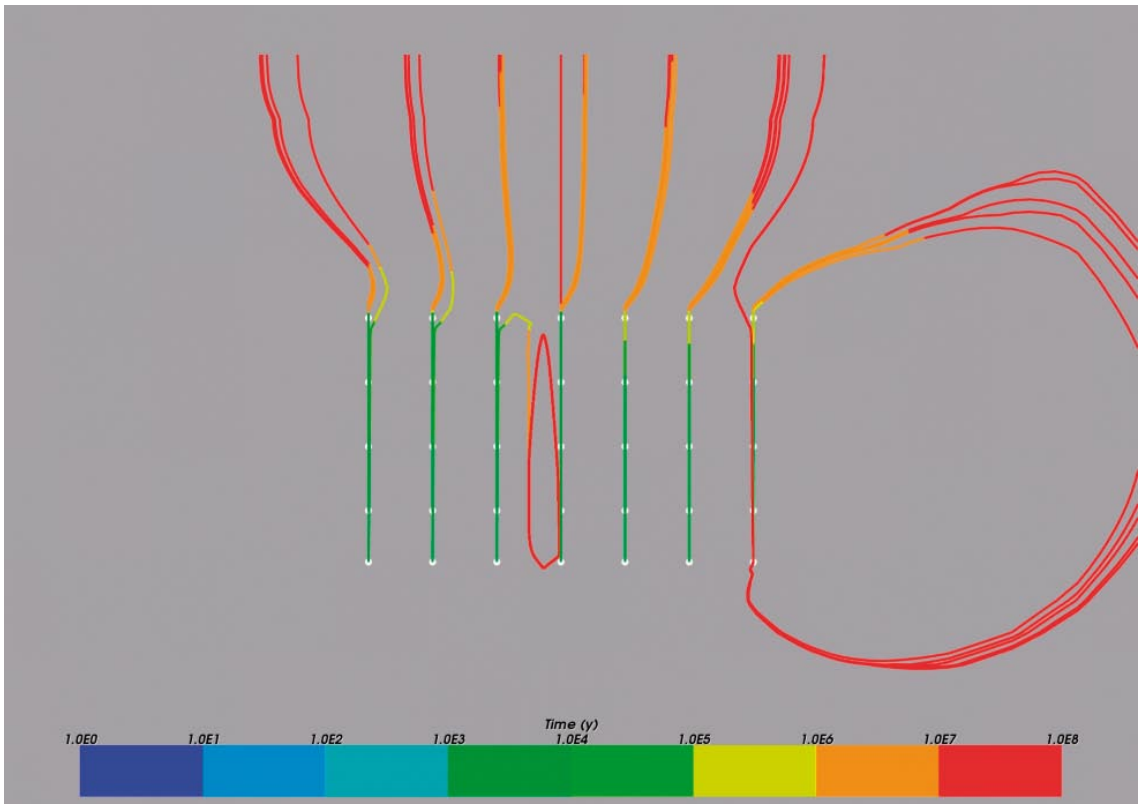

Figure 3-3. *Case 1. Vertical section showing flow paths coloured by travel time along the paths. Particle release time = 10 years.*

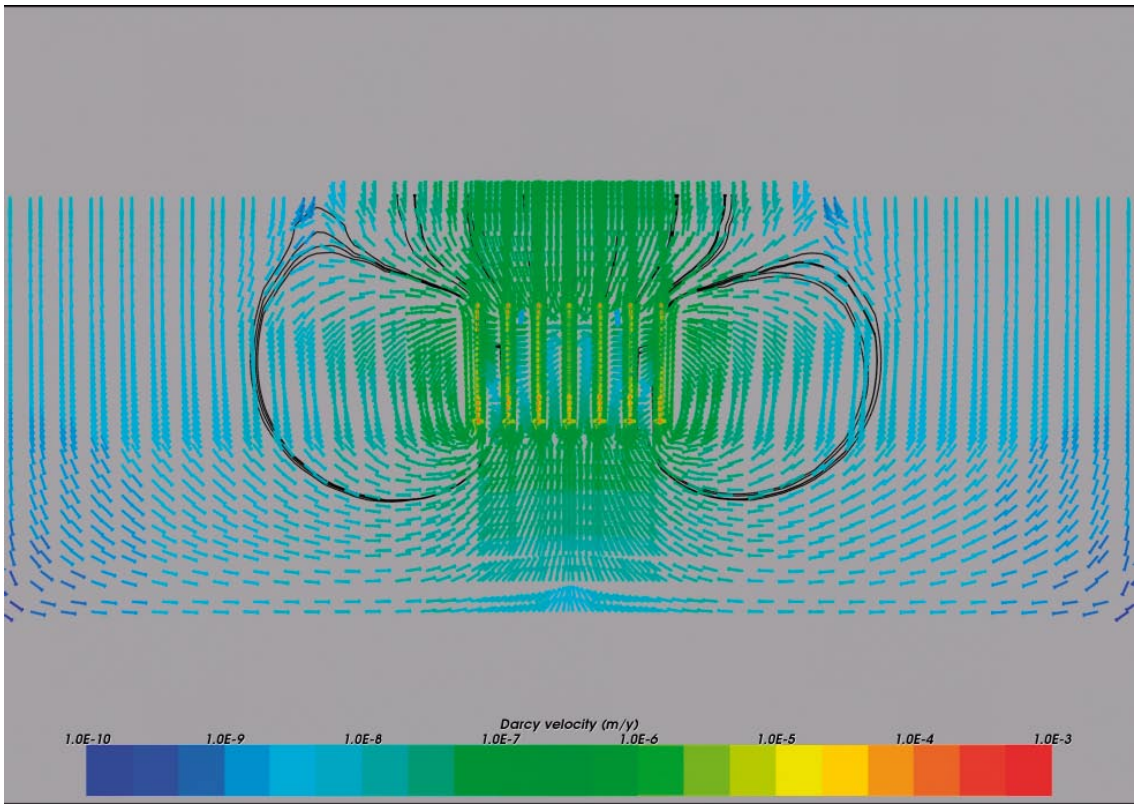

Figure 3-4. *Case 1. Vertical section through the middle of the model showing Darcy velocity vectors. Flow paths are superimposed for illustration. Time = 100 years.*

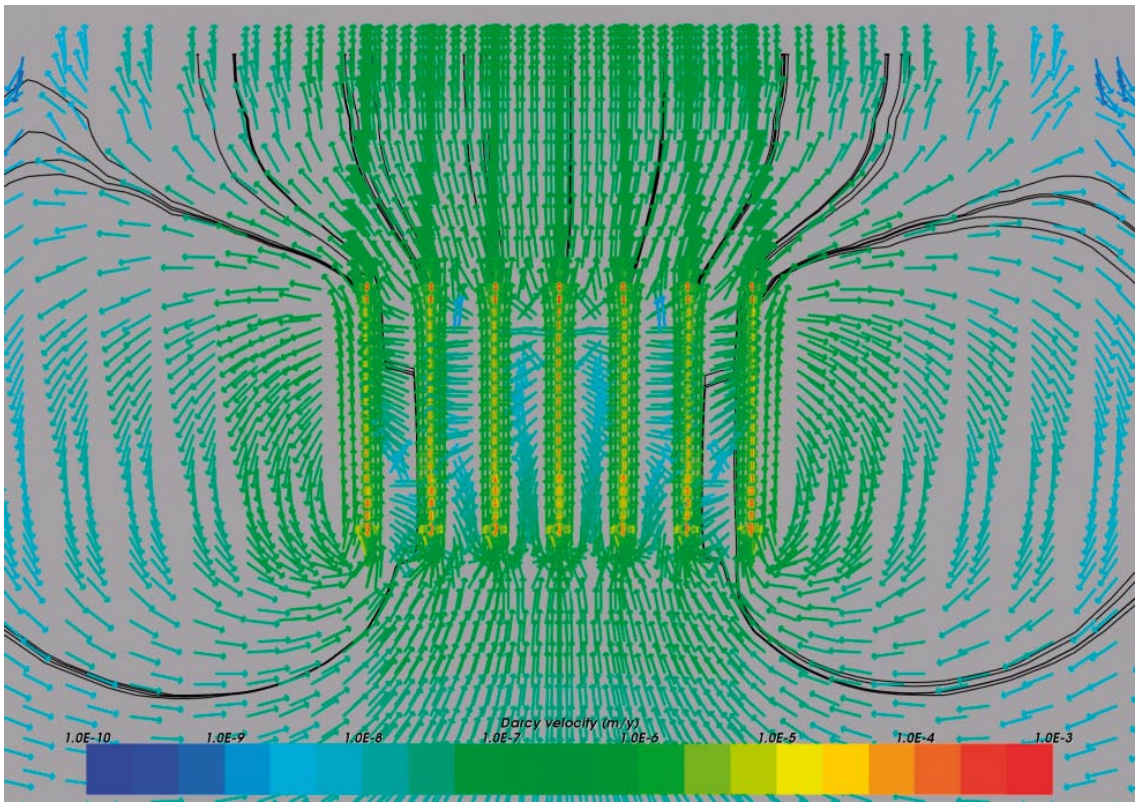

Figure 3-5. *Case 1. Close-up view of a vertical section showing Darcy velocity vectors. Flow paths are superimposed for illustration. Time = 100 years.*

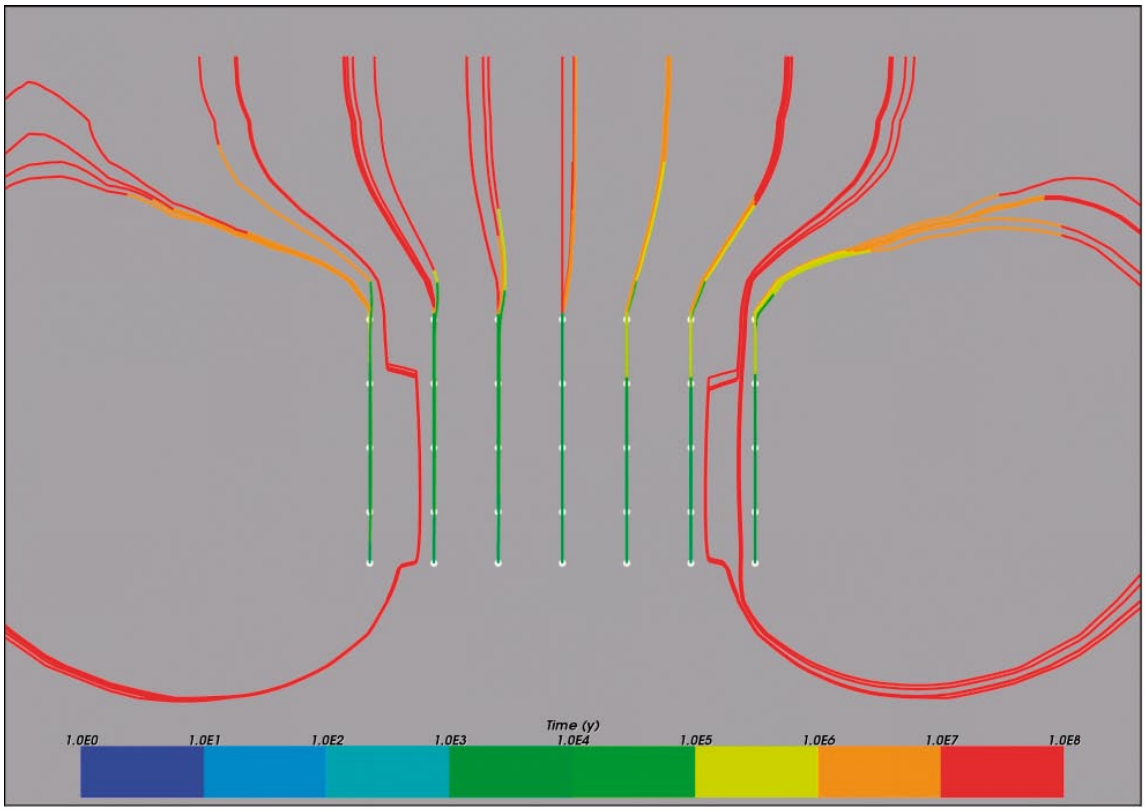

Figure 3-6. *Case 1. Vertical section showing flow paths coloured by travel time along the paths. Particle release time = 100 years.*

3.2.2 Case 2. Head gradient

In this variant, the head applied as a top boundary condition has changed from a uniform value as was used in the Base Case, to a 1% head gradient sloping down from west to east (left to right in the pictures). Given the size of the model this means that the head in the western part of the model will be set to 190.5 m linearly decreasing over the top surface down to zero in the eastern part of the model.

Compared to the Base Case, the applied head gradient increases the horizontal flow in the upper more permeable layers of the rock; see Figure 3-7–Figure 3-8. This change in the flow field skews the flow paths of the released particles and sends them in an eastward direction following the top layers of rock. The order of magnitude of the Darcy velocities and the travel time remain virtually unchanged compared to the base case when the head gradient is applied.

3.2.3 Case 3. Homogeneous rock properties

This variant is based on Case 2 but the increased permeability in the top layers of the model is changed so that the rock has homogeneous properties throughout the model domain. The permeable top of the model in the Base Case model transports a major part of the water entering the model through the top surface. The aim with this case is to see if more groundwater penetrates into the deep rock if the properties aremade homogeneous.

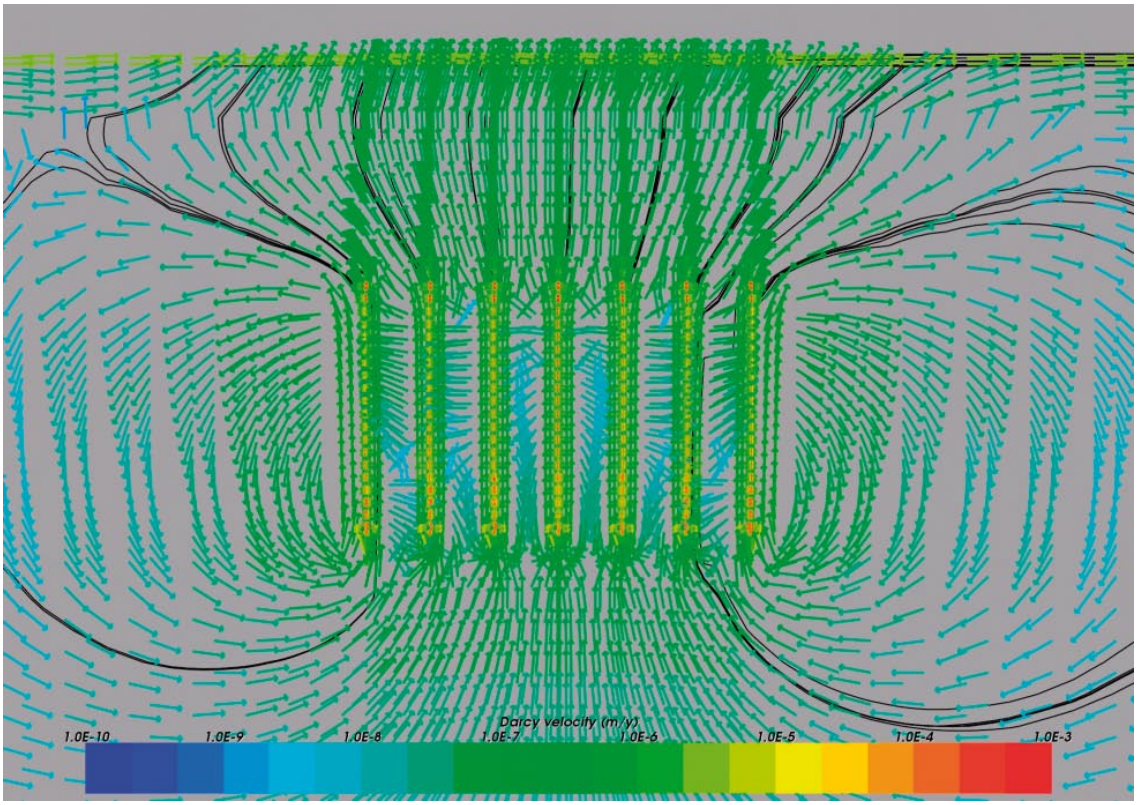

Figure 3-7. *Case 2. Close-up view of a vertical section showing Darcy velocity vectors. Flow paths are superimposed for illustration. Time = 100 years.*

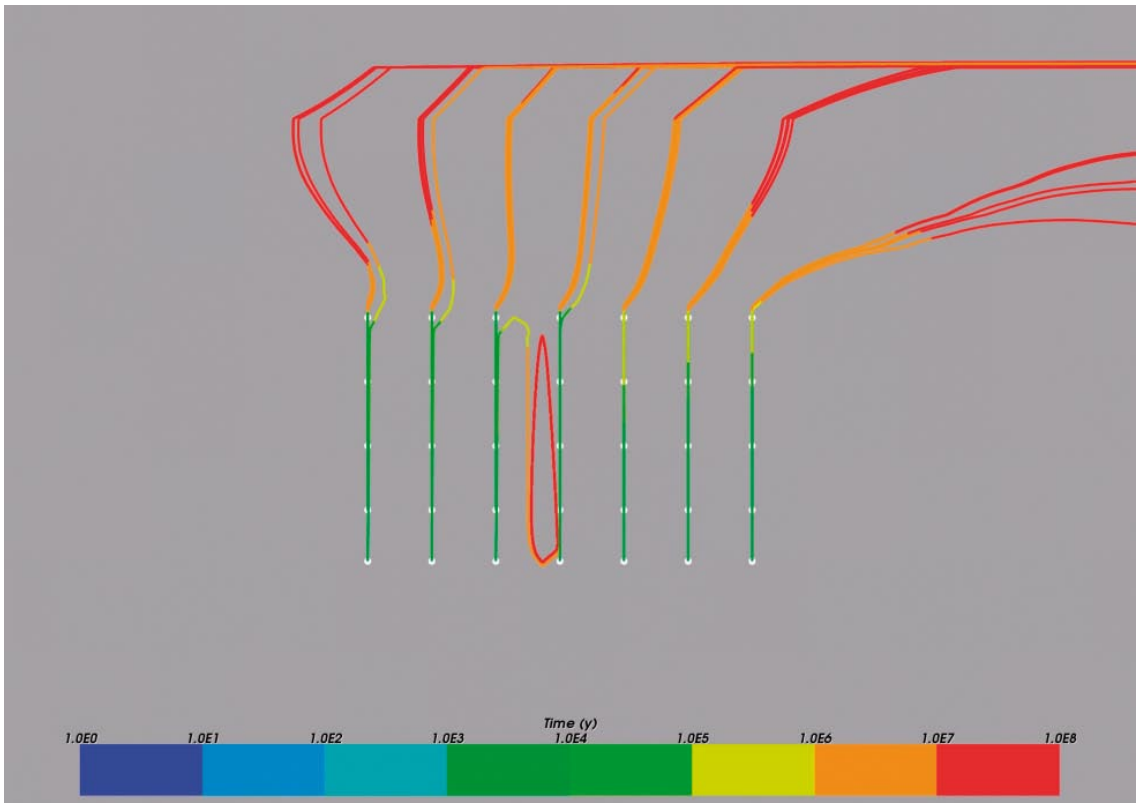

Figure 3-8. *Case 2. Vertical section showing flow paths coloured by travel time along the paths. Particle release time = 100 years.*

Figure 3-9–Figure 3-11 show the results after 100 years of simulation and the differences compared to Case 2 are significant. The flow field is no longer directed horizontally in the top layers. Instead, the flow direction outside of the repository area is more vertical and the groundwater penetrates deeper down into the model entering the boreholes from beneath. The Darcy velocities in the upper layers have decreased due to the lower permeabilities of the shallow rock. The over all Darcy velocities are still in the same range as in Case 2. The flow paths are also more vertical and symmetric above the repository compared to Case 2 where the particles bent eastwards when reaching the upper layers of the rock. The range of travel times is still roughly the same as before, i.e. 10^6–10^8 years.

3.3 Sensitivity to structural model

3.3.1 Case 4. Single fracture zone (slope +60°)

This is the first in a series of variants aiming on investigating the effects of adding one or more fracture zones to the structural model. In this variant, one single 50 m thick fracture zone is included in the model. The fracture zone is sloping +60° and cuts through the centre borehole at Z = –3,000 m, see the purple feature in Figure 3-12. The contrast in permeability between the more permeable fracture zone and the surrounding rock is two orders of magnitude (100 times). Apart from the fracture zone, this variant has the same properties as Case 2, i.e. 1% head gradient as a top boundary condition and increased permeability in the top layers of the model.

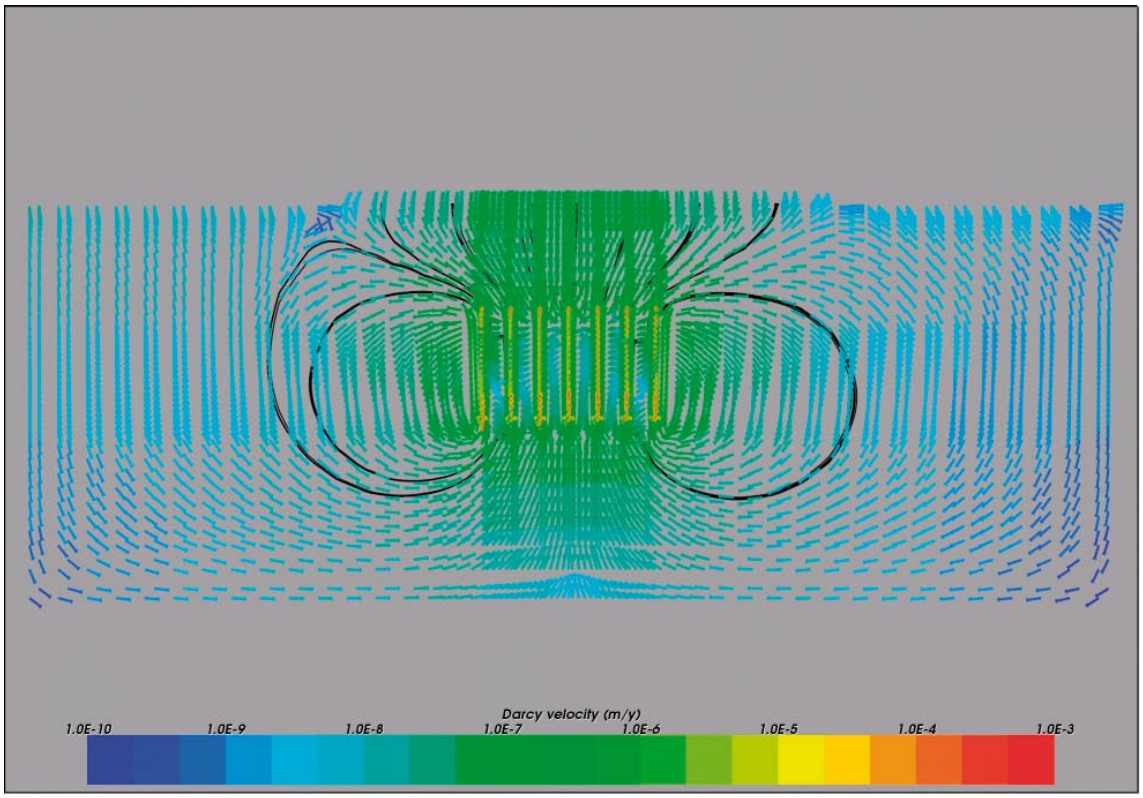

Figure 3-9. *Case 3. Vertical section through the middle of the model showing Darcy velocity vectors. Flow paths are superimposed for illustration. Time = 100 years.*

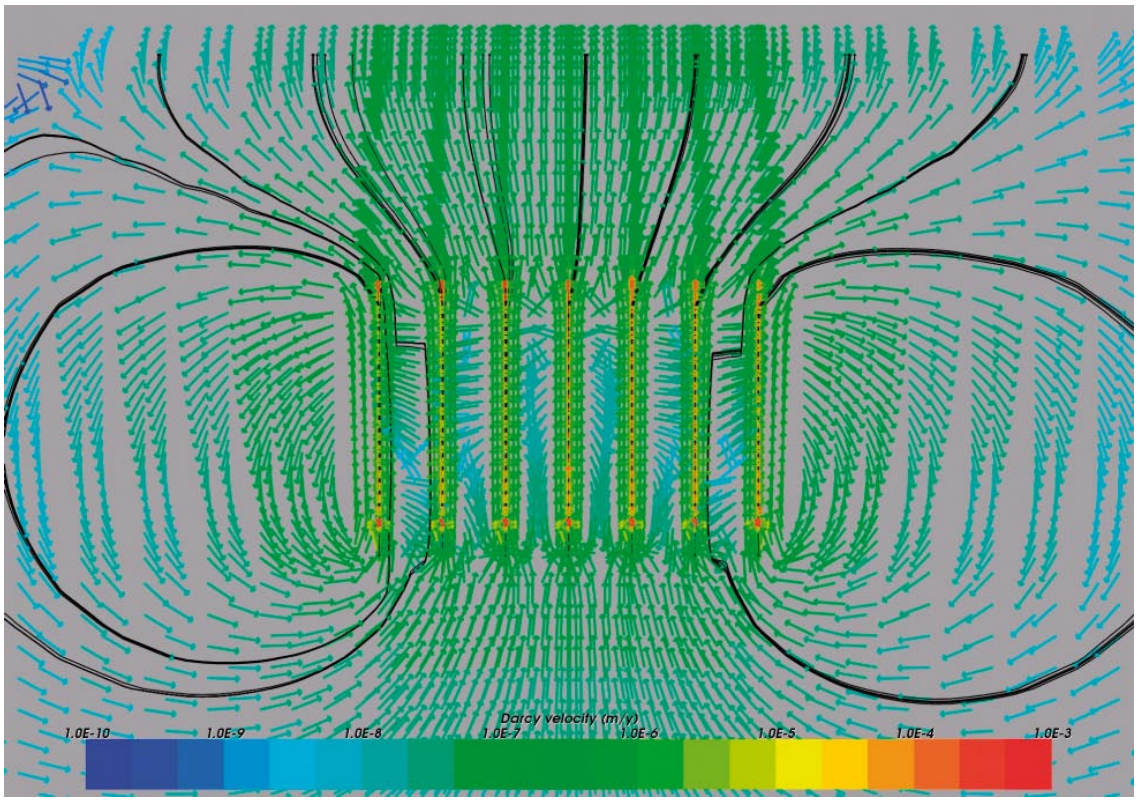

Figure 3-10. *Case 3. Close-up view of a vertical section showing Darcy velocity vectors. Flow paths are superimposed for illustration. Time = 100 years.*

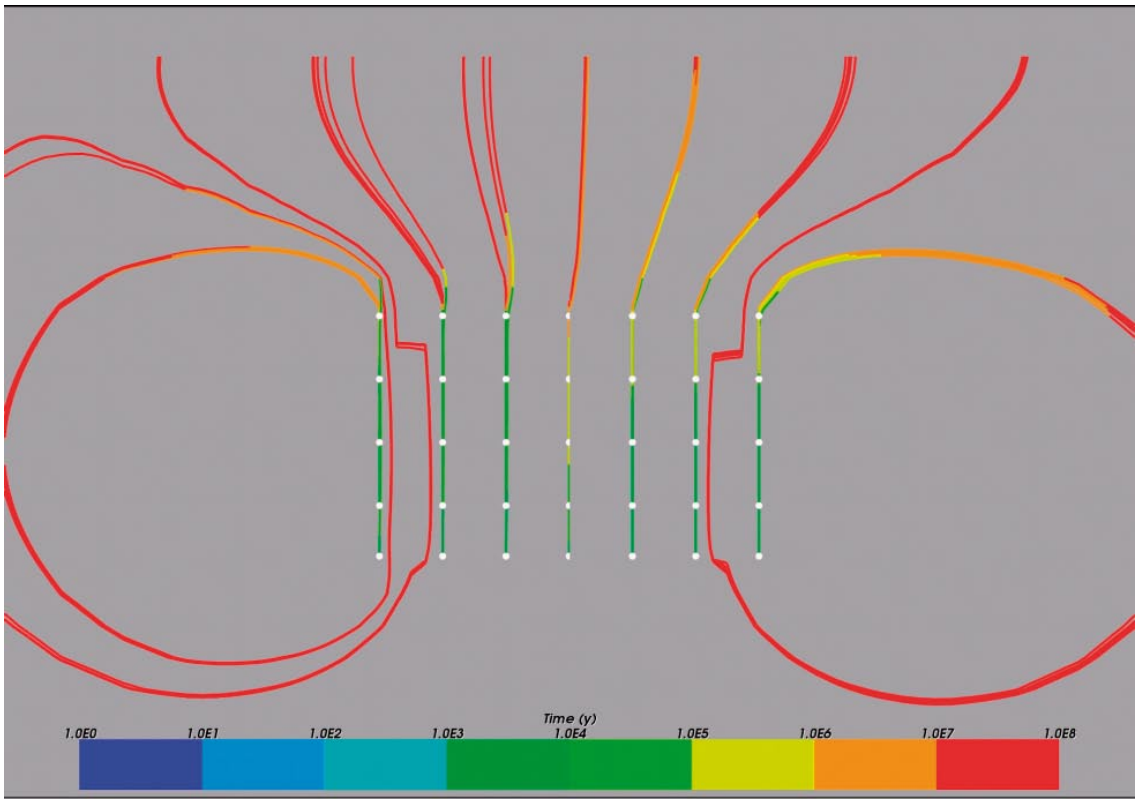

Figure 3-11. *Case 3. Vertical section showing flow paths coloured by travel time along the paths. Particle release time = 100 years.*

The effects of adding a high permeable structure to the model can be seen in Figure 3-12 and Figure 3-13. The groundwater flow in the immediate vicinity of the fracture zone is directed along the fracture. As expected, the Darcy velocity also increases inside the fracture zone. On the other hand, looking at the parts of the fracture that are outside of the repository area, the change in Darcy velocity is not that obvious. The reason for this is the coarser discretisation in the peripheral areas of the model resulting in decreased contrast between the fracture and the rock. This effectively wipes out the effect of the fracture zone, see Figure 3-14. In order to capture the full effect of an implicitly added fracture the grid discretisation needs to be no larger than the size of the represented feature, in this case 50 m.

Compared to Case 2, we here see a slightly increased Darcy velocity throughout the model. The flow pattern is what we would expect from a model combining the head gradient and a sloping fracture zone, i.e. increased Darcy velocities in the top layers of the model and in the vicinity of the fracture zone. Overall, the results do not differ much and the travel times are still in the range of 10^6–10^8 years. However, this conclusion should be treated with some caution since the effects of fracture zones are highly dependent on the physical properties and geometries of the fractures and the discretisation of the model.

3.3.2 Case 5. Single fracture zone (slope –60°)

In this variant, the fracture zone was rotated counter clock wise compared to Case 4 to an angle of –60°. Apart from this change, the two variants have the same physical properties. The idea with changing the slope of the fracture is to align the zone with the head gradient. Contrary to what one might intuitively expect, the direction of the resulting flow through the entire fracture zone is upwards towards the west, i.e. against the top head gradient in the upper part of the rock. The explanation given is that the energy required for the groundwater to flow against the head gradient is still less than that of choosing the other way through the rock.

Apart from this, the effects on flow and performance measures are not significant compared to the previous variants.

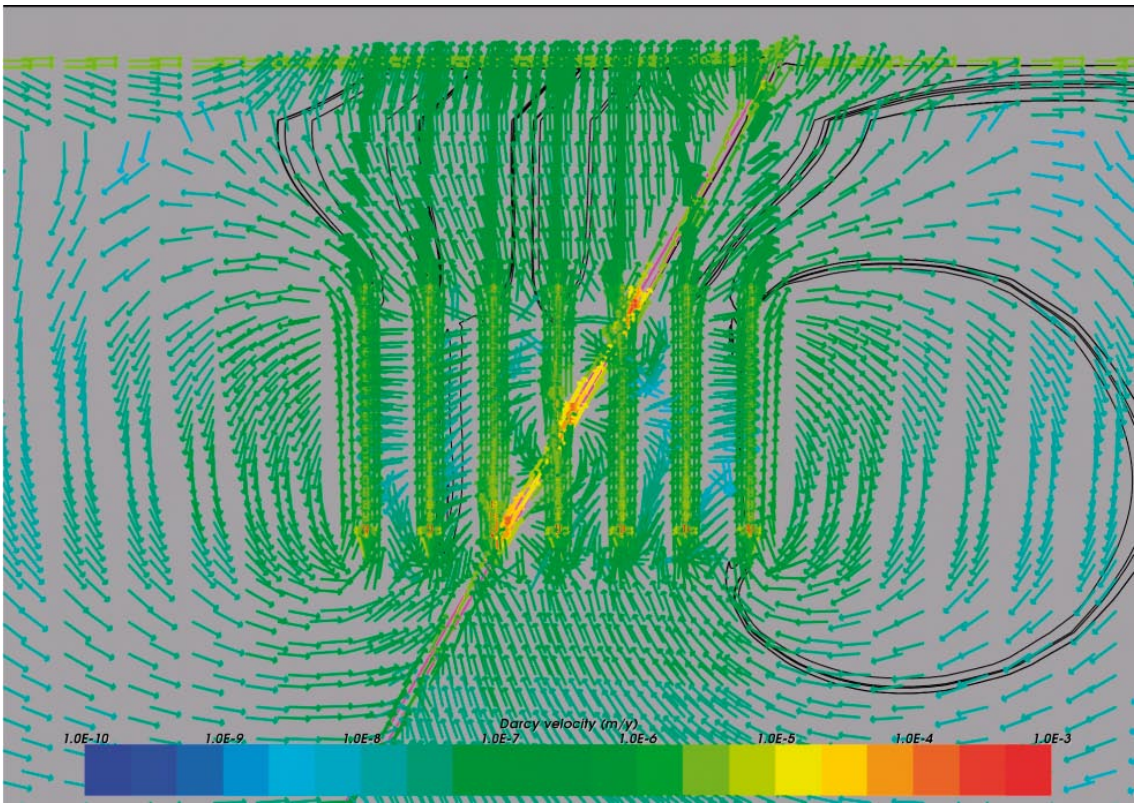

Figure 3-12. *Case 4. Close-up view of a vertical section showing Darcy velocity vectors. Flow paths are superimposed for illustration. Time = 100 years.*

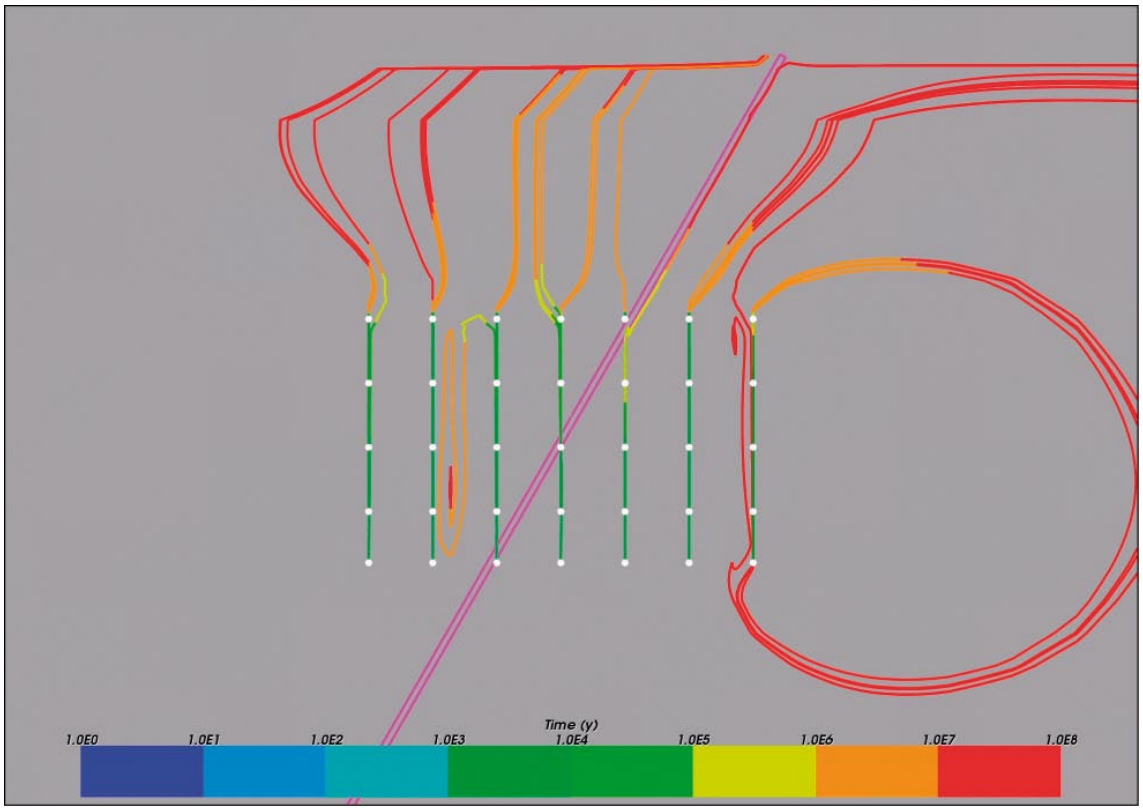

Figure 3-13. *Case 4. Vertical section showing flow paths coloured by travel time along the paths. Particle release time = 100 years.*

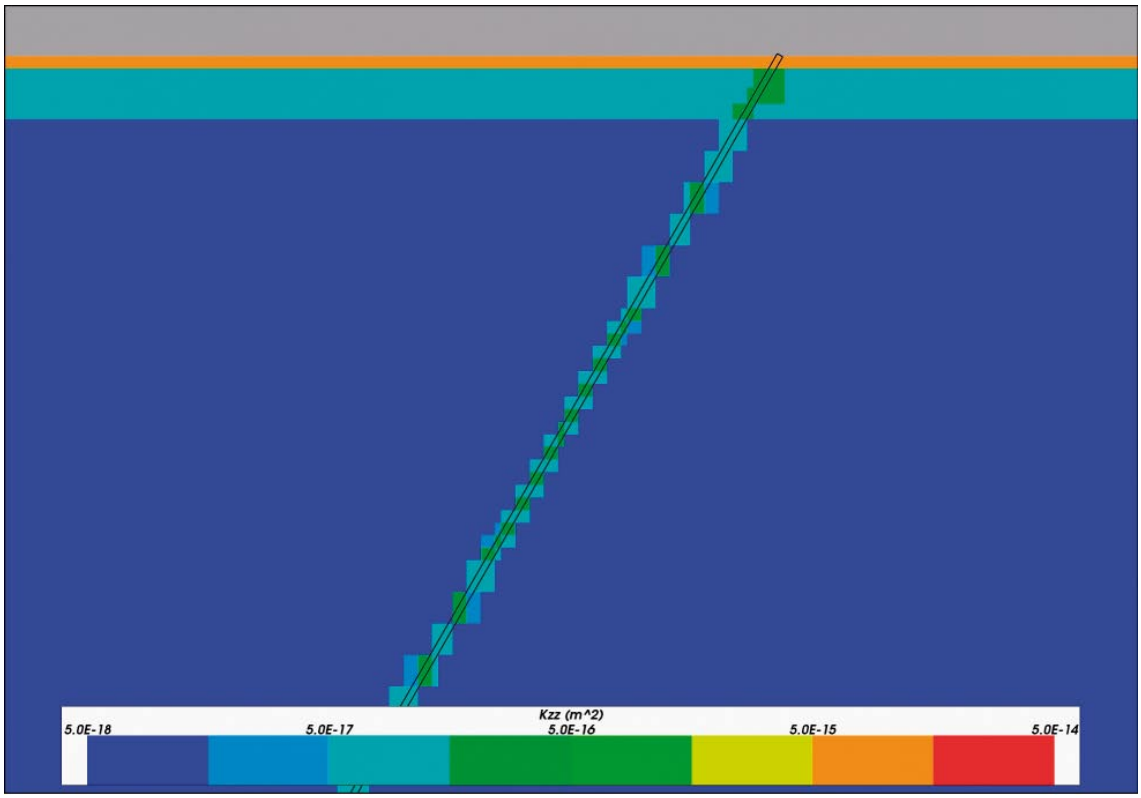

Figure 3-14. *Case 4. Vertical cross section showing the permeability. One fracture zone was included using the Implicit Fracture Zone (IFZ) method.*

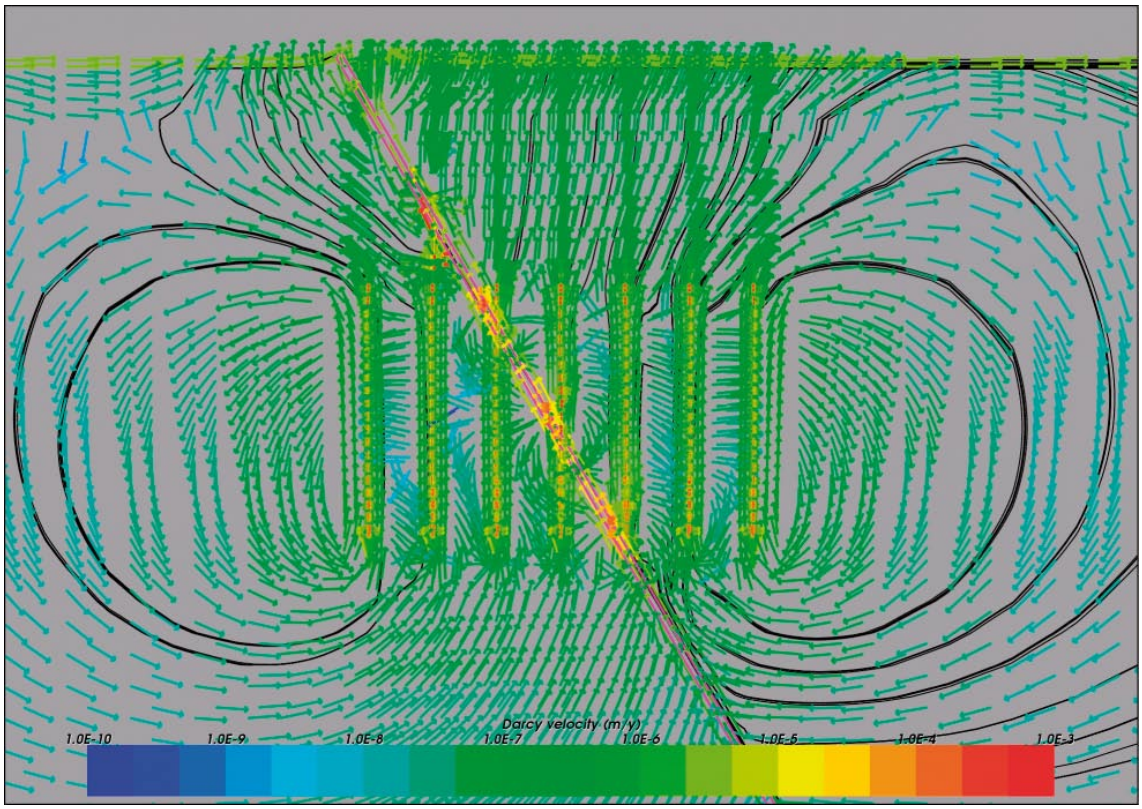

Figure 3-15. *Case 5. Close-up view of a vertical section showing Darcy velocity vectors. Flow paths are superimposed for illustration. Time = 100 years.*

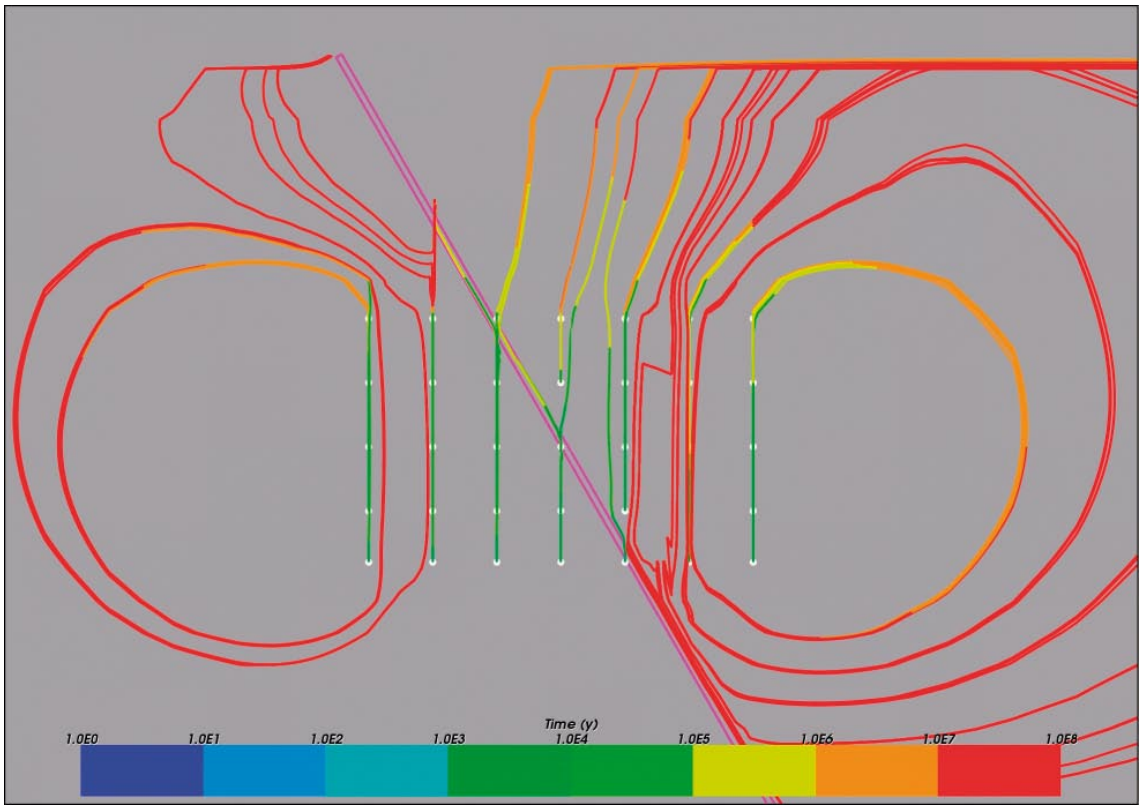

Figure 3-16. *Case 5. Vertical section showing flow paths coloured by travel time along the paths. Particle release time = 100 years.*

3.3.3 Case 6. Connected regional fracture zones

The fracture zones included in Cases 4 and 5 did not have the expected effect on the groundwater flow. The idea of Case 6 is to include structural features that would lead shallow head gradients and groundwater deep into the rock and possibly disturb the stable situation initially formed. In order to allow for this, a set of three connected fracture zones was used. All fractures have a thickness of 100 m, which is twice as thick as the fracture zones that were applied in Cases 4 and 5. All other physical properties of the fracture zones and the rest of the model stay unchanged.

The results are presented in Figure 3-17 and Figure 3-18. The main observations from Case 4 and 5 are still valid. Flow is still directed upward through the upper part of the vertical fracture zone upstream. Darcy velocities are increased in the intersections between the boreholes and the sloping fracture zone. However, even if the paths of the released particles change slightly due to the new flow field, the overall performance of the repository does not change.

3.3.4 Case 7. Disconnected regional fracture zones

This variant explores the effects of a more complex fracture network. In total, this model includes four fractures, see Figure 3-19. The two in the middle are sloping –60° and +60° respectively and crossing each other at Z = –3,000 m. These have the same properties as the fractures in Case 4 and 5. The two remaining regional fracture zones are vertical and have a thickness of 100 m. They are hydraulically disconnected from the two zones in the centre.

Again, the idea is to allow the hydraulic gradient to propagate downward from the surface and for the groundwater to penetrate deeper into the model by including regional fracture zones outside of the repository area. The effects of the regional fracture zones on the groundwater

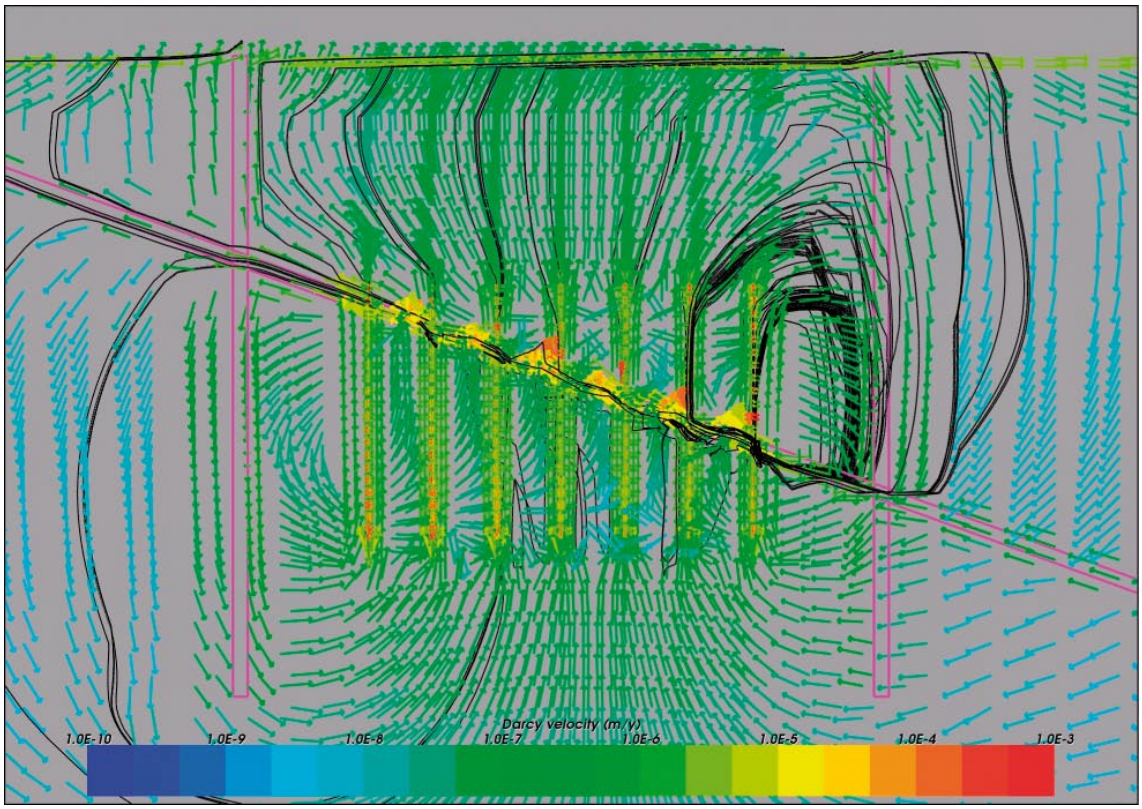

Figure 3-17. *Case 6. Close-up view of a vertical section showing Darcy velocity vectors. Flow paths are superimposed for illustration. Time = 100 years.*

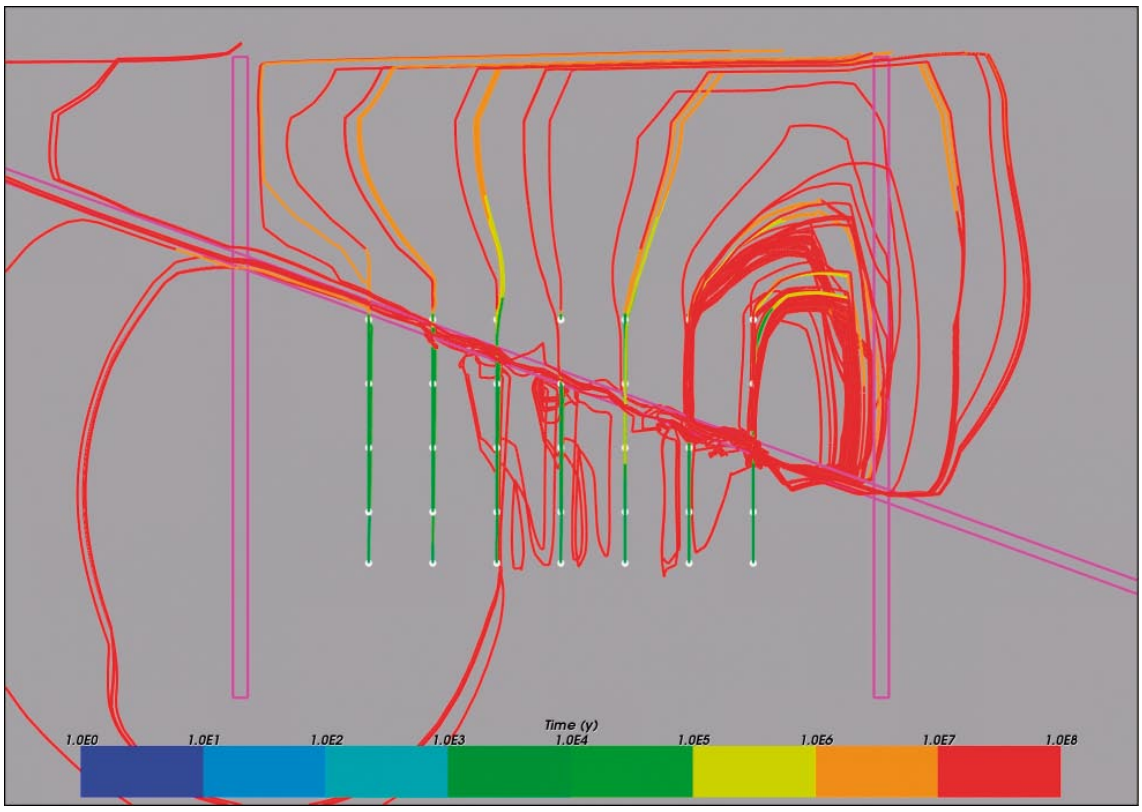

Figure 3-18. *Case 6. Vertical section showing flow paths coloured by travel time along the paths. Particle release time = 100 years.*

flow are clear, see Figure 3-19 and Figure 3-20. Flow along the vertical regional fractures is enhanced in a downward direction. In addition, localised convection cells are formed in the volumes between the outer boreholes and the regional fractures, which is clearly seen in the particle tracking. Apart from this, a general increase of the Darcy velocities is found in the rock above the repository and this is reflected in the performance measures where the hypothetical travel time range now decreases down to 10^5 years for some of the released particles.

This variant clearly shows how sensitive the model is to the structural representation of the rock domain and the hydraulically active features that are present.

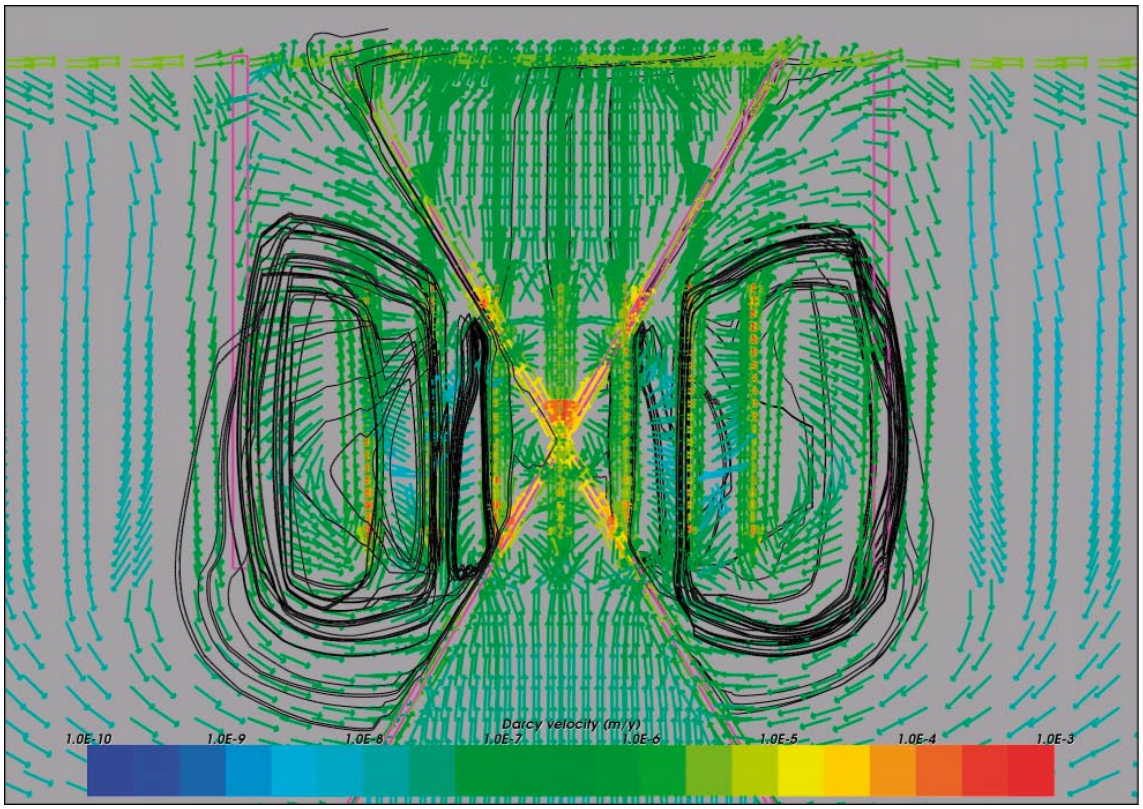

Figure 3-19. *Case 7. Close-up view of a vertical section showing Darcy velocity vectors. Flow paths are superimposed for illustration. Time = 100 years.*

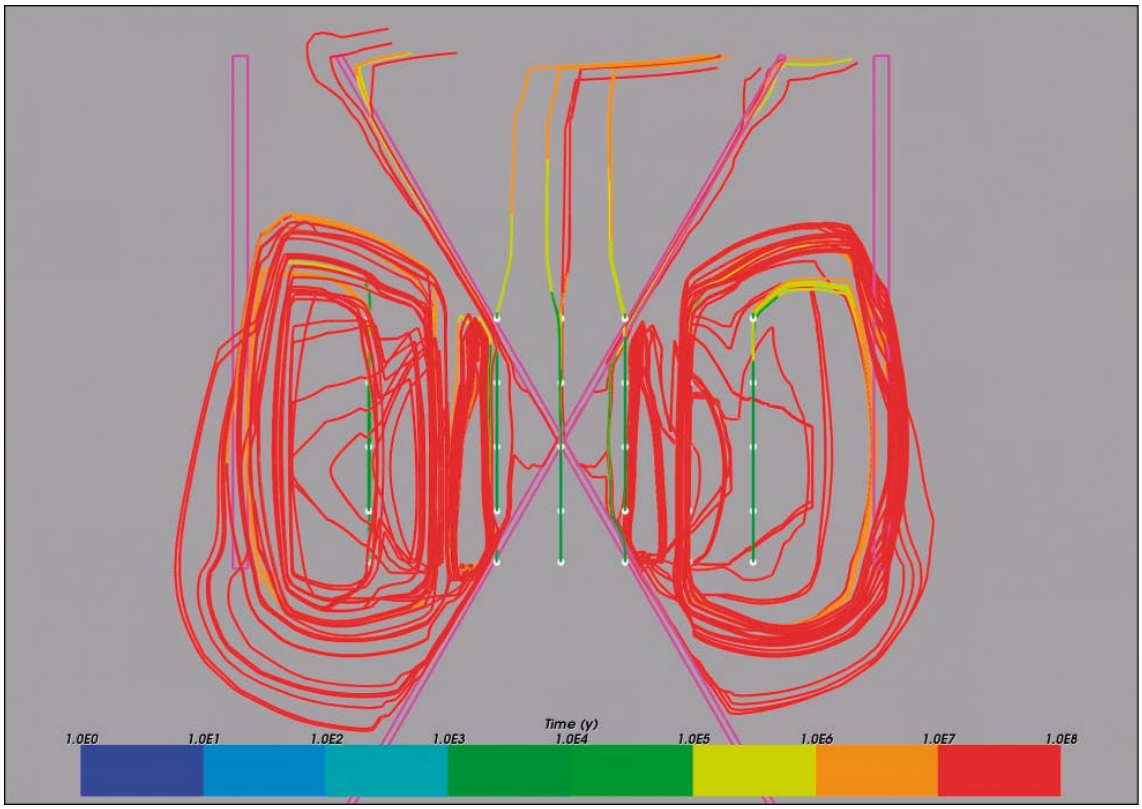

Figure 3-20. *Case 7. Vertical section showing flow paths coloured by travel time along the paths. Particle release time = 100 years.*

3.3.5 Case 8. HCD model Laxemar v1.2

This variant is based on Case 3 where a head gradient of 1% was applied to the top boundary and rock properties did not vary with depth. In addition to this, the Hydraulic Conductor Domain (HCD) model from the site investigation of Laxemar v1.2 was included in the present variant. This set of fracture zones is a result of the extensive hydrogeologic investigations performed in the Laxemar area. The geometries of the fracture zones have been determined from studies of surface lineaments and cores from borehole drillings. Physical properties based on measurements and simulations have been assigned to all fractures. However, it should be noted that in the site modelling, additional structural information is used in terms of an upscaled stochastic discrete fracture network (DFN) that is combined with the HCD to form a complete description of the structural model. The DFN part of the modelling is outside the scope of this project and therefore not used here. This of course means that a significant amount of connectivity is missing in the present model. In addition, the fracture zones used in the site modelling were only defined down to Z = –2,100 m. Thus, no information was available for the deep rock beneath this level. This of course is not satisfying when the repository is located at a depth of 2,000–4,000 m. On the other hand, discretisation is coarser in the present model that applied in the site modelling meaning that the representation of the fracture network will not be very good at depth. Consequently, this variant should be used only as an indication on the potential effects of a realistic fracture network. The effect of extending some fracture zones into the deeper lying rock is studied in Case 9, see Section 3.3.6.

In Figure 3-21 and Figure 3-22, the results for Case 8 are presented. In the figures, the intersections between fracture zones and the plane of cross-section have been drawn using pink lines. It is clear that the effect of the irregular fracture network on the groundwater flow is mainly restricted to the upper 2,000 m of the rock. The horizontal fracture zone above the repository acts like a shield, directing the groundwater rising from the repository depth in the horizontal direction before it reaches the surface. In addition, the Darcy velocities in the upper region of the rock have decreased. Still the overall effect of including the fracture network is not significant. However, this is not unexpected because of general lack of connectivity, fracture representation below Z = –2,000 m and insufficient grid discretisation.

3.3.6 Case 9. Extended HCD model Laxemar v1.2

The fracture network model used in Case 8 was only defined down to Z = –2,100 m. Since the results showed that the groundwater flow was left rather undisturbed below this level, it was decided that an extended version of the fracture network should be modelled. Thus, in the present variant the vertical fractures were extended down to Z = –5,000 m, see Figure 3-23, while all other properties were kept unchanged compared to Case 8. The results are shown in Figure 3-24–Figure 3-27 for both 10 years and 100 years of simulation time.

The effects of the fracture network can now be seen in the model. Vertical flows now occur in the fracture zones that were extended down to a depth of 5,000 m. The Darcy velocities are increased throughout the entire model, which is reflected in the calculated range of hypothetical travel time that in this variant comes down to 10^5 years for a few particles. Clearly, we need to be able to represent the hydro-geological structures of the deep rock in order to capture the more conservative scenarios of the model.

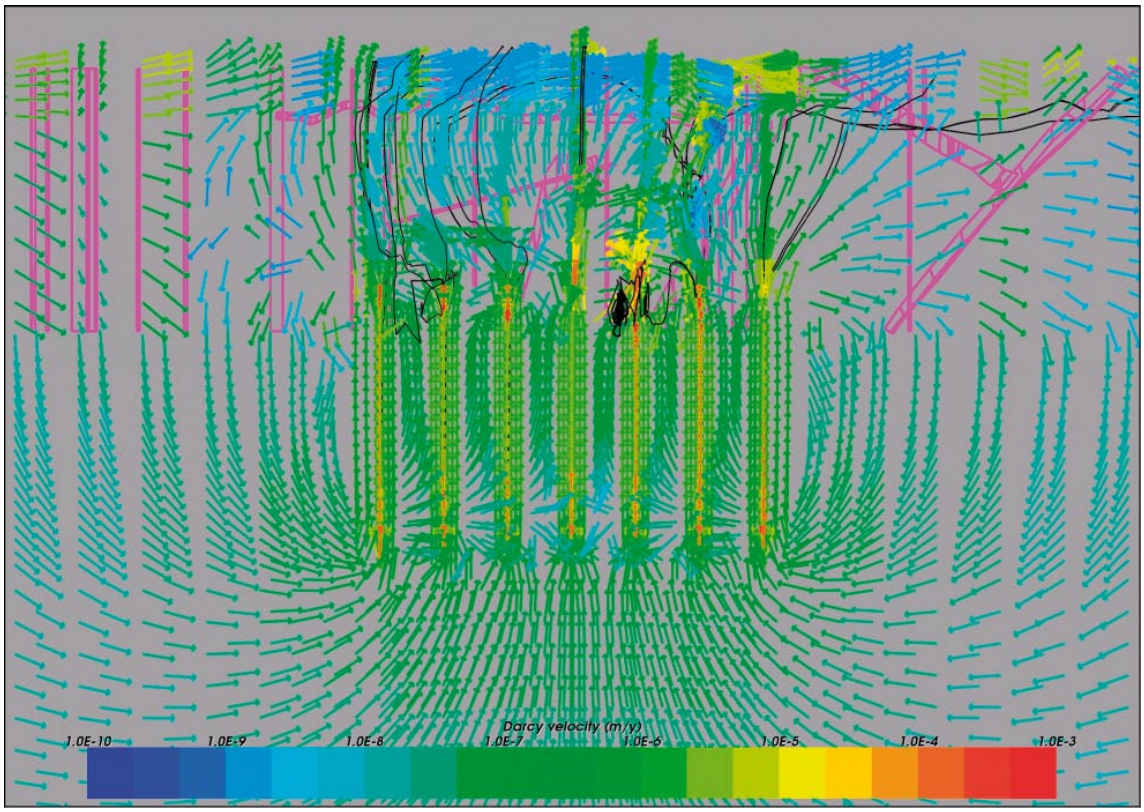

Figure 3-21. *Case 8. Close-up view of a vertical section showing Darcy velocity vectors. Flow paths are superimposed for illustration. Time = 100 years.*

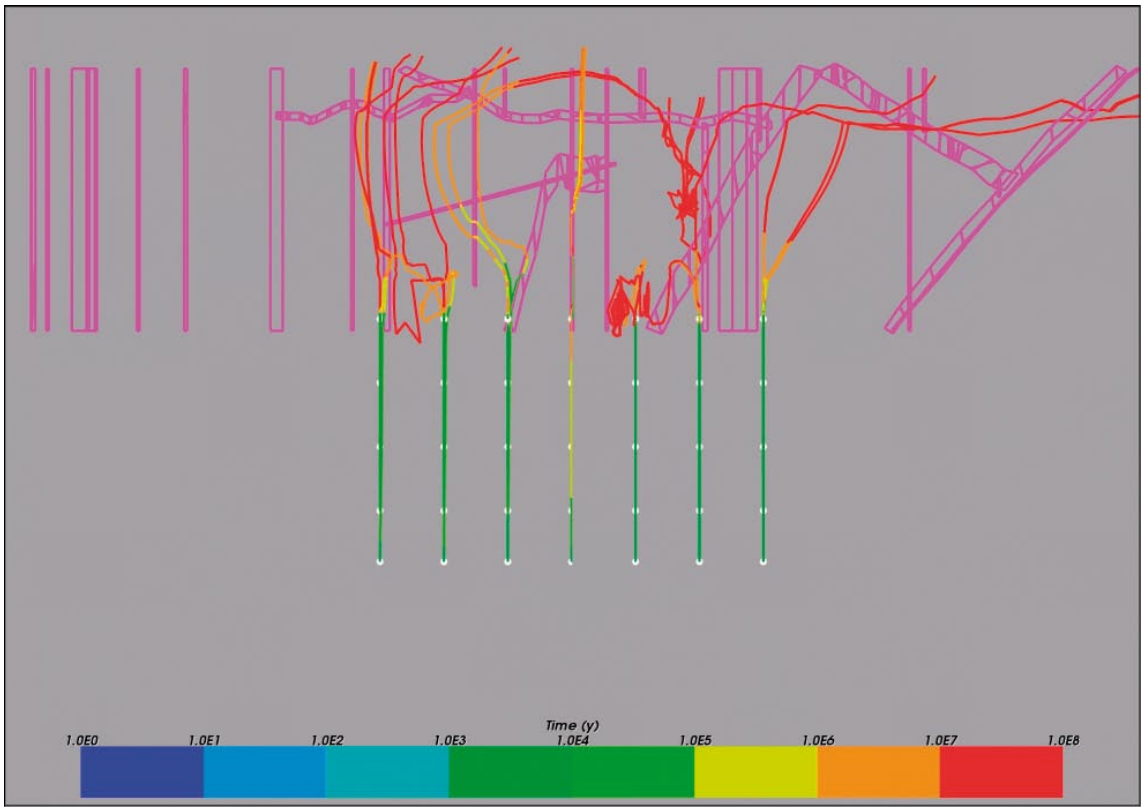

Figure 3-22. *Case 8. Vertical section showing flow paths coloured by travel time along the paths. Particle release time = 100 years.*

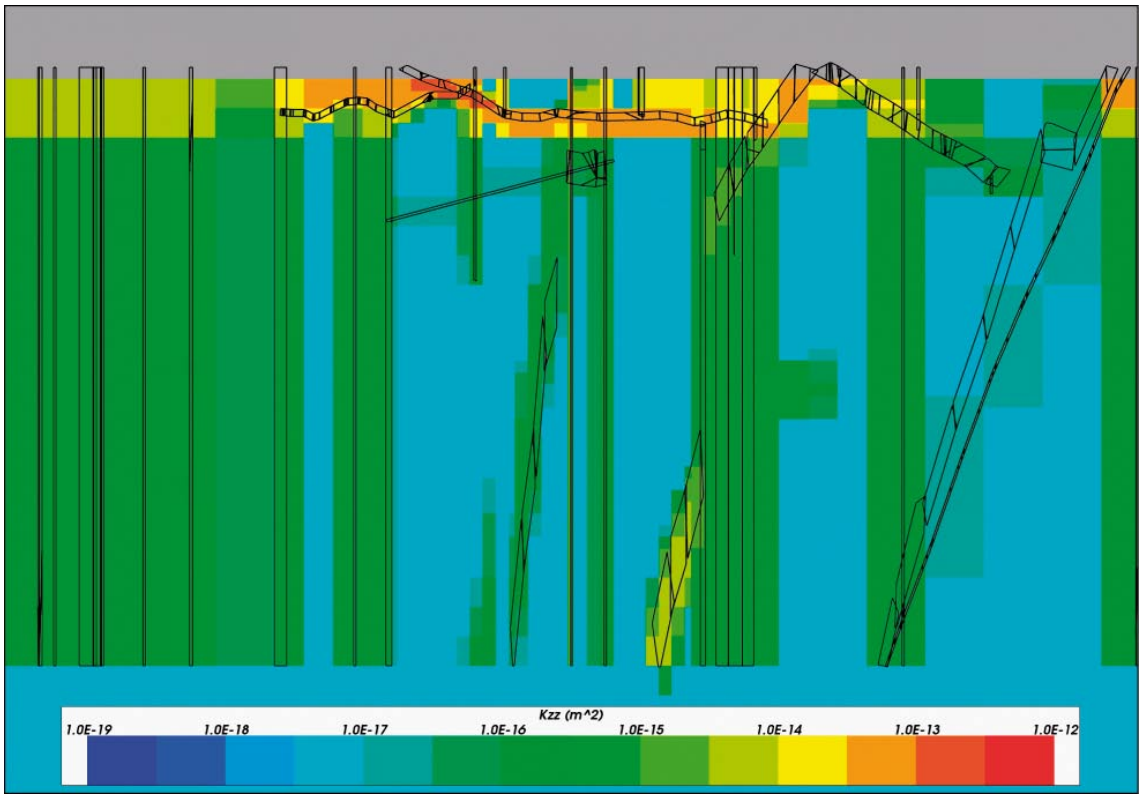

Figure 3-23. *Case 9. Vertical cross section showing the permeability. A modified version of the hydraulic conductor domain (HCD) model from the site investigation of Laxemar v1.2 was included using the Implicit Fracture Zone (IFZ) method.*

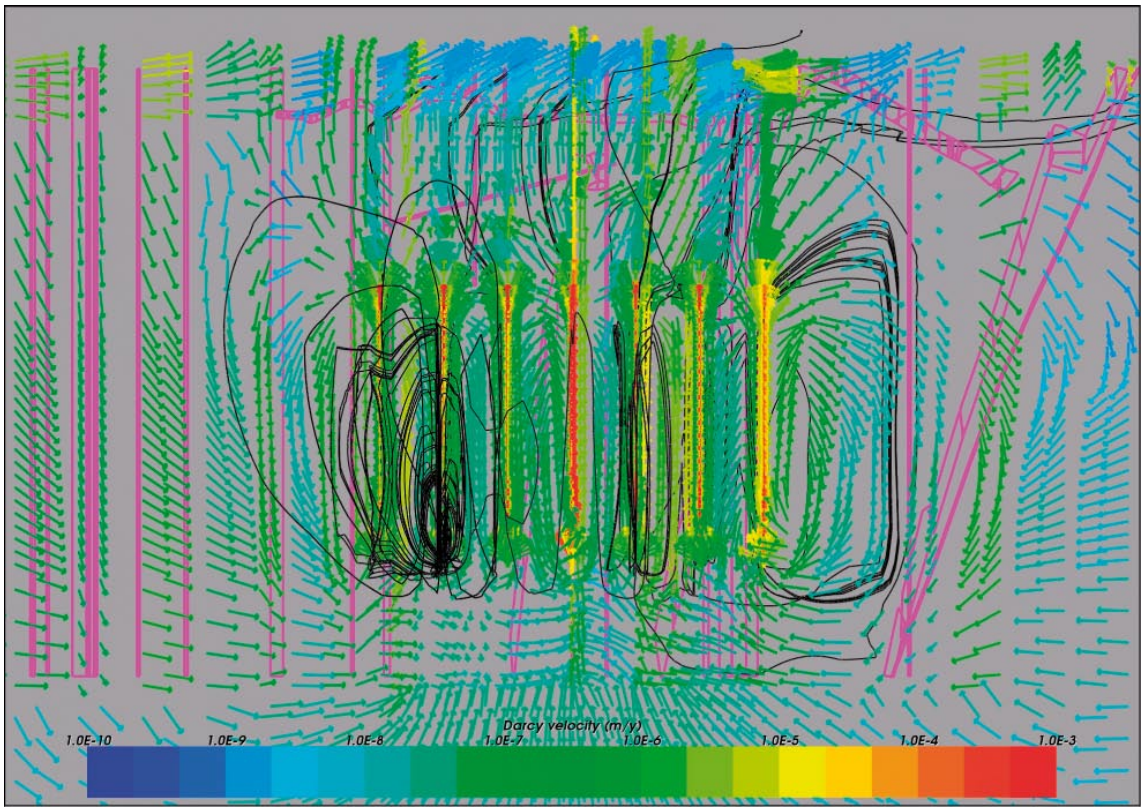

Figure 3-24. *Case 9. Close-up view of a vertical section showing Darcy velocity vectors. Flow paths are superimposed for illustration. Time = 10 years.*

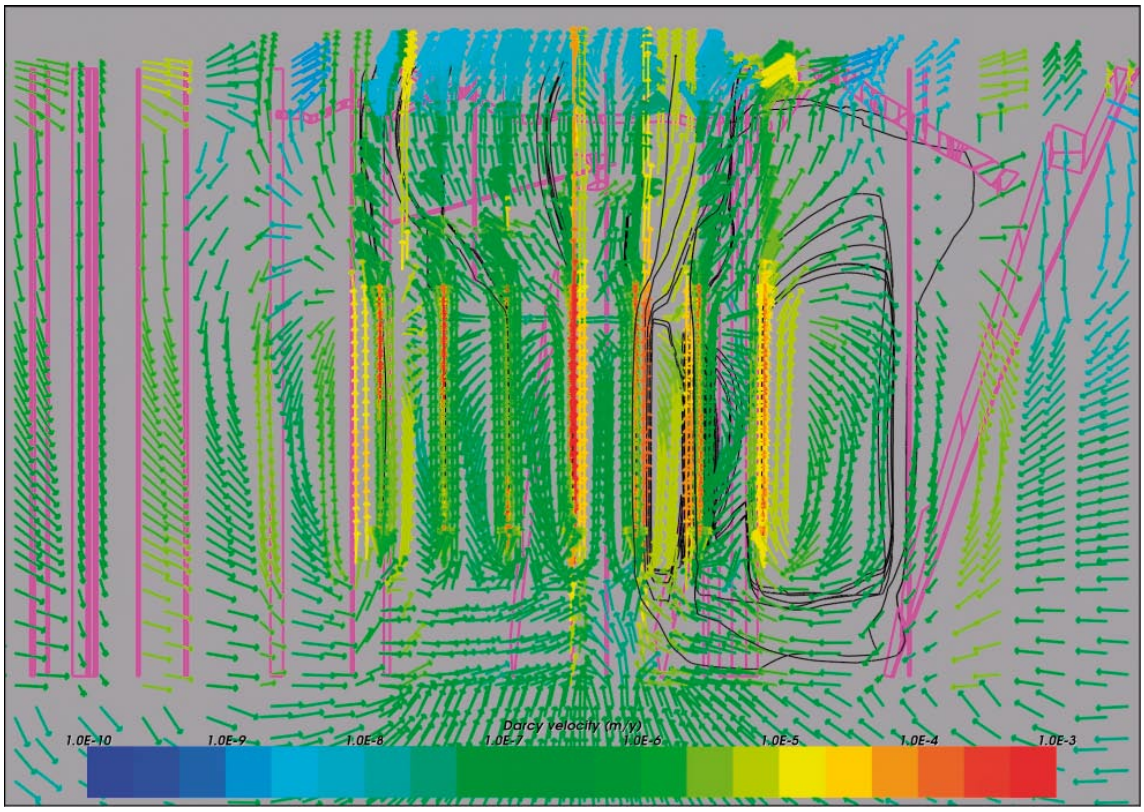

Figure 3-25. *Case 9. Close-up view of a vertical section showing Darcy velocity vectors. Flow paths are superimposed for illustration. Time = 100 years.*

Figure 3-26. *Case 9. Vertical section showing flow paths coloured by travel time along the paths. Particle release time = 10 years.*

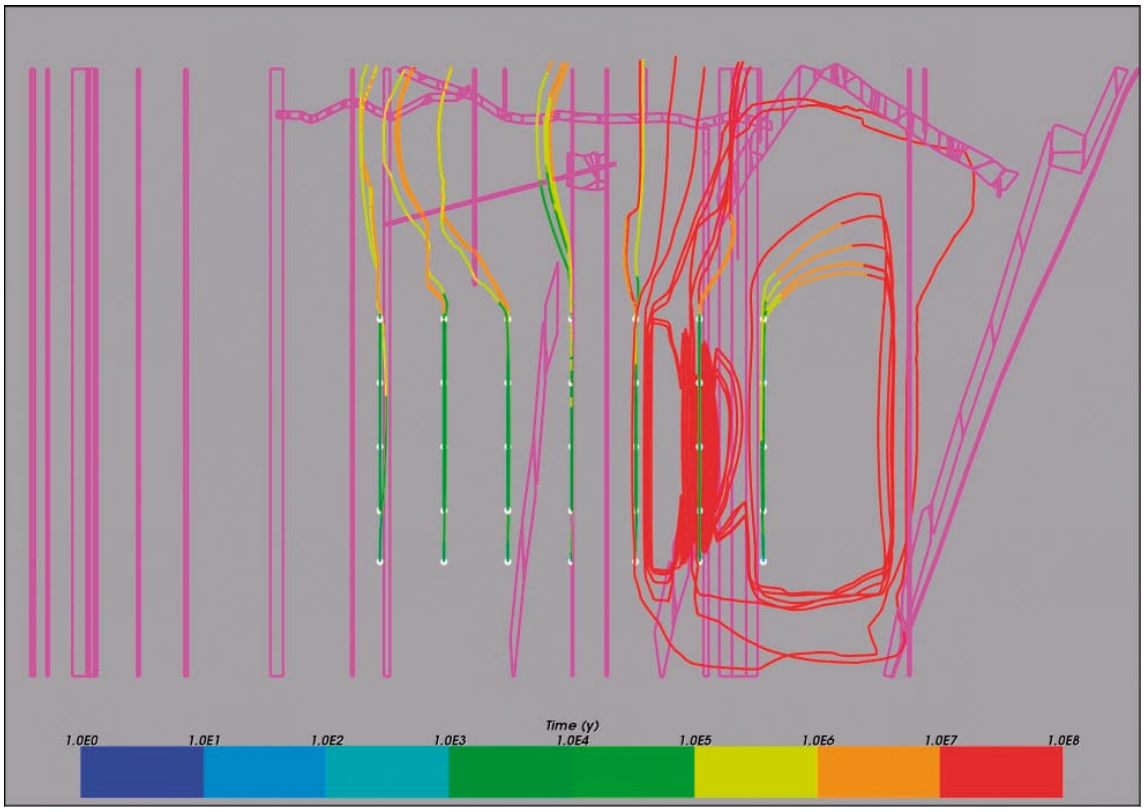

Figure 3-27. *Case 9. Vertical section showing flow paths coloured by travel time along the paths. Particle release time = 100 years.*

3.4 Sensitivity to borehole properties

This section examines the effects of poor backfill properties in the boreholes. The upper part of the boreholes, i.e. down to 2,000 m depth, includes various materials such as concrete, asphalt and bentonite. The deeper section of the boreholes, between 2,000 and 4,000 m depth include the buffer material and the DZ around the boreholes. Both the depths and the different physical properties of these materials at these depths are varied.

3.4.1 Case 10. Increased borehole permeability at Z = 0 to –500 m

This variant is based on Case 3 using the 1% head gradient on top and homogeneous permeability in the rock. The physical properties for the top 500 m of the boreholes (concrete and asphalt) are changed to buffer properties, i.e. the permeability is increased by 20 times.

There are no significant changes to the flow field, Darcy velocities or travel times compared to the previous variants, see Figure 3-28 and Figure 3-29.

3.4.2 Case 11. Increased borehole permeability at Z = –500 to –2,000 m

In this variant, which is based on Case 3, the physical properties of the bentonite for the borehole sections between 500 and 2,000 m depth are changed to buffer and DZ properties. This increases the permeability 20–100 times in the section where the bentonite is placed.

Figure 3-30 and Figure 3-31 show the results for Case 11. The results are very similar to Case 10 and there are no significant changes to the flow field or Darcy velocities. However, the calculated hypothetical travel times for the released particles are slightly shorter than for Case 10. The reason is most likely the greater borehole length with higher permeability in this variant.

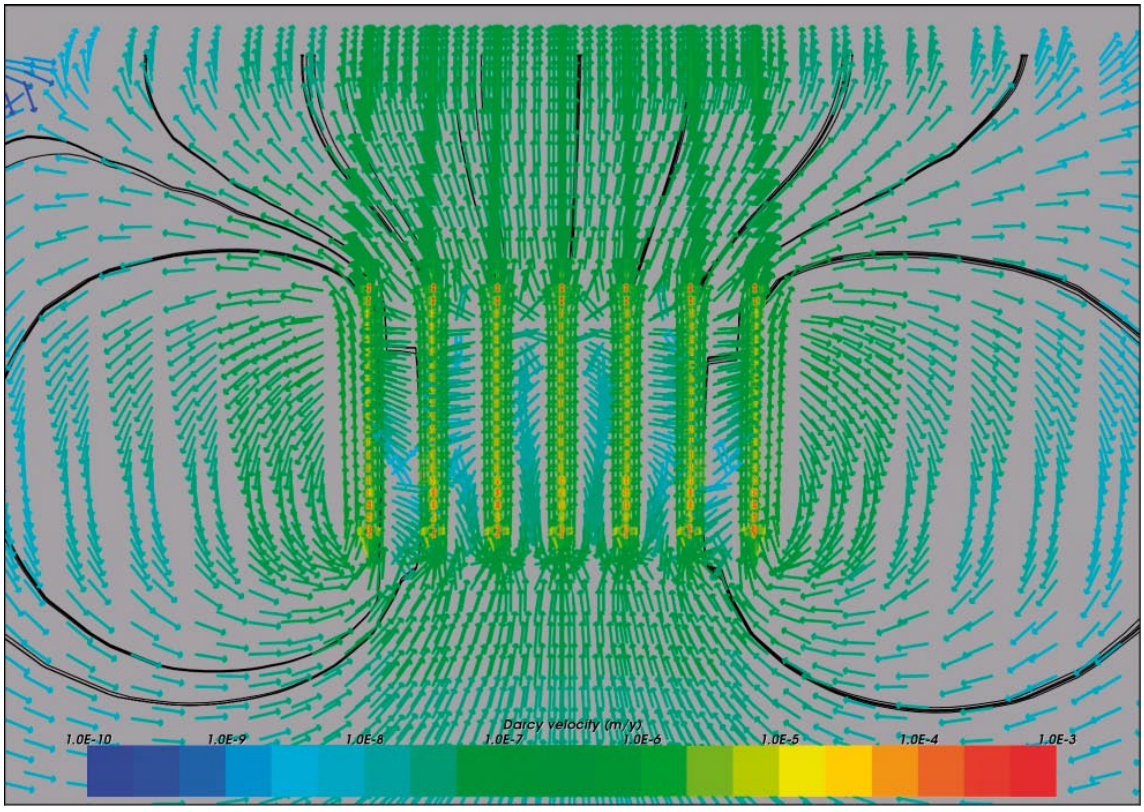

Figure 3-28. *Case 10. Close-up view of a vertical section showing Darcy velocity vectors. Flow paths are superimposed for illustration. Time = 100 years.*

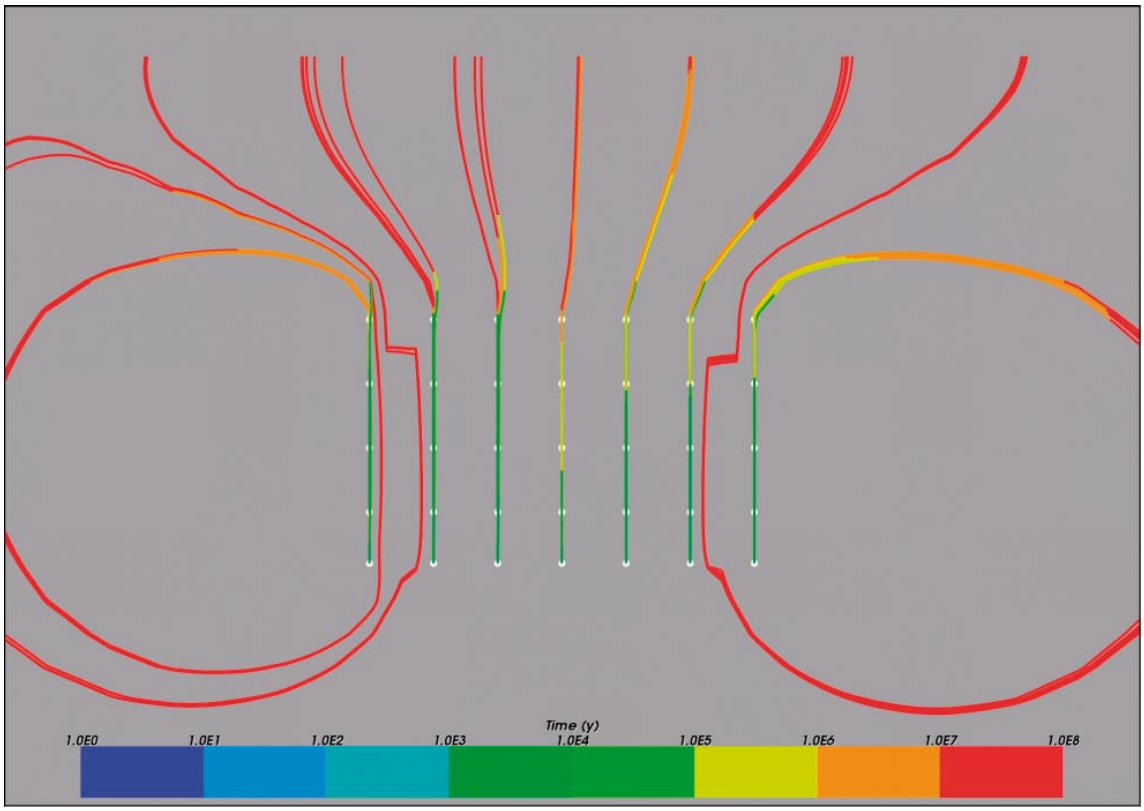

Figure 3-29. *Case 10. Vertical section showing flow paths coloured by travel time along the paths. Particle release time = 100 years.*

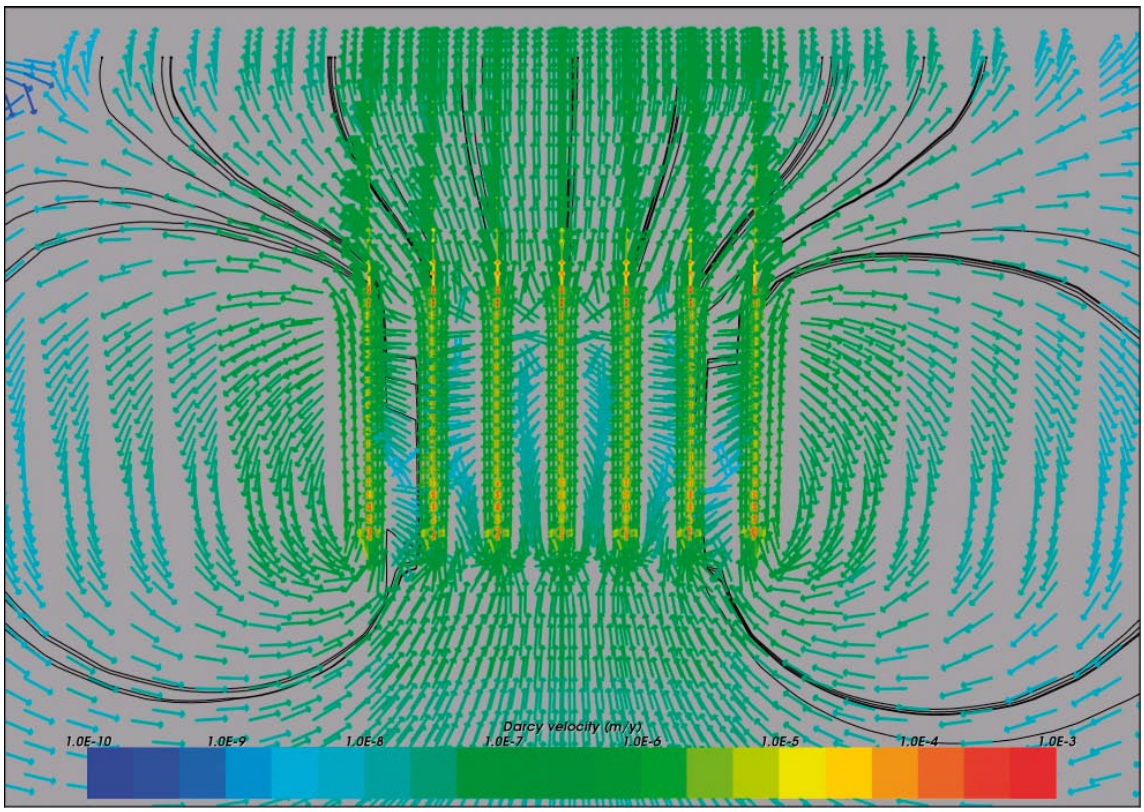

Figure 3-30. *Case 11. Close-up view of a vertical section showing Darcy velocity vectors. Flow paths are superimposed for illustration. Time = 100 years.*

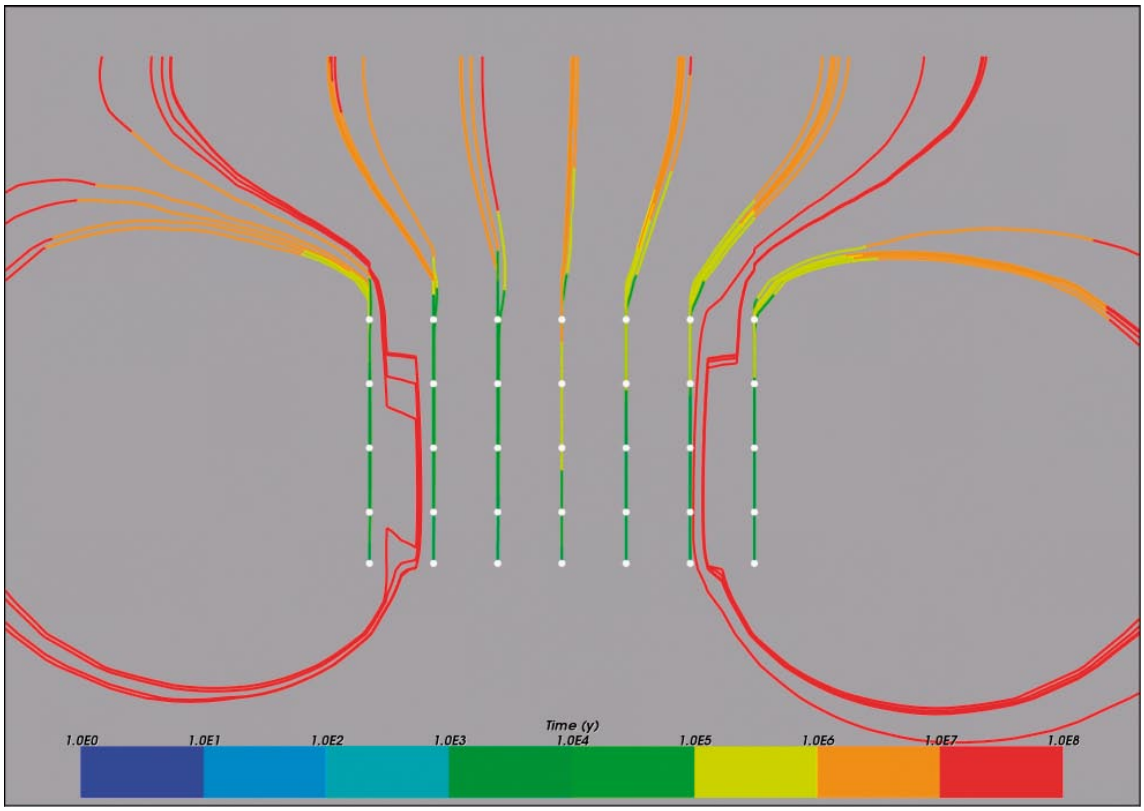

Figure 3-31. *Case 11. Vertical section showing flow paths coloured by travel time along the paths. Particle release time = 100 years.*

3.4.3 Case 12. Increased borehole permeability at Z = 0 to –2,000 m

Also this variant is based on the properties of Case 3. However, in this third variant of increased borehole permeability, the physical properties of the concrete, asphalt and bentonite for the borehole sections from the surface level down to Z = –2,000 m are changed to the buffer and DZ properties. This increases the permeability 20–100 times in the borehole section above the canisters all the way up to the surface of the model compared to Case 3.

The results are presented in Figure 3-32 and Figure 3-33. The changes compared to Case 11 are very small, so adding the extra permeability to the top 500 m of the boreholes does not affect the results. In fact, the travel times were even slightly shorter in Case 11 than in this case.

3.4.4 Case 13. Increased borehole permeability

In the fourth variant including increased borehole permeability, the permeability of all materials in the borehole assigned a value corresponding to 10 times the original value of the buffer. This means that the concrete, asphalt, bentonite, buffer and DZ in the boreholes all have the same physical properties from the surface level down to Z = –4,000 m corresponding to the bottom of the boreholes. Apart from these changes, this variant is based on the properties of Case 3.

Figure 3-34–Figure 3-36 present the results for Case 13 and as expected, we can now see some changes in the Darcy velocities inside the boreholes. The increased flows inside the repository affect the flow outside the repository as well. The increased velocities are also reflected in the calculated range of hypothetical travel times where we can see a slight decrease.

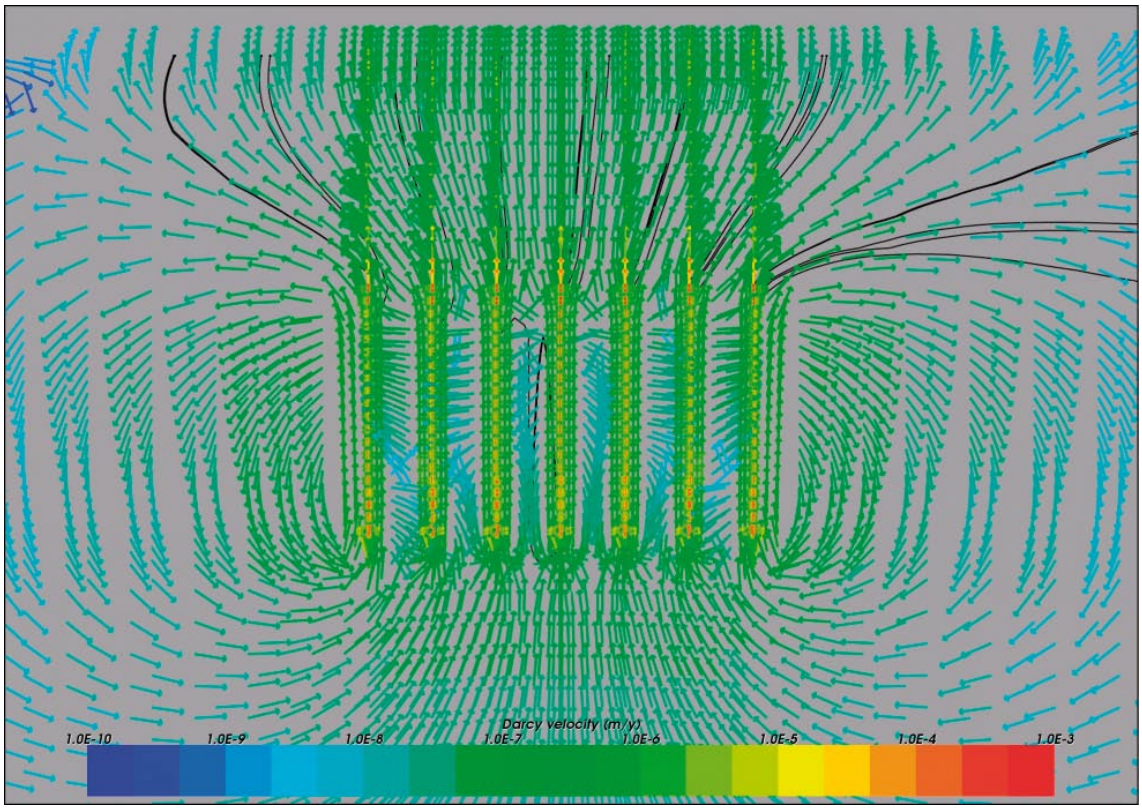

Figure 3-32. *Case 12. Close-up view of a vertical section showing Darcy velocity vectors. Flow paths are superimposed for illustration. Time = 100 years.*

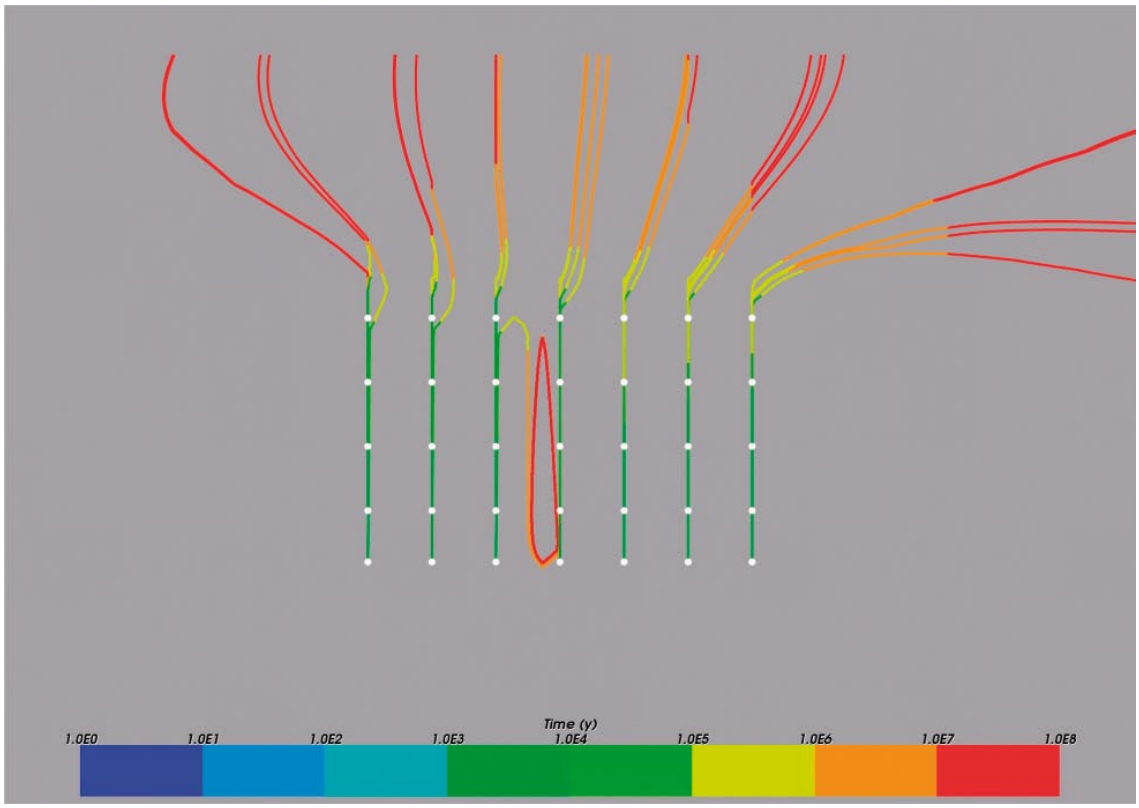

Figure 3-33. *Case 12. Vertical section showing flow paths coloured by travel time along the paths. Particle release time = 100 years.*

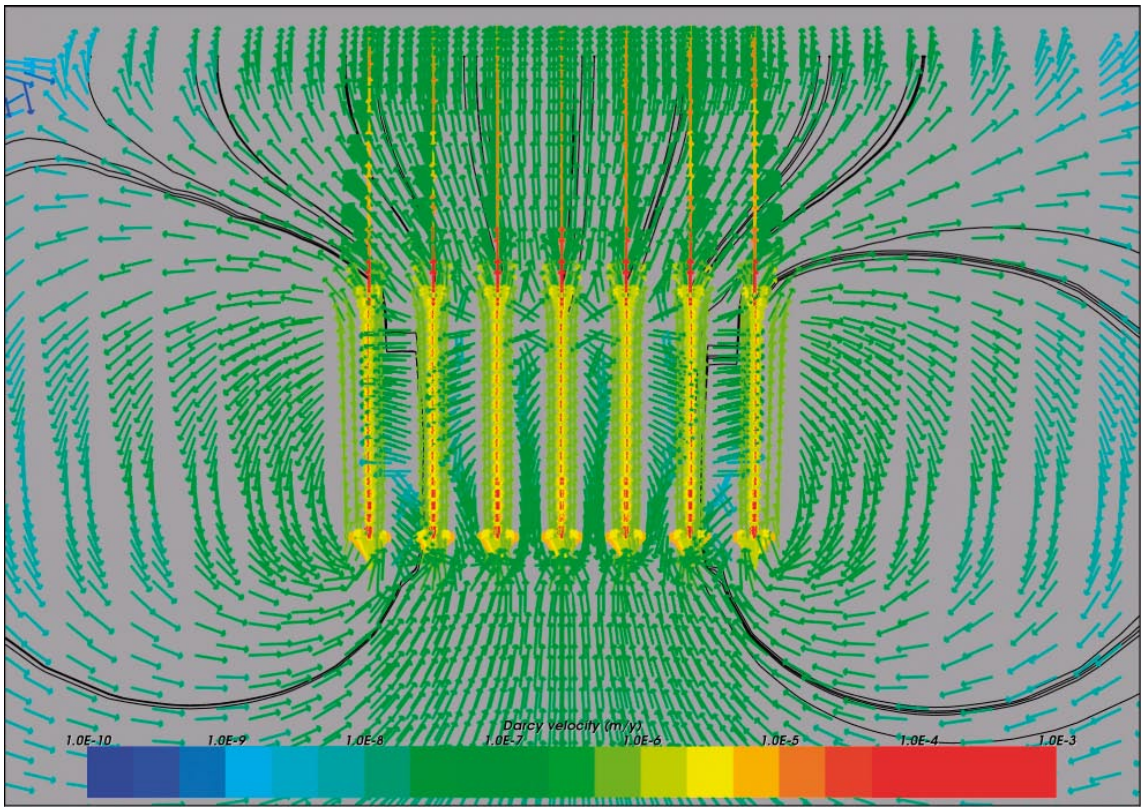

Figure 3-34. *Case 13. Close-up view of a vertical section showing Darcy velocity vectors. Flow paths are superimposed for illustration. Time = 100 years.*

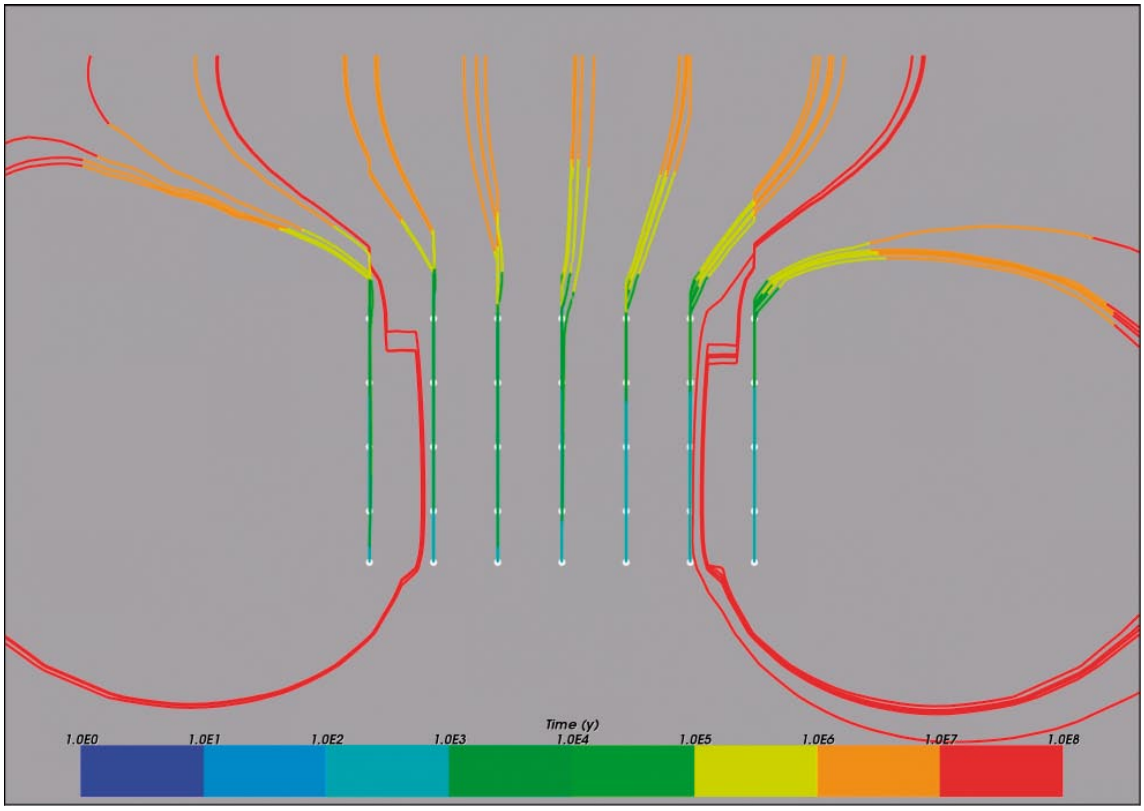

Figure 3-35. *Case 13. Vertical section showing flow paths coloured by travel time along the paths. Particle release time = 100 years.*

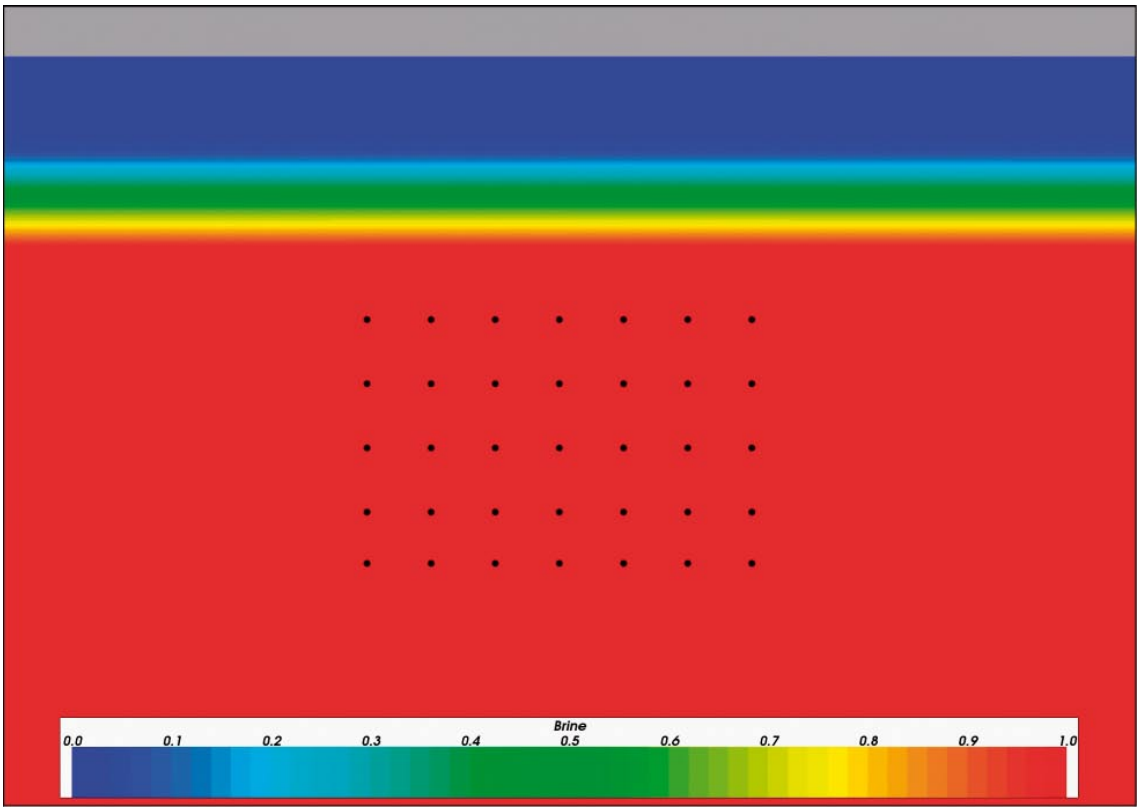

Figure 3-36. *Case 13. Vertical section showing the distribution of Brine. Black points indicate the release positions for the particles. Time = 100 years.*

In Figure 3-36, the distribution of Brine on a vertical section through the middle of the model is shown after 100 years of simulation. It is clear that the saline water has not moved at all. Obviously, the flow velocities are far too small to be able to move to saline water from the depths of the model. This means that the repository will reside well below the interface between the freshwater higher up in the model and the dense saline water deeper down in the rock.

3.5 Sensitivity to heat and salt IC

This section explores the models sensitivity to heat generated within the canisters and to the presence of saline groundwater at depth. In addition, the effects of initially filling the boreholes with freshwater is studied. Because the disposal slurry is anticipated to consist of bentonite and fresh water, the latter is a most likely scenario.

3.5.1 Case 14. No heat source in boreholes

The model is based on Case 3, with a 1% head gradient on the top surface and homogeneous rock permeability. This variant explores the effects off removing the heat source from the boreholes. This is accomplished by simply setting the heat generation to zero and keeping all the other physical parameters the same as before. It should be noted that the geothermal gradient is still present and taken account for in the model.

The effect of removing the heat source on the groundwater flow pattern is significant, see Figure 3-37 and Figure 3-38. There are no longer any convection cells caused by by buoyancy. Consequently, the flow is effectively horizontal following the path (downward flow in the west and upward flow in the east) expected from the applied head gradient. The higher permeability of the boreholes reinforces the flow along the holes and they act as conductors sending groundwater deep down into the model where the flows are enhanced in a downward direction in the western part of the repository and upward in the eastern part.

The highest Darcy velocities are found at the bottom of the boreholes where water is being flushed out from the boreholes into the rock. The Darcy velocity is 3–4 orders of magnitude lower in this variant compared to the variants including the heat source. This fact, in combination with the horizontal flow pattern, results in calculated hypothetical travel times that are generally longer than 10^8 years.

3.5.2 Case 15. Freshwater IC with single fracture zone (slope –60°)

The model is based on Case 5 and uses a 1% head gradient applied as a top boundary condition, increased permeability in the top layers and one fracture zone, sloping –60°. This variant explores the effects of replacing the stabilising brine in the model and starting the simulation with pure freshwater throughout the model domain. Salt is only allowed to diffuse into the model through the bottom boundary.

Comparing the results to the corresponding variant including brine, Case 5, it is evident that the flow pattern is not much affected by the absence of brine in the model, see Figure 3-39 and Figure 3-40. The Darcy velocities increase slightly which can be seen in the travel times for the released particles. The changes are however, minor and the range stays roughly the same as in Case 5.

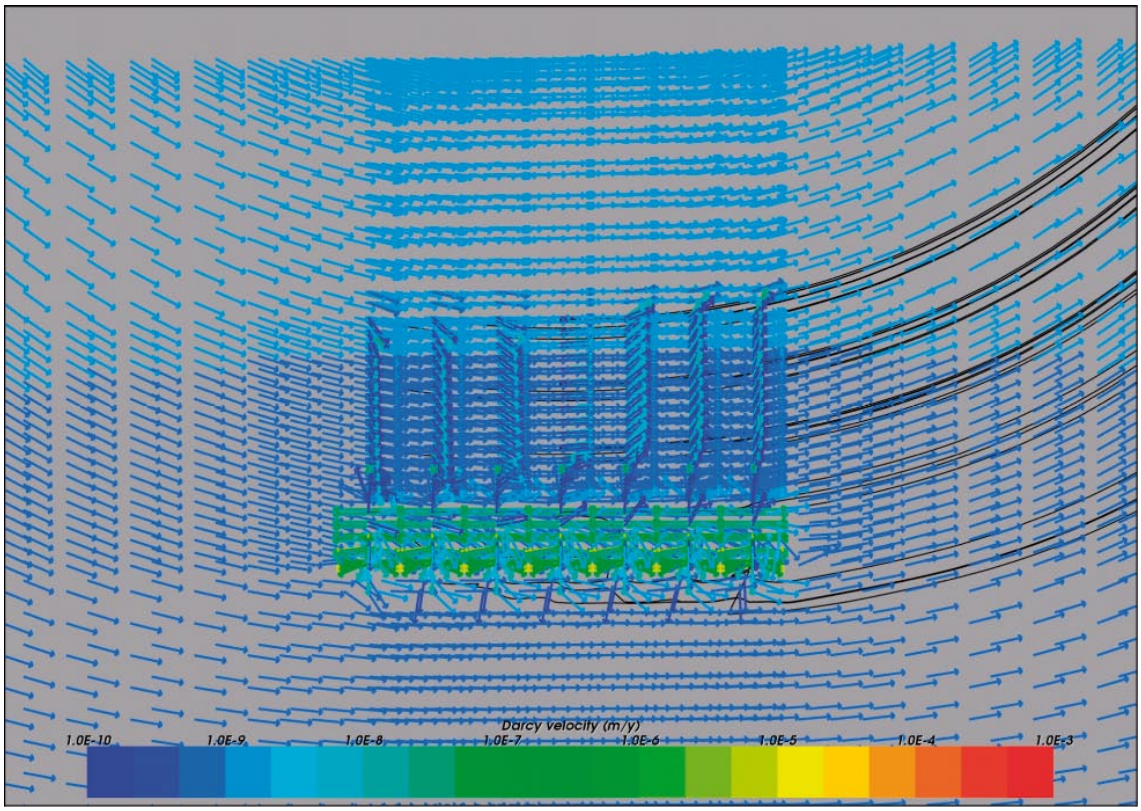

Figure 3-37. *Case 14. Close-up view of a vertical section showing Darcy velocity vectors. Flow paths are superimposed for illustration. Time = 100 years.*

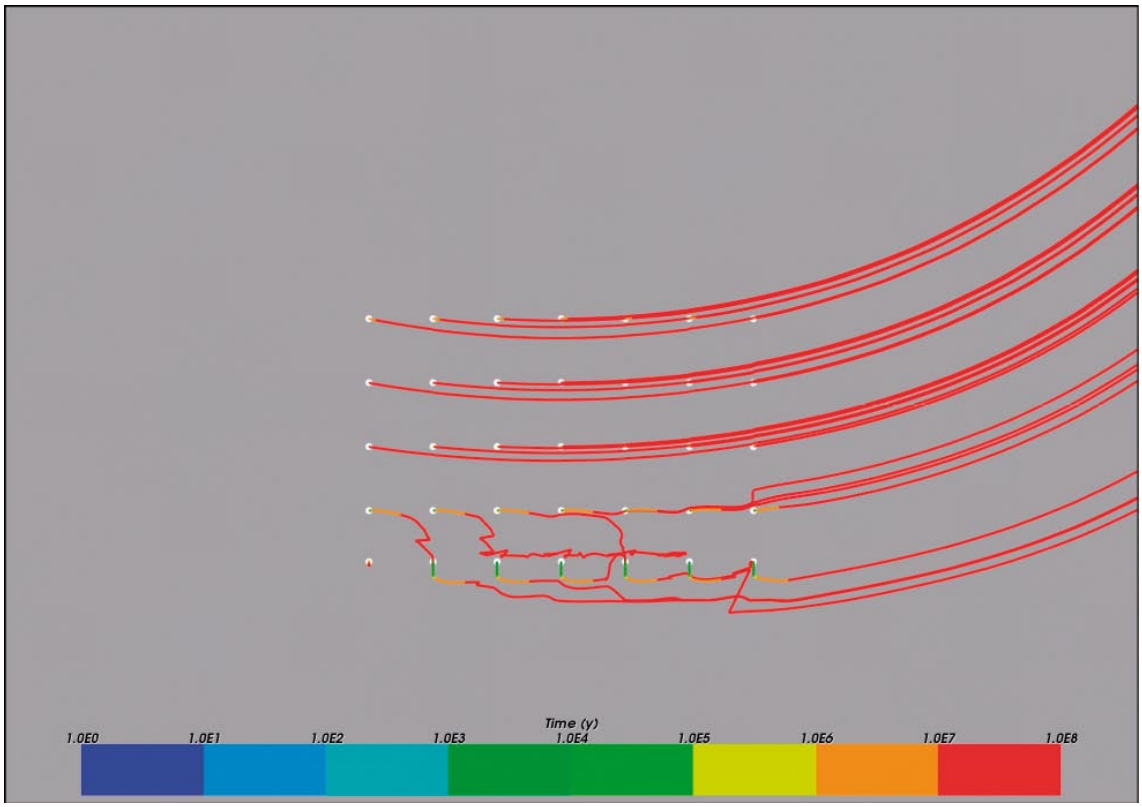

Figure 3-38. *Case 14. Vertical section showing flow paths coloured by travel time along the paths. Particle release time = 100 years.*

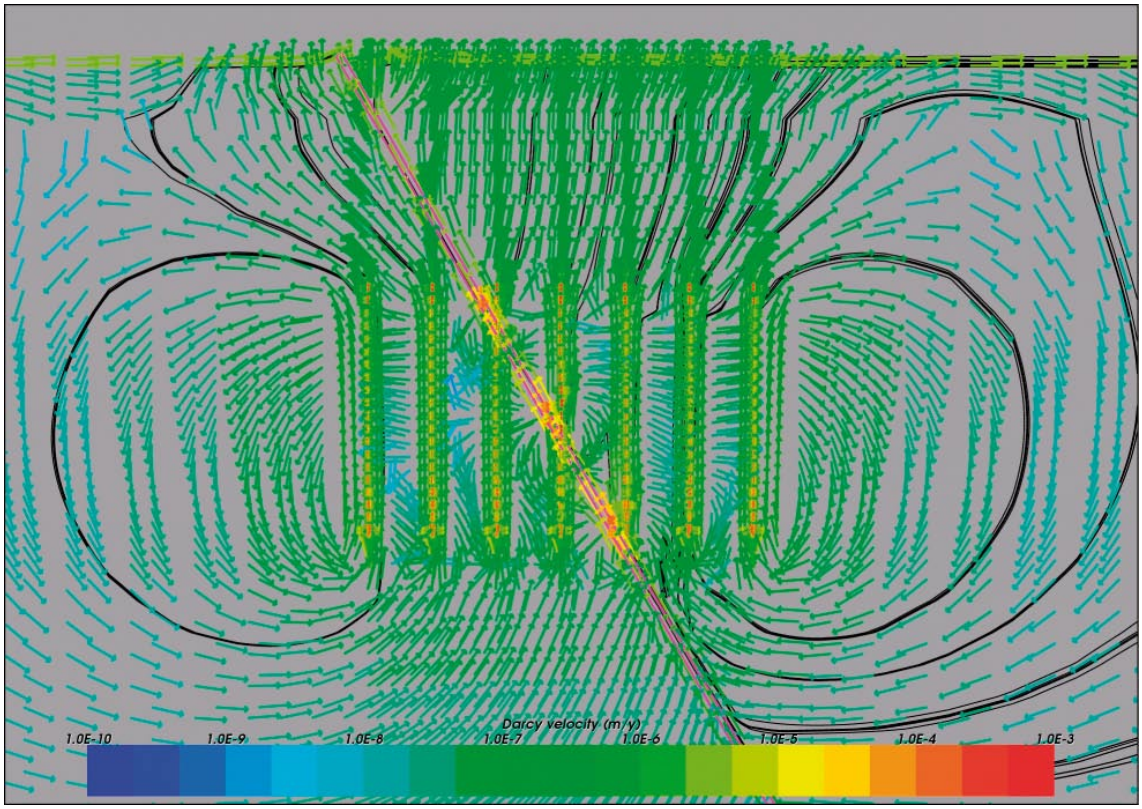

Figure 3-39. *Case 15. Close-up view of a vertical section showing Darcy velocity vectors. Flow paths are superimposed for illustration. Time = 100 years.*

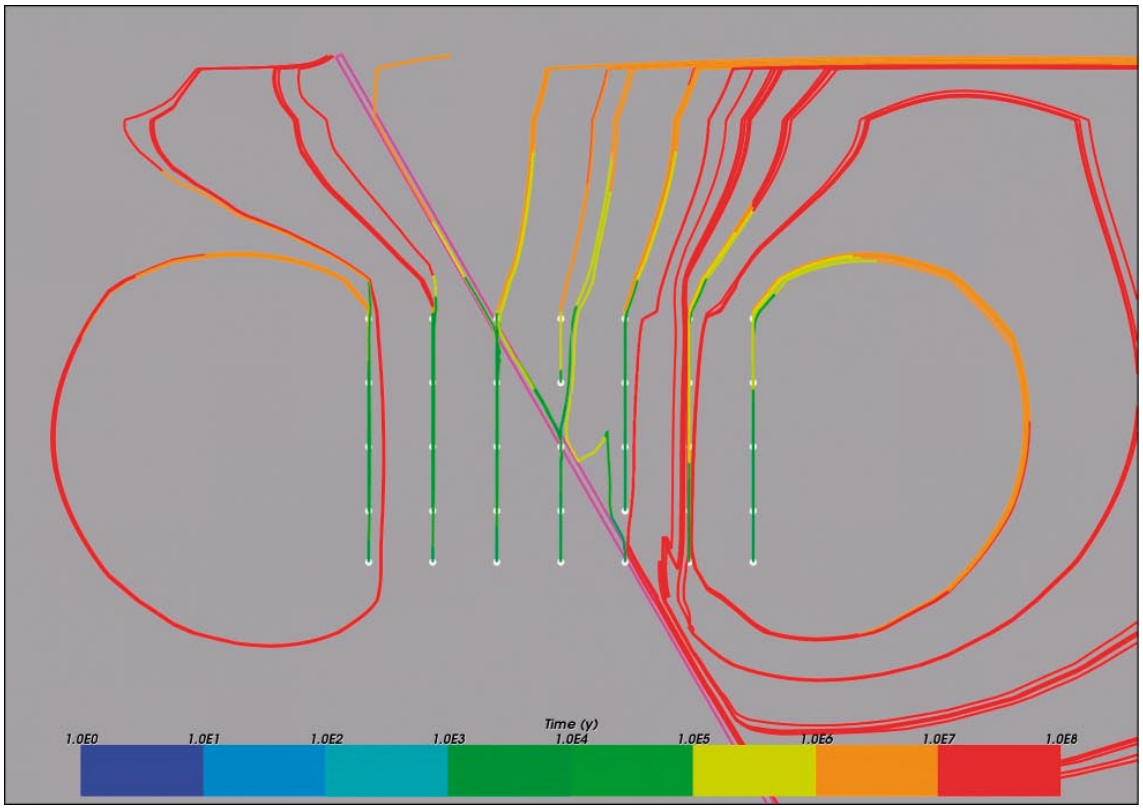

Figure 3-40. *Case 15. Vertical section showing flow paths coloured by travel time along the paths. Particle release time = 100 years.*

3.5.3 Case 16. Freshwater IC with fracture zone (slope –60°) and no heat generation in boreholes

This variant is based on Case 15 but with the heat source removed from the boreholes. Thus, the model is uses a 1% head gradient applied as a top boundary condition, increased permeability in the top layers, freshwater initial condition and one fracture zone, sloping –60°. Again, it should be noted that the geothermal gradient is still present and accounted for in the model.

The effect of removing the heat source on the groundwater flow pattern is significant, see Figure 3-41 and Figure 3-42. There are no longer any convection cells caused by buoyancy. Consequently, the flow is effectively horizontal following the path (downward flow in the west and upward flow in the east) expected from the applied head gradient. The included fracture zone now works as a conductor sending groundwater deep down into the model. The same effect, although smaller, can be seen in the boreholes where the flows are enhanced in a downward direction in the western part of the repository and upward in the eastern part. The highest Darcy velocities are found at the bottom of the boreholes where water is flushed out from the boreholes into the rock. The Darcy velocity is 3–4 orders of magnitude lower in this variant compared to the variants where the heat source was included. This fact in combination with the horizontal flow pattern results in travel times that are generally greater than 10^8 years.

3.5.4 Case 17. Freshwater filled boreholes

The following variants in this section investigate the effects of initially filling the boreholes with fresh water. Given the suggested methods for emplacing the canister and the buffer material in the boreholes this is actually a likely scenario when building the repository.

This variant is based on Case 3, with a 1% head gradient on the top surface and homogeneous rock permeability. The difference is that in the present variant the boreholes initially are filled with freshwater to a radius of 2.0 m from 4,000 m depth all the way up to the surface.

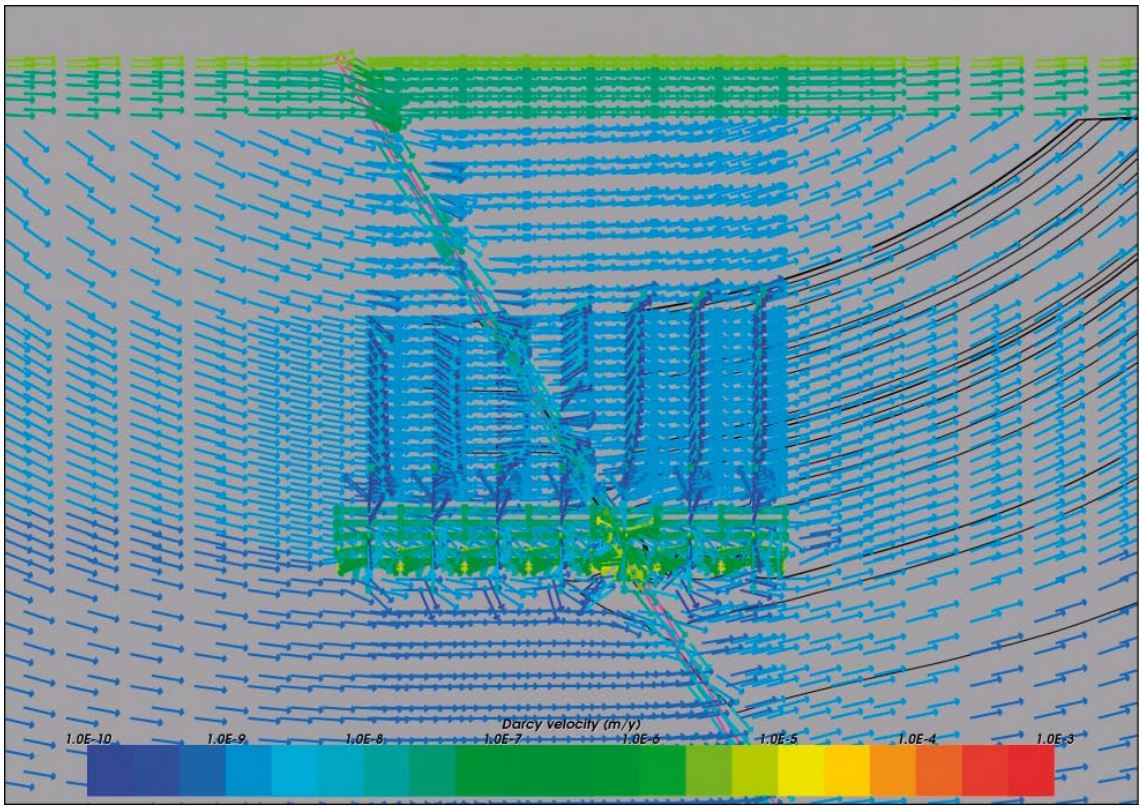

Figure 3-41. *Case 16. Close-up view of a vertical section showing Darcy velocity vectors. Flow paths are superimposed for illustration. Time = 100 years.*

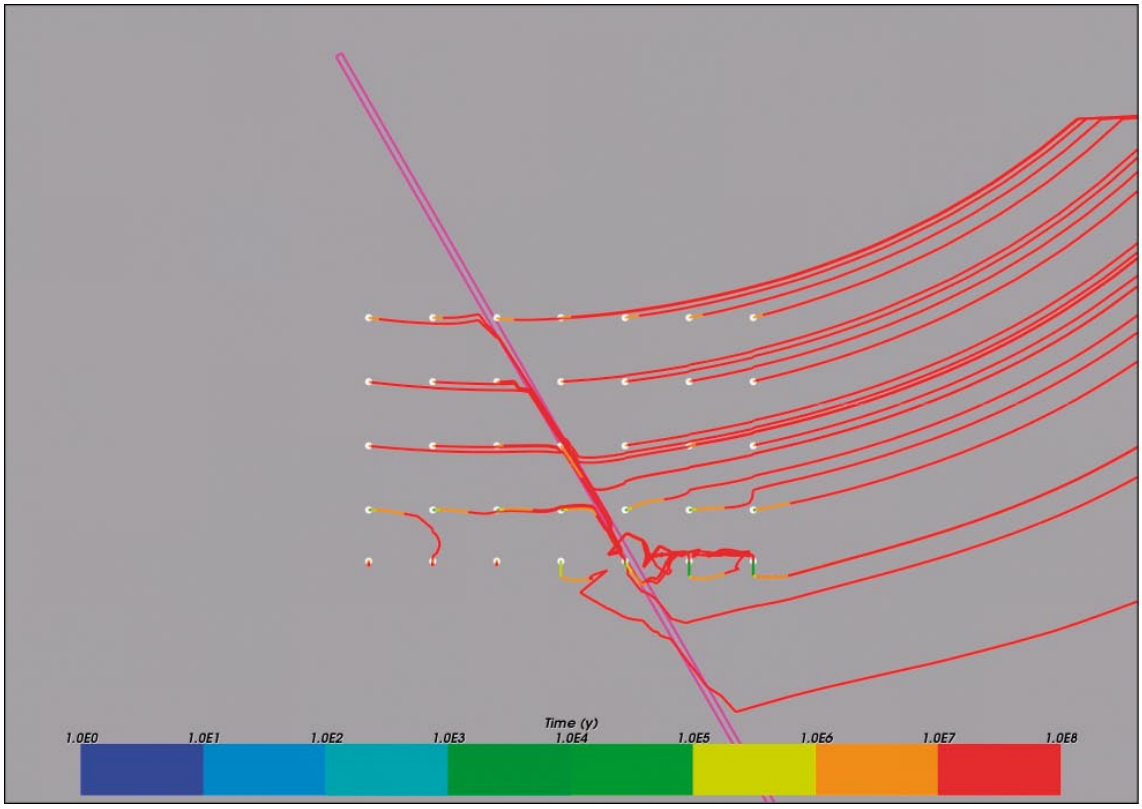

Figure 3-42. *Case 16. Vertical section showing flow paths coloured by travel time along the paths. Particle release time = 100 years.*

The results are presented in Figure 3-43–Figure 3-46 for 10 and 100 years of simulation time respectively. The effect from having the freshwater initially in the boreholes is not very pronounced. The expected effect of rapid flushing of the lighter freshwater is absent and the flow field remains mainly unchanged. The travel times do not differ much from the previous variants and stay within the same range as before.

3.5.5 Case 18. Freshwater filled boreholes with increased permeability

This variant is based on Case 17 with freshwater filled boreholes but with an increased permeability. The permeability of all materials in the borehole is assigned a value that is 10 times the original value of the buffer. This means that the concrete, asphalt, bentonite, buffer and DZ in the boreholes all have the same physical properties from the surface level down to Z = –4,000 m, corresponding to the bottom of the boreholes.

Figure 3-47–Figure 3-50 show the results for Case 18 for 10 and 100 years of simulation time respectively. Compared to the results from Case 17, the effects on Darcy velocity inside the boreholes is much more pronounced in the present variant. The flow direction inside the boreholes is more vertical as one would expect from the changes made to the model. This is also reflected in the calculated hypothetical travel times for the released particles where most of the particles now are found in the range 10^5–10^6 years.

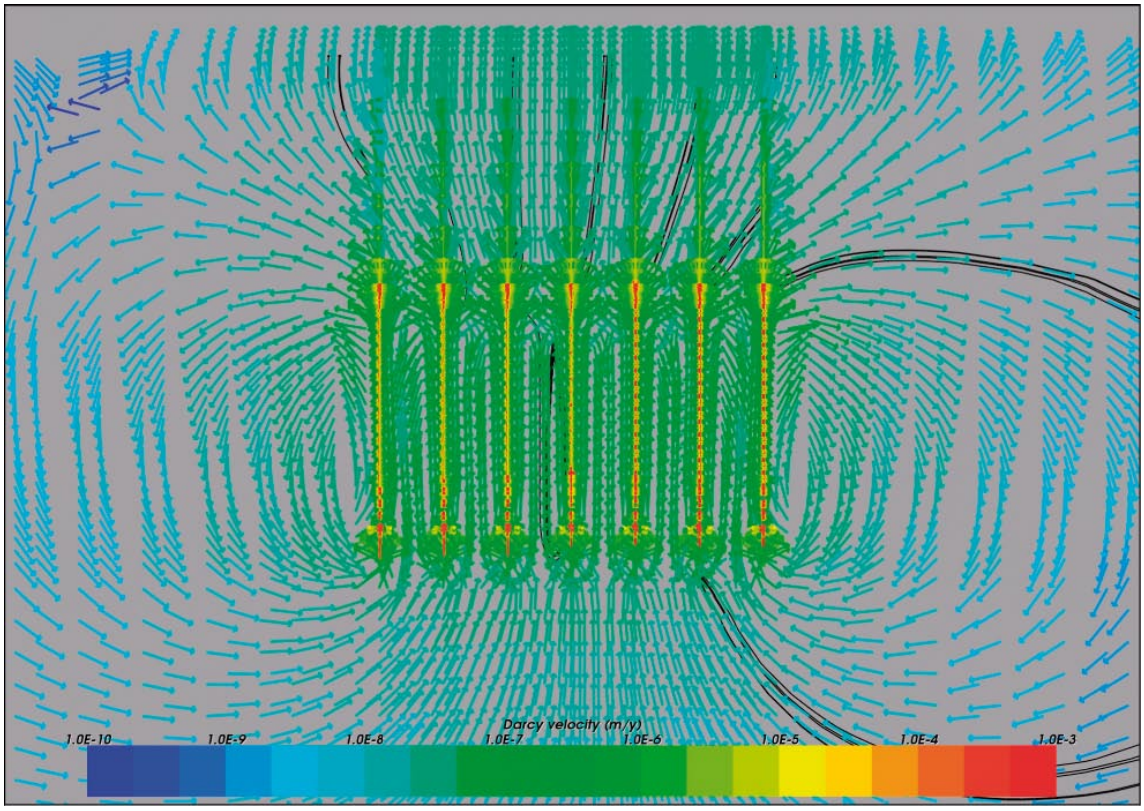

Figure 3-43. *Case 17. Close-up view of a vertical section showing Darcy velocity vectors. Flow paths are superimposed for illustration. Time = 10 years.*

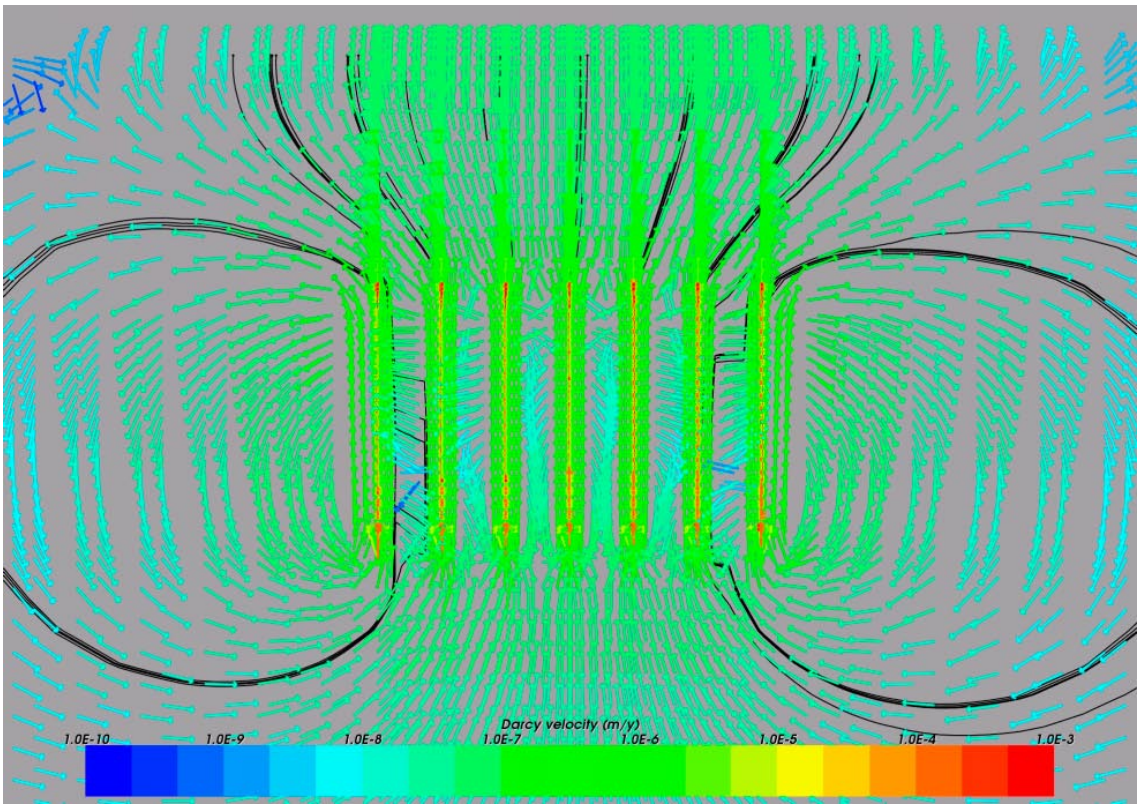

Figure 3-44. *Case 17. Close-up view of a vertical section showing Darcy velocity vectors. Flow paths are superimposed for illustration. Time = 100 years.*

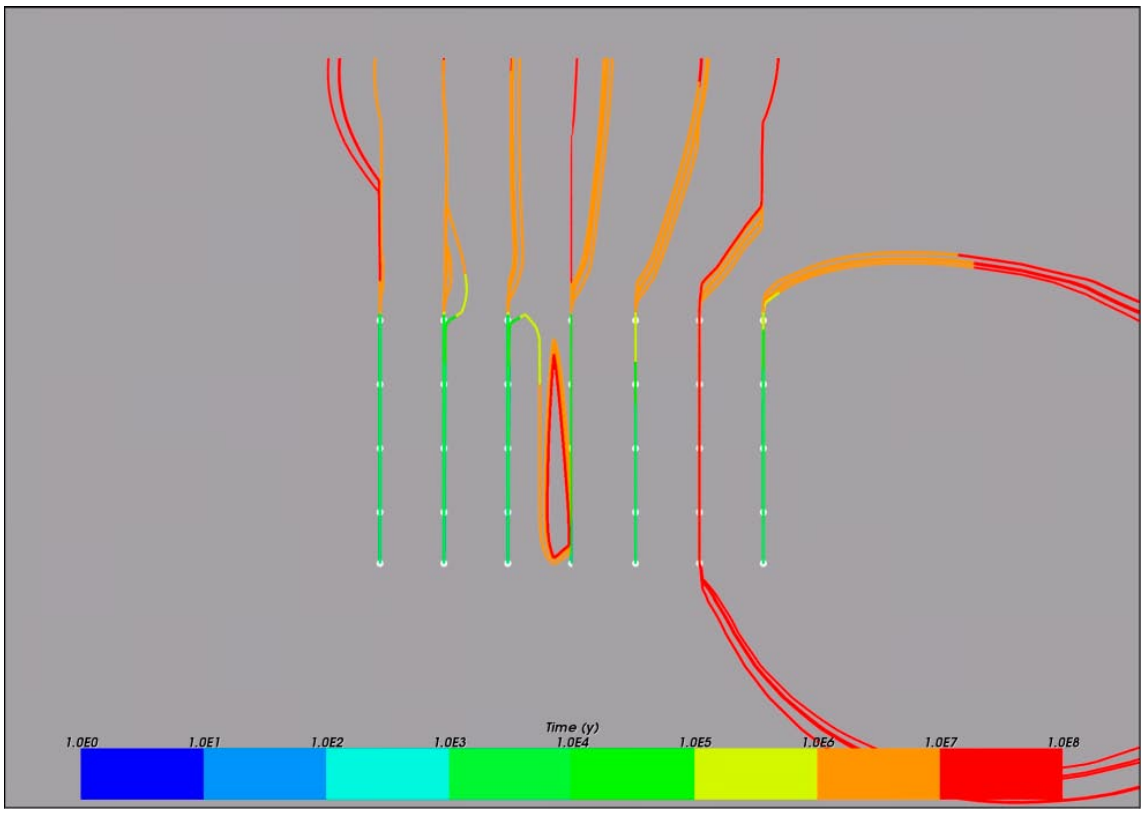

Figure 3-45. *Case 17. Vertical section showing flow paths coloured by travel time along the paths. Particle release time = 10 years.*

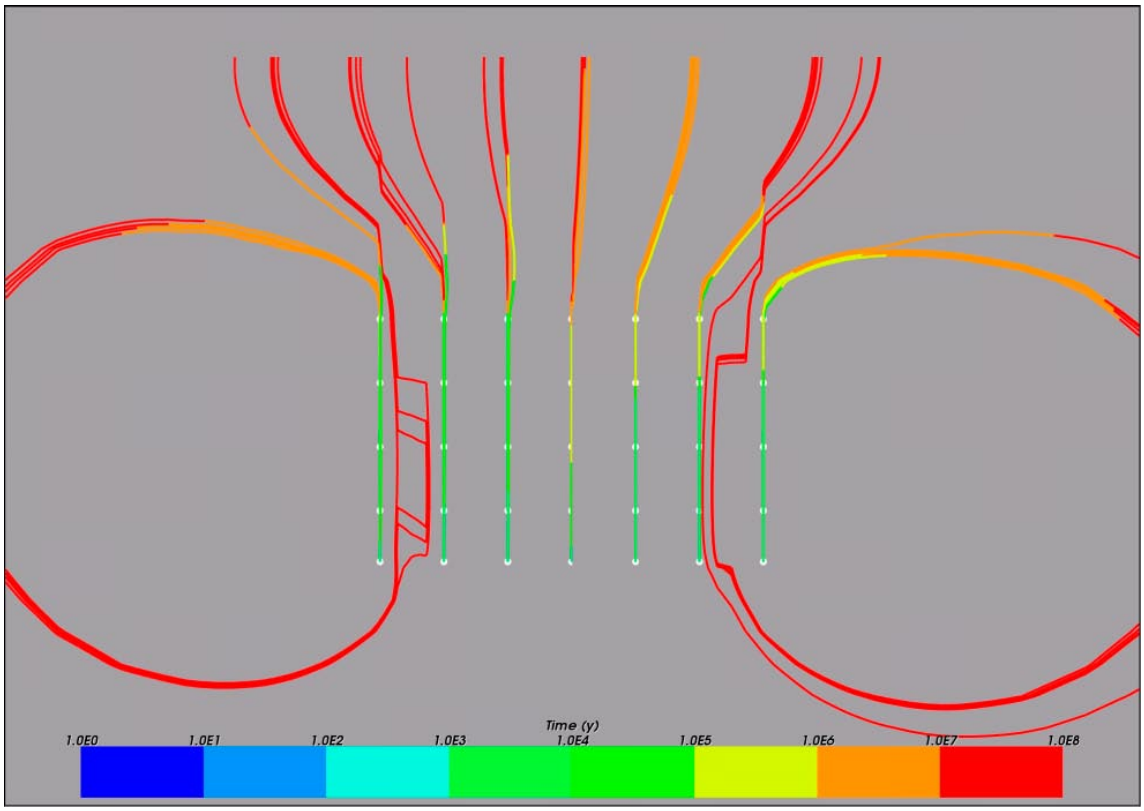

Figure 3-46. *Case 17. Vertical section showing flow paths coloured by travel time along the paths. Particle release time = 100 years.*

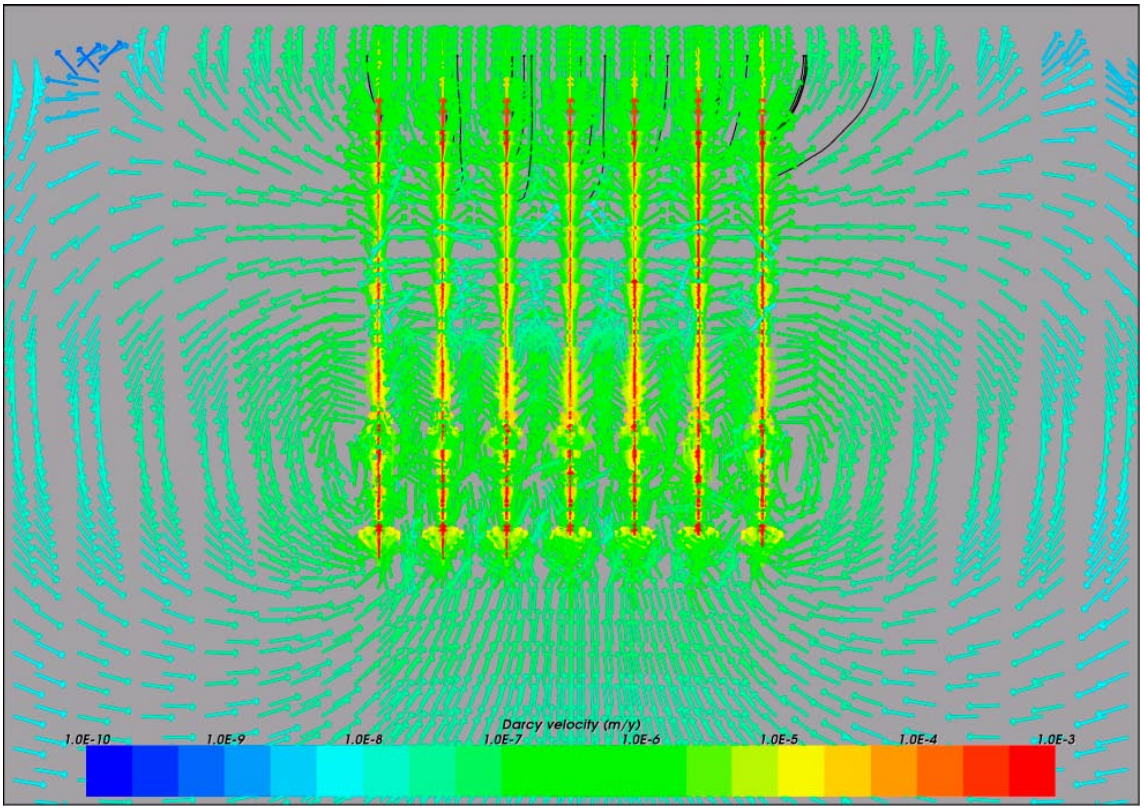

Figure 3-47. *Case 18. Close-up view of a vertical section showing Darcy velocity vectors. Flow paths are superimposed for illustration. Time = 10 years.*

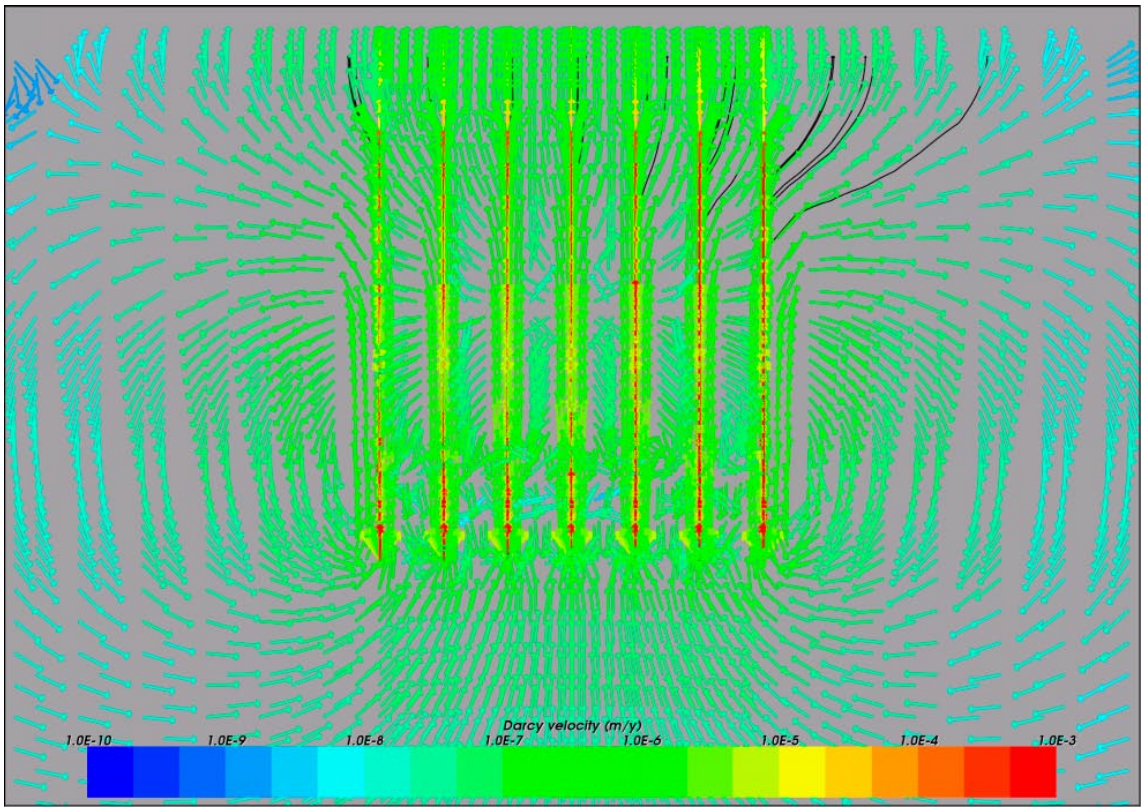

Figure 3-48. *Case 18. Close-up view of a vertical section showing Darcy velocity vectors. Flow paths are superimposed for illustration. Time = 100 years.*

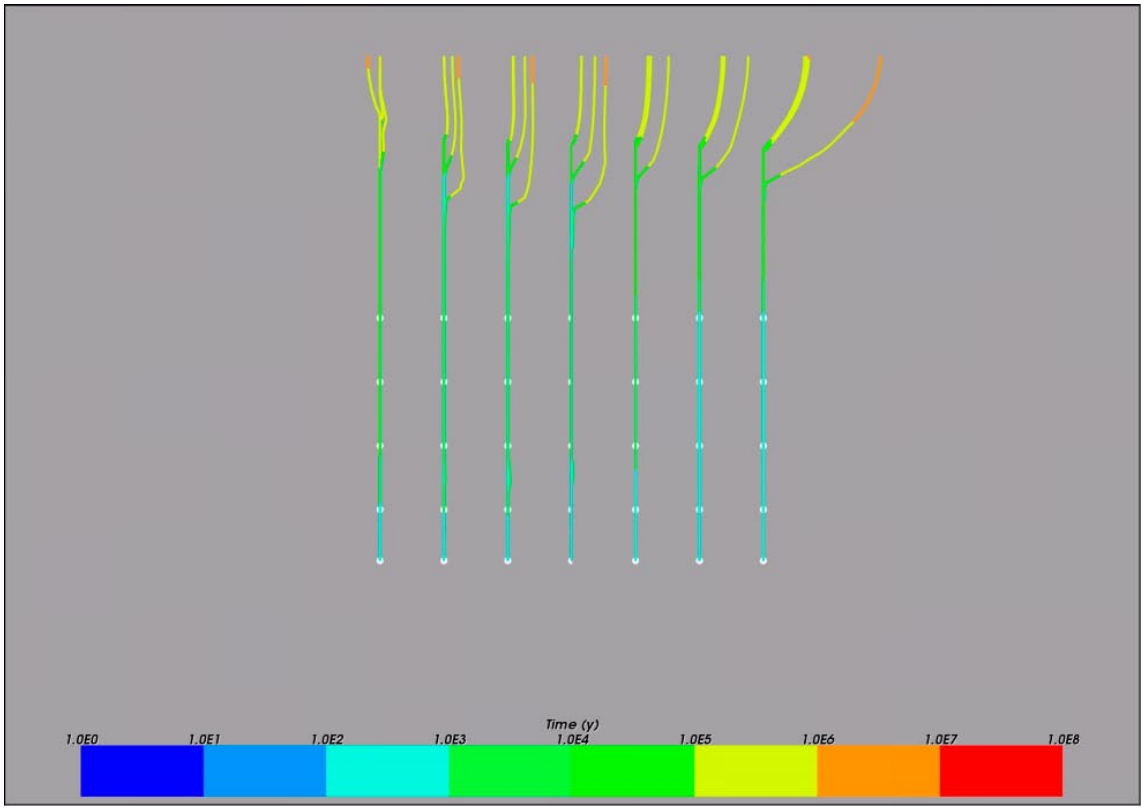

Figure 3-49. *Case 18. Vertical section showing flow paths coloured by travel time along the paths. Particle release time = 10 years.*

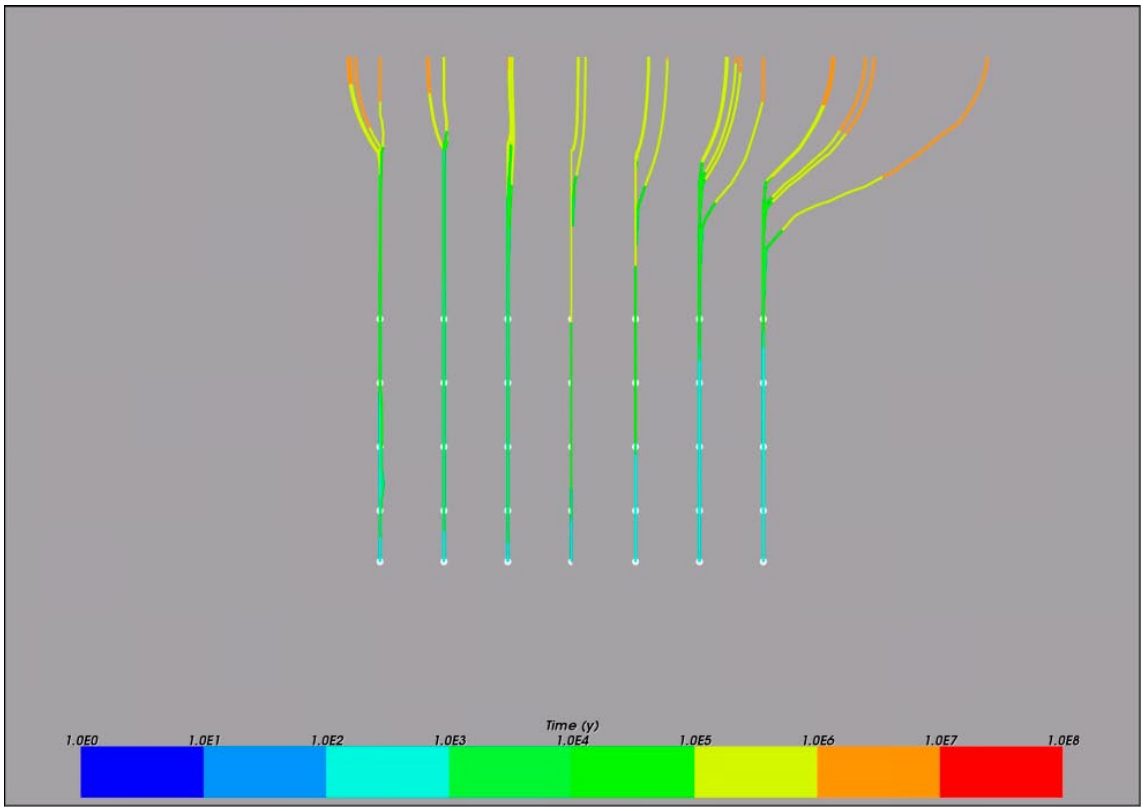

Figure 3-50. *Case 18. Vertical section showing flow paths coloured by travel time along the paths. Particle release time = 100 years.*

3.5.6 Case 19. Freshwater filled boreholes with connected regional fractures

In the present variant, based on Case 18, four connected fracture zones with a width of 100 m are included. The properties of the fractures are the same as for the boreholes, i.e. a permeability 10 times the original value of the buffer.

In Figure 3-51–Figure 3-54 the results for Case 19 are presented for 10 and 100 years of simulation time respectively. The effects on the flow field of including the fracture zones are significant. Darcy velocities in the intersections between the fracture zones and the boreholes have increased but the overall velocities do not differ much. Even if there are significant disturbances in the flows around the repository, the effect on the travel times for the released particles is reversed to the effect on the flow velocities. The explanation could be that the particle paths are no longer monotonously vertical as in Case 18 but rather complex and with many particles becoming stuck due to problems with the numerics.

3.5.7 Case 20. Freshwater filled boreholes and nearby rock

This variant is an extreme version of Case 17. Instead of having the freshwater in the boreholes to a radius of 2.0 m we here put freshwater in a rock volume surrounding the boreholes with a radius of 50.0 m from 4,000 m depth all the way up to the surface. The variant is based on Case 3, with a 1% head gradient on the top surface and homogeneous rock permeability.

In Figure 3-55–Figure 3-58 the results for Case 19 are presented for 10 and 100 years of simulation time. It is clear that the flow field and Darcy velocities are significantly affected by the large amount of freshwater initially present in the boreholes and the surrounding rock. The calculated hypothetical travel times are about one order of magnitude lower than for Case 17 and the effect is of almost the same order as when the permeabilities inside the boreholes were changed in Case 18.

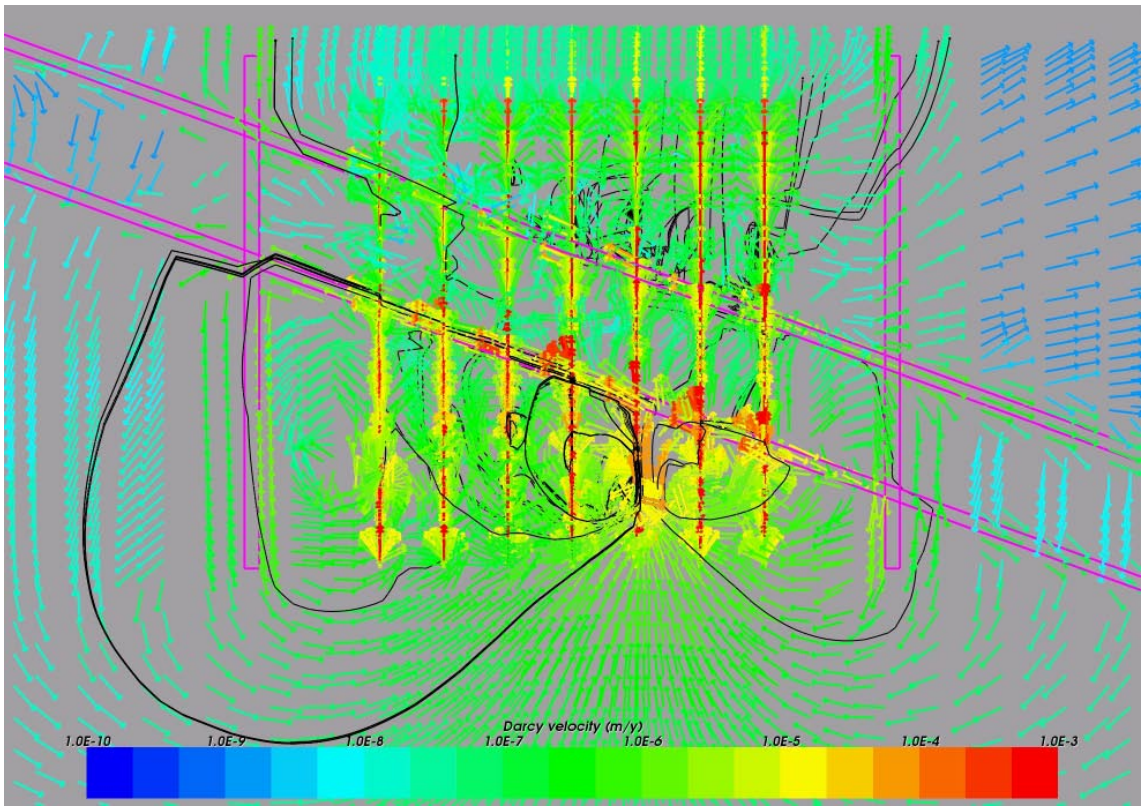

Figure 3-51. *Case 19. Close-up view of a vertical section showing Darcy velocity vectors. Flow paths are superimposed for illustration. Time = 10 years.*

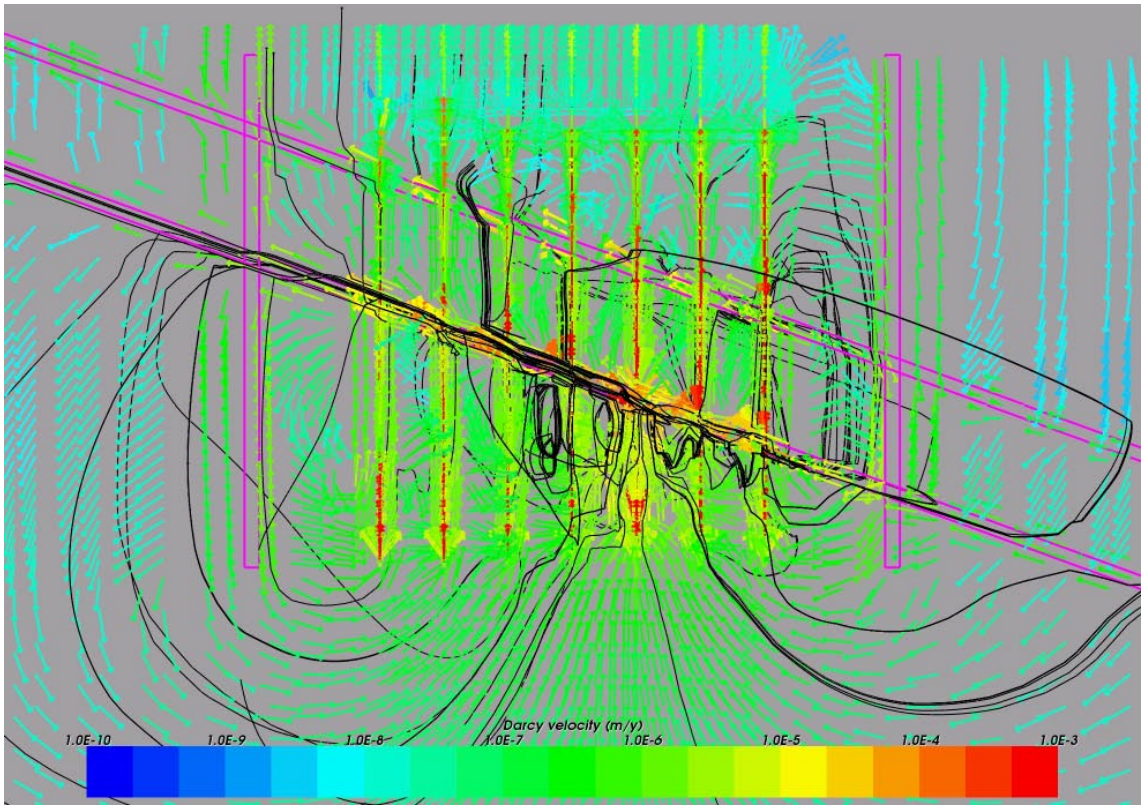

Figure 3-52. *Case 19. Close-up view of a vertical section showing Darcy velocity vectors. Flow paths are superimposed for illustration. Time = 100 years.*

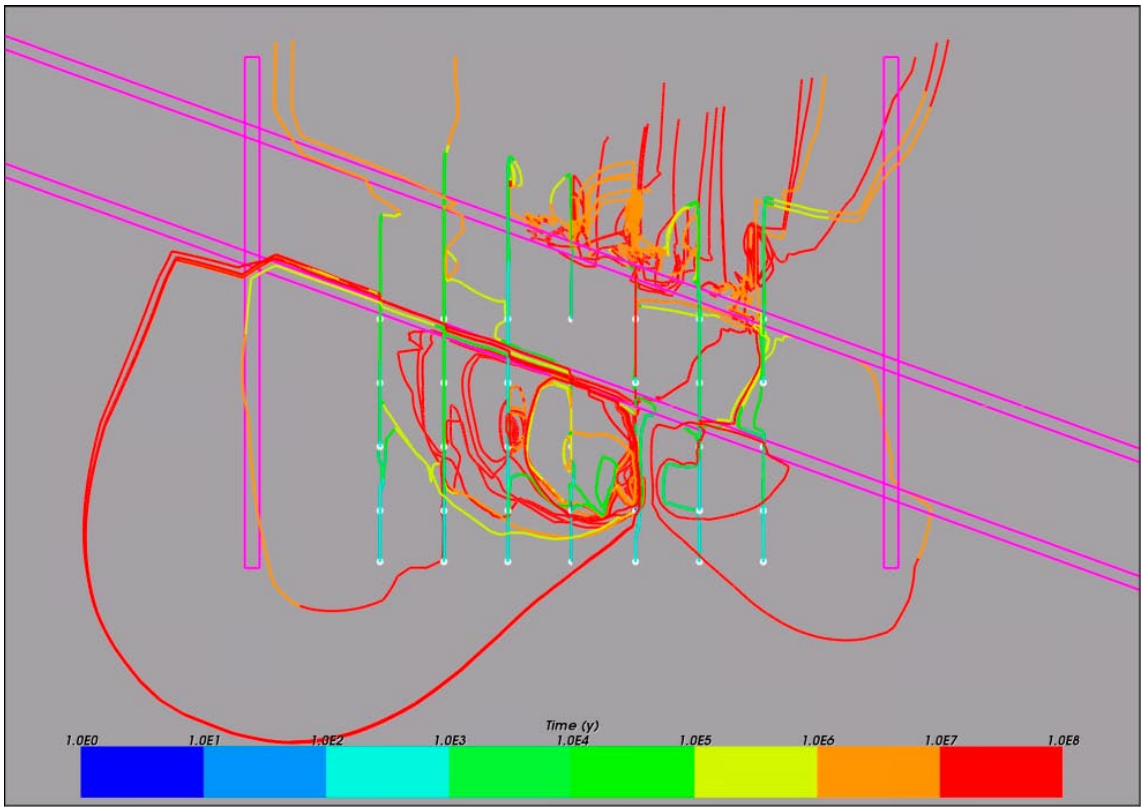

Figure 3-53. *Case 19. Vertical section showing flow paths coloured by travel time along the paths. Particle release time = 10 years.*

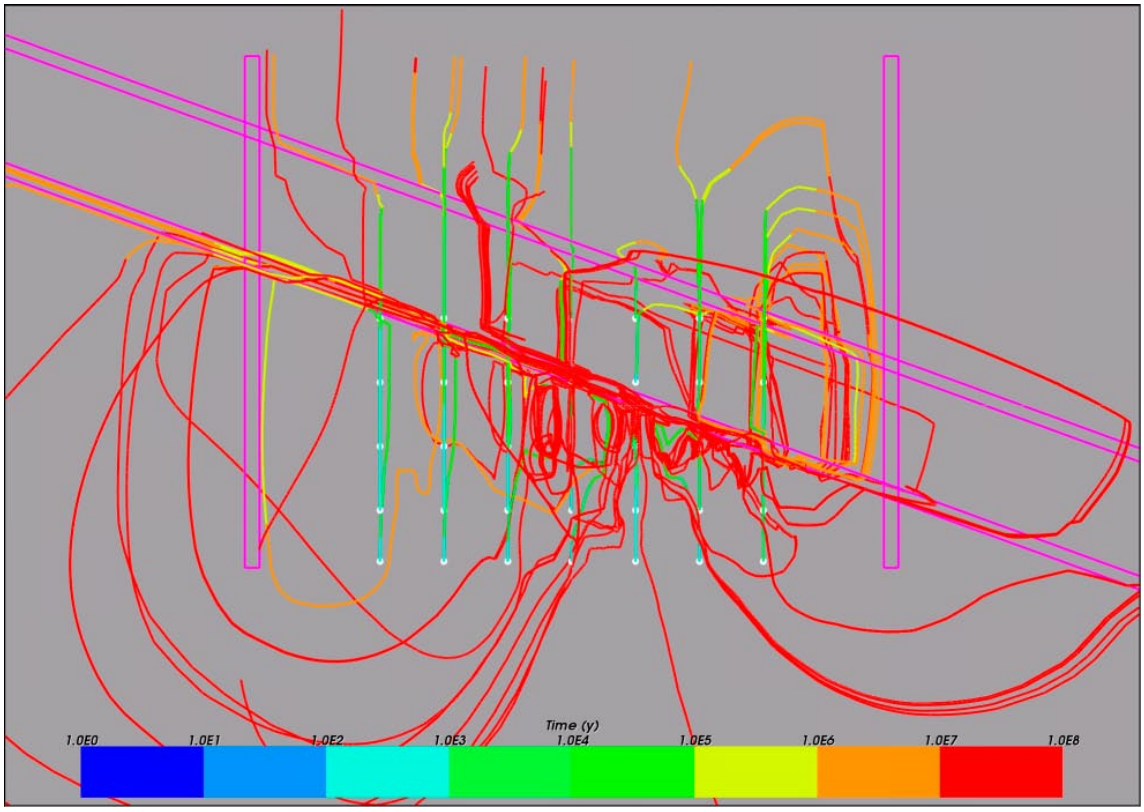

Figure 3-54. *Case 19. Vertical section showing flow paths coloured by travel time along the paths. Particle release time = 100 years.*

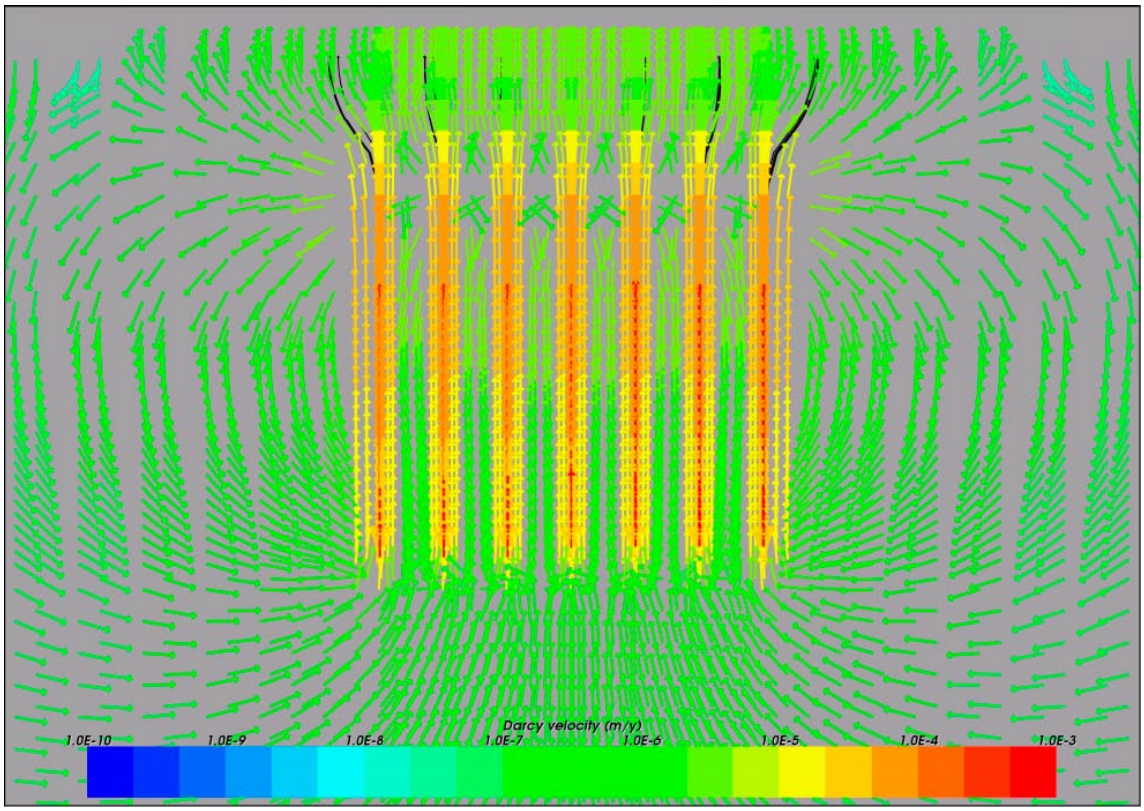

Figure 3-55. *Case 20. Close-up view of a vertical section showing Darcy velocity vectors. Flow paths are superimposed for illustration. Time = 10 years.*

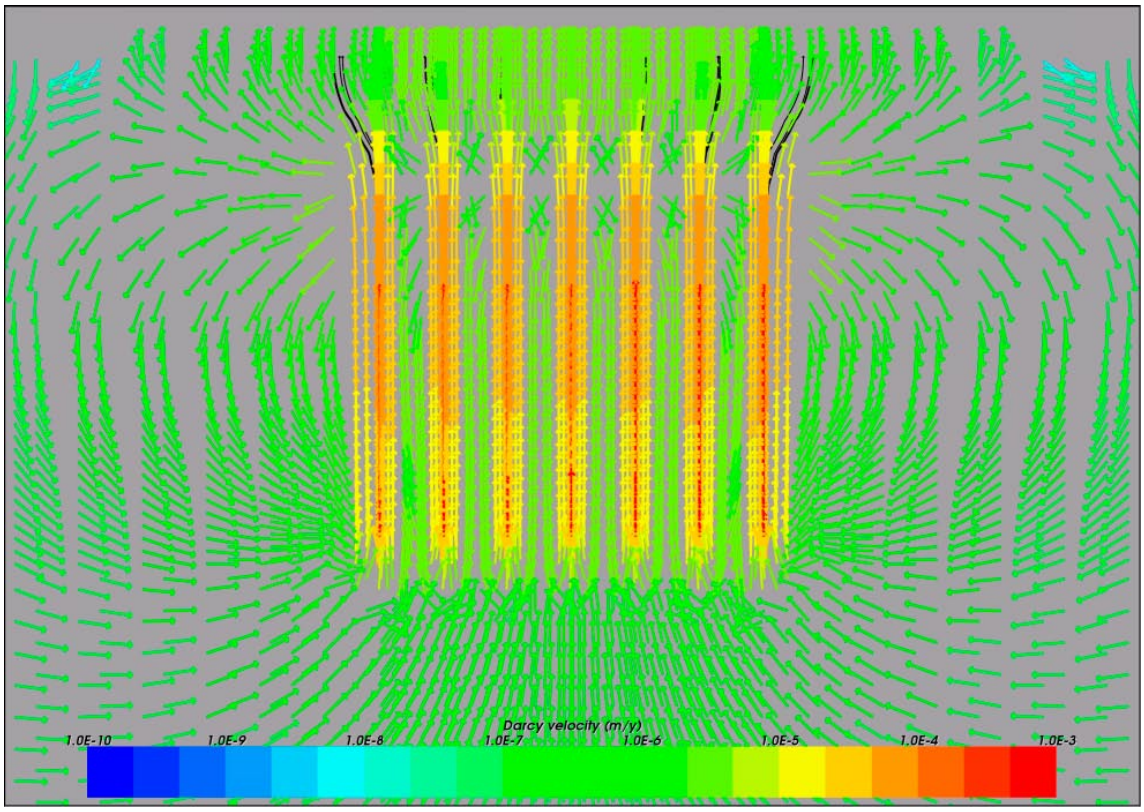

Figure 3-56. *Case 20. Close-up view of a vertical section showing Darcy velocity vectors. Flow paths are superimposed for illustration. Time = 100 years.*

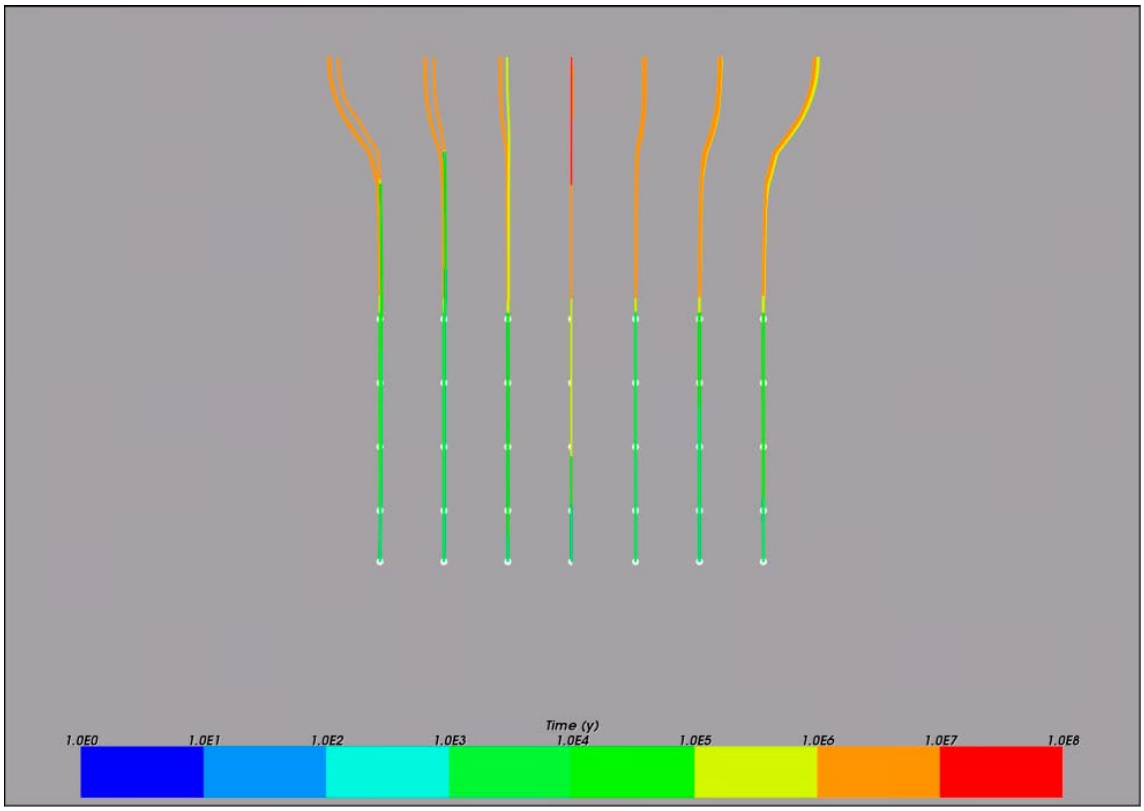

Figure 3-57. *Case 20. Vertical section showing flow paths coloured by travel time along the paths. Particle release time = 10 years.*

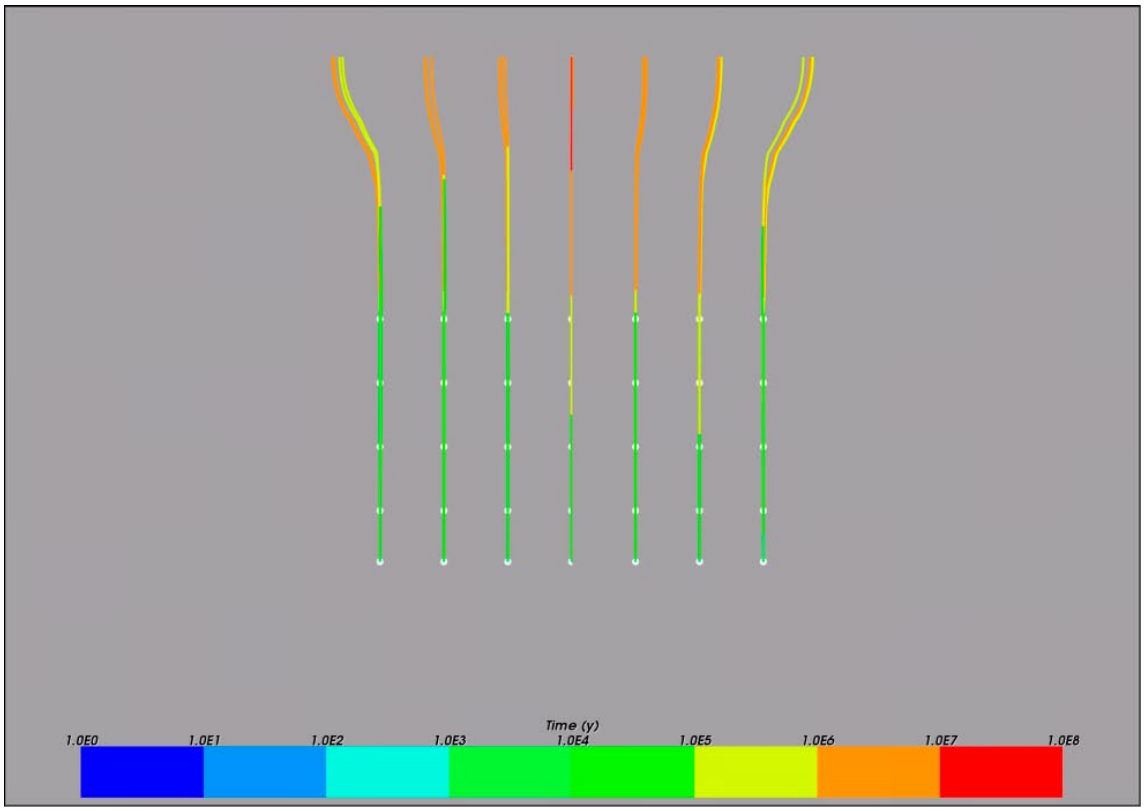

Figure 3-58. *Case 20. Vertical section showing flow paths coloured by travel time along the paths. Particle release time = 100 years.*

3.6 Sensitivity to borehole depth

In the present section, a couple of variants are presented that are aimed to study the effects of placing the canisters higher up in the rock. In the original concept the boreholes are drilled down to 4,000 m depth and the canister are placed between Z = –2,000 and –4,000 m. In these vaariants the canisters are placed 1,000 m higher up in the boreholes, i.e. between Z = –1,000 and –3,000 m. The upper part of the canister section therefore resides in the middle of the initial transition from freshwater to brine, which occurs between 700 and 1,500 m depth in the model. Thus, there is potentially a risk for faster transport from the canisters up to the surface since the canisters are no longer well below the interface of the stabilising brine. A more trivial fact is that the 1,000 m shorter pathways for the released particles will reduce the travel times.

3.6.1 Case 21. Shallower boreholes

This variant is based on Case 3 with a 1% head gradient on the top surface and homogeneous rock permeability. The repository has been moved 1,000 m higher up in the rock with the canisters placed in the interval Z = –1,000 to –3,000 m.

Compared to Case 3, where the boreholes are at a 1,000 m deeper level, the calculated hypothetical travel times for the particles are one order of magnitude shorter, see Figure 3-59 and Figure 3-60.

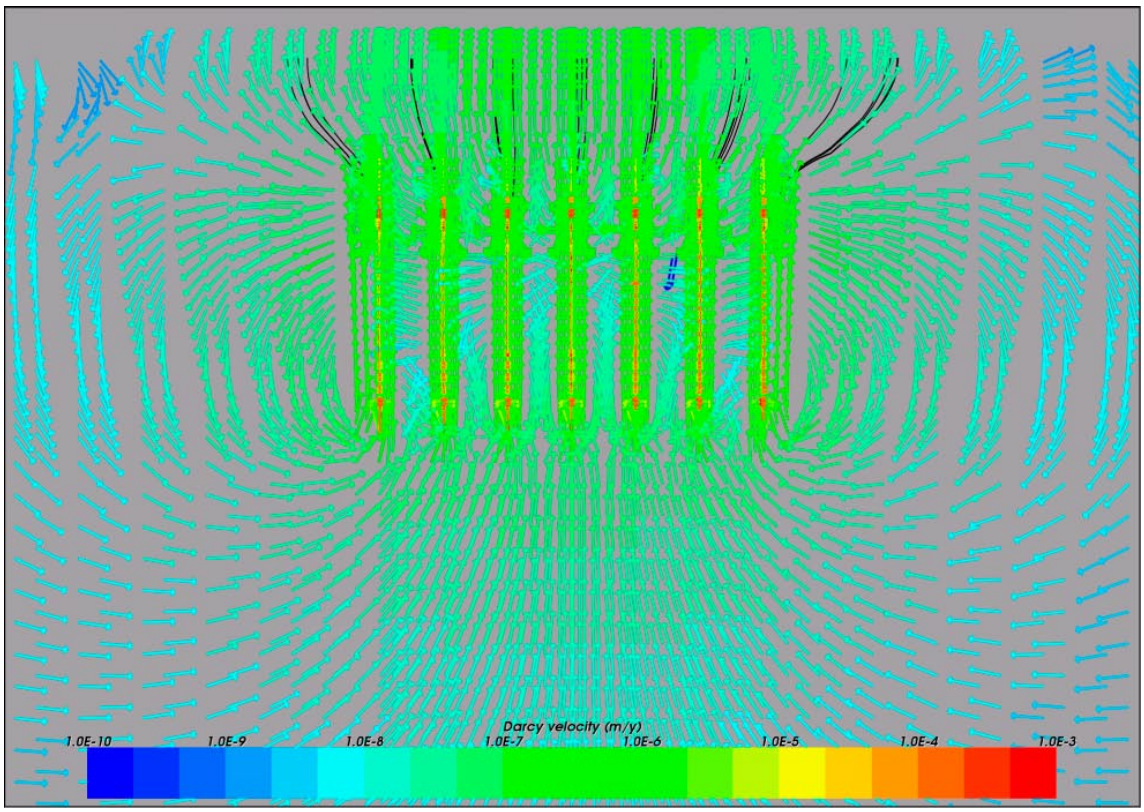

Figure 3-59. *Case 21. Close-up view of a vertical section showing Darcy velocity vectors. Flow paths are superimposed for illustration. Time = 100 years.*

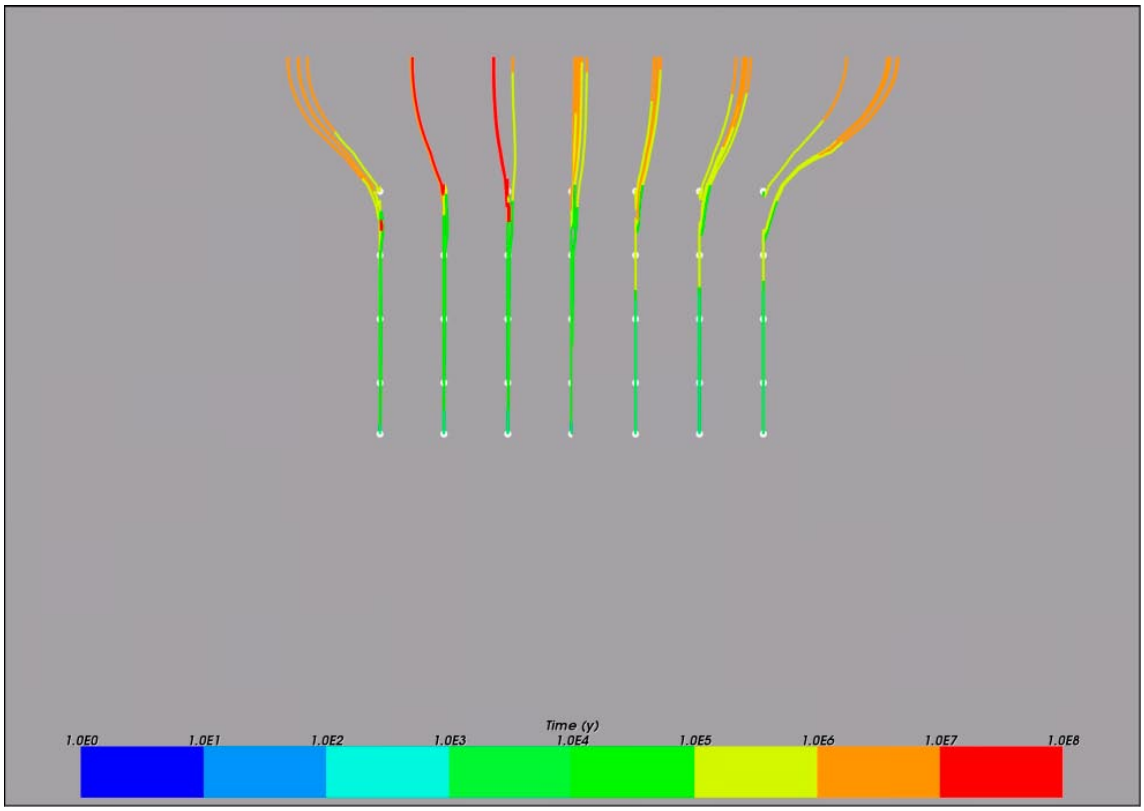

Figure 3-60. *Case 21. Vertical section showing flow paths coloured by travel time along the paths. Particle release time = 100 years.*

3.6.2 Case 22. Shallower boreholes with connected regional fractures

Case 22 was set up as a more complex variant of Case 21 with the addition of four connected fracture zones with a width of 100 m. The permeability of all materials in the boreholes was set to a value corresponding to 10 times the original value of the buffer. This means that the concrete, asphalt, bentonite, buffer and DZ in the boreholes all have the same physical properties from the surface level down to Z = –3,000 m, corresponding to the bottom of the shallower boreholes. The properties of the fractures are the same as for the boreholes.

The results presented in Figure 3-61 and Figure 3-62 show that the fracture zones affect the flow field and that some particles find new ways through the connected network of fractures. However, most particles choose broadly the way as in Case 21, i.e. more or less straight up through the rock above the repository. The travel times are therefore not affected much compared to Case 21.

3.7 Additional cases

A few additional variants were set up combining some of the most interesting variants simulated previously. These additional variants could be viewed upon as potential “worst case scenarios” given the specification of the used model and the tested sensitivities. Finally, one variant with a more refined model grid was set up in order investigate the effects of finer discretisation, which could potentially be of great importance for the results.

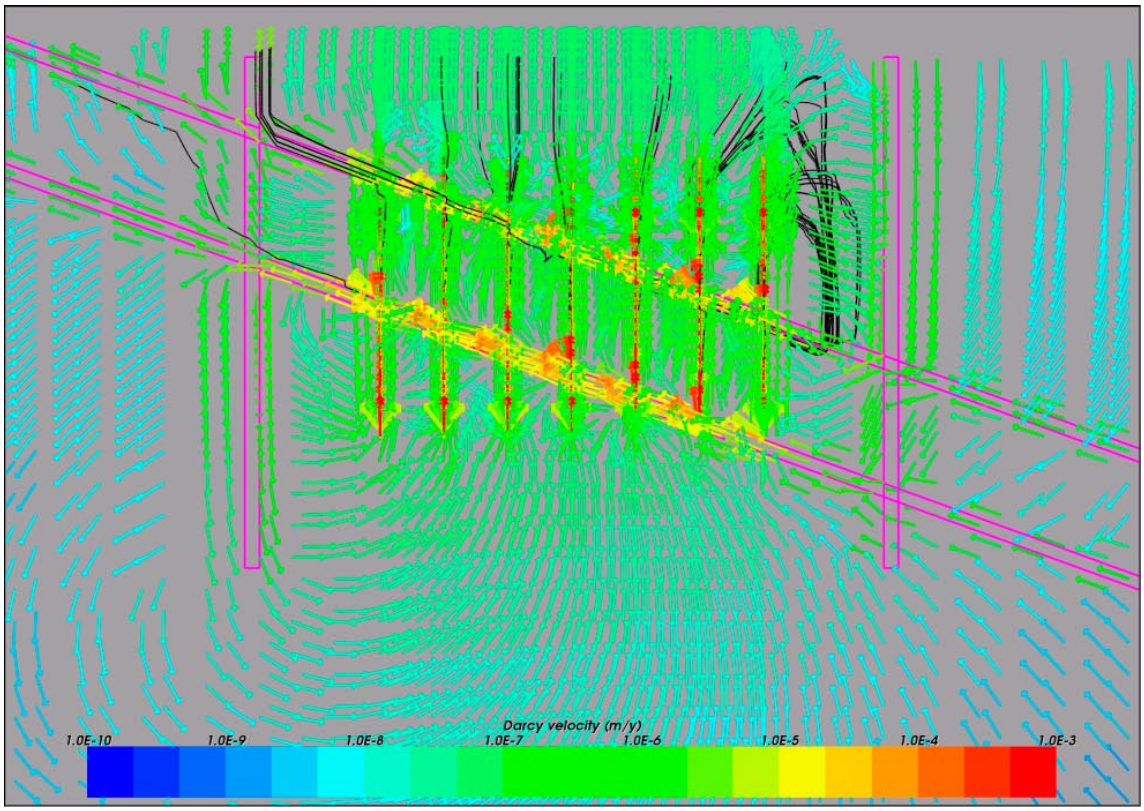

Figure 3-61. *Case 22. Close-up view of a vertical section showing Darcy velocity vectors. Flow paths are superimposed for illustration. Time = 100 years.*

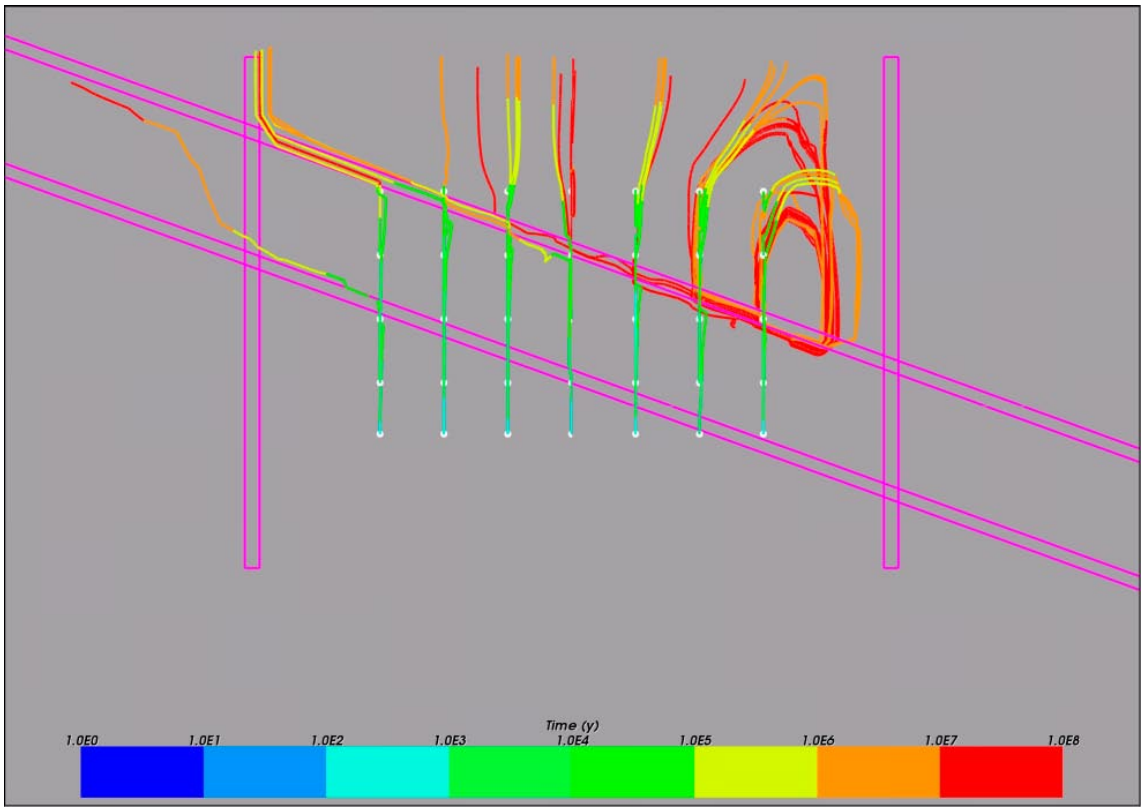

Figure 3-62. *Case 22. Vertical section showing flow paths coloured by travel time along the paths. Particle release time = 100 years.*

3.7.1 Case 23. Combined case 1

The first additional case is a combination of the following features found to be of certain interest in the performed sensitivities:

- heat source in canisters,
- 1% head gradient as top boundary condition,
- increased depth dependent rock permeability,
- fracture network model modified from POM Laxemar v1.2 so that the vertical zones extend to 5,000 m depth,
- boreholes initially filled with freshwater to a radius of 2.0 m,
- increased permeabilities in backfill, buffer and DZ material of boreholes.

The results are presented in Figure 3-63 and Figure 3-64. The flow field is rather horizontal which is an effect of the increased permeabilities in the upper parts of the rock. The Darcy velocities are generally high particularly in the boreholes. There is a wide range of calculated hypothetical travel times for the released particles. The fastest particles reach the top surface in about 10^4 years. This is one order of magnitude faster than seen in any of the previous variants and show that the simulated performance of the repository is rather sensitive to the model properties that are being used. The particles with very long travel times correspond to circulating flow paths and should not be regarded in the analysis.

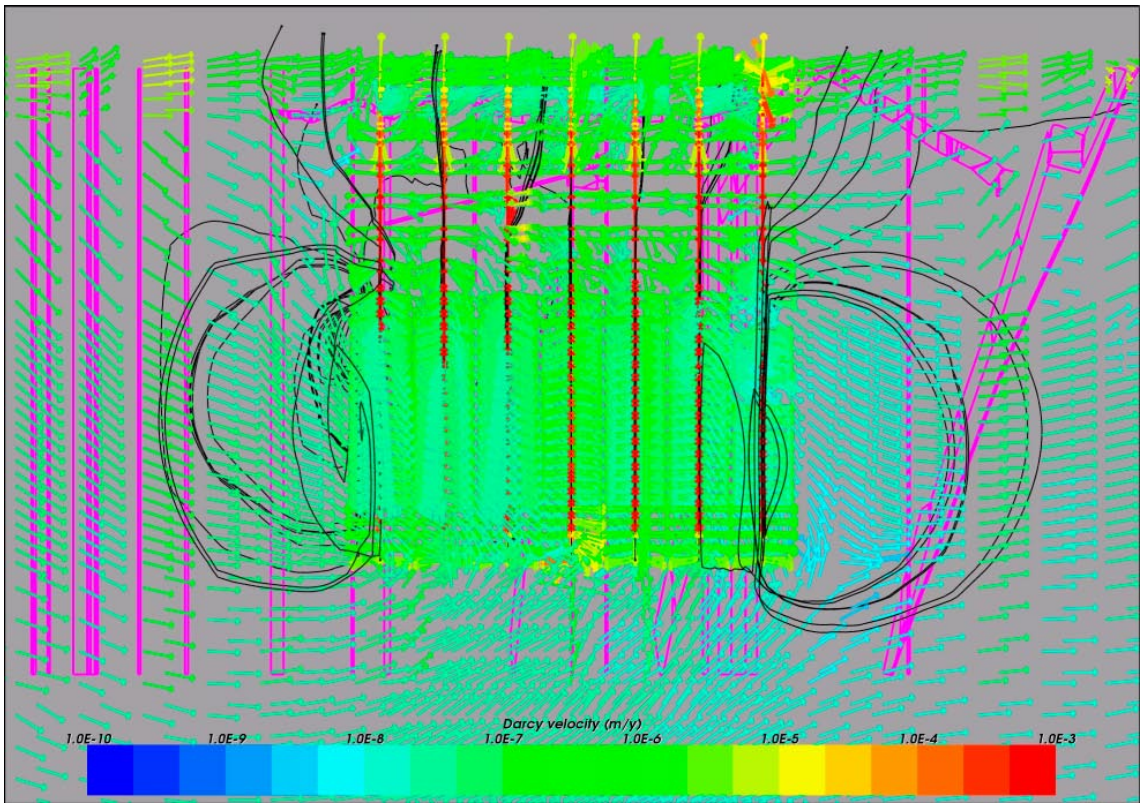

Figure 3-63. *Case 23. Close-up view of a vertical section showing Darcy velocity vectors. Flow paths are superimposed for illustration. Time = 100 years.*

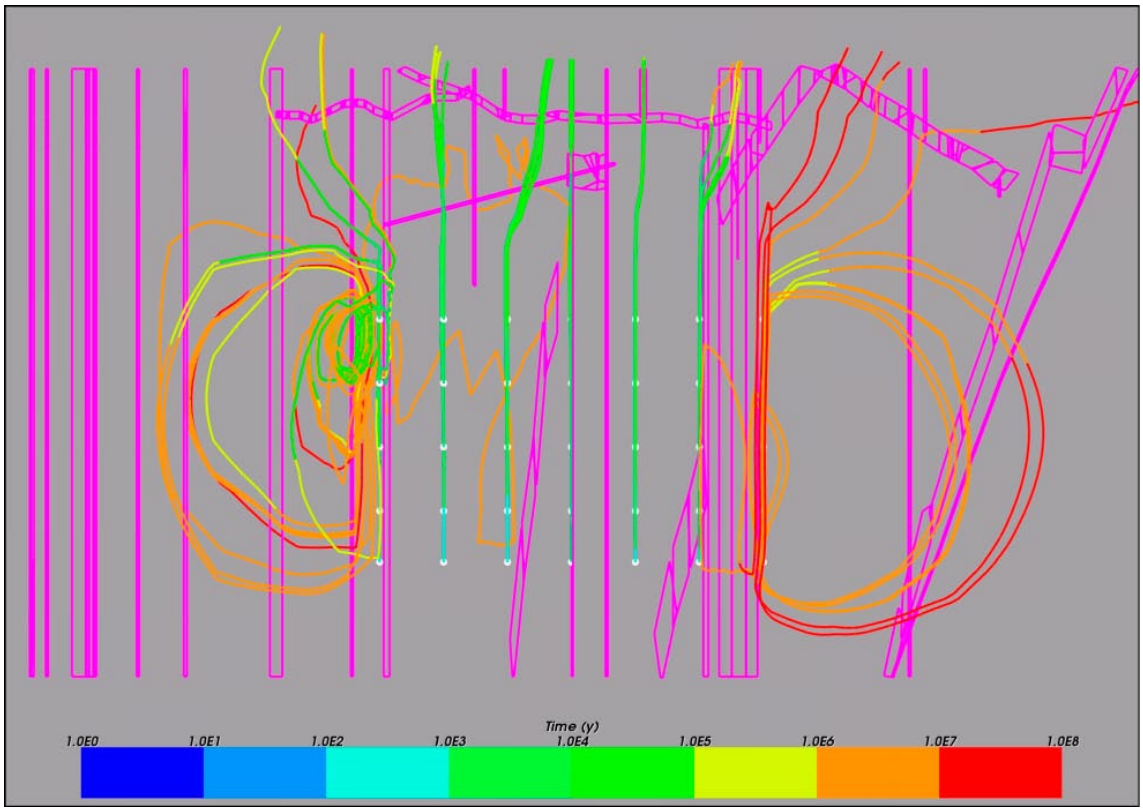

Figure 3-64. *Case 23. Vertical section showing flow paths coloured by travel time along the paths. Particle release time = 100 years.*

3.7.2 Case 24. Combined case 2

The second additional case is based on the first with the change of having the shallower boreholes. Hence, the main features of the model are:

- heat source in canisters,
- 1% head gradient as top boundary condition,
- increased depth dependent rock permeability,
- fracture network model modified from POM Laxemar v1.2 so that the vertical zones extend to 5,000 m depth,
- boreholes initially filled with freshwater to a radius of 2.0 m,
- increased permeabilities in backfill, buffer and DZ material of boreholes,
- shallower boreholes, canisters placed at a depth interval of Z = –1,000 to –3,000 m.

The results are presented in Figure 3-65 and Figure 3-66. The flow pattern is similar to the previous variant with the difference following a shallower placed repository. The Darcy velocities are broadly the same but the travel times are, as expected, over all faster, the latter being a direct effect of the shorter paths from the repository to the top surface. The flow paths are also more vertical in this case compared to Case 23 where we saw some circulating particles.

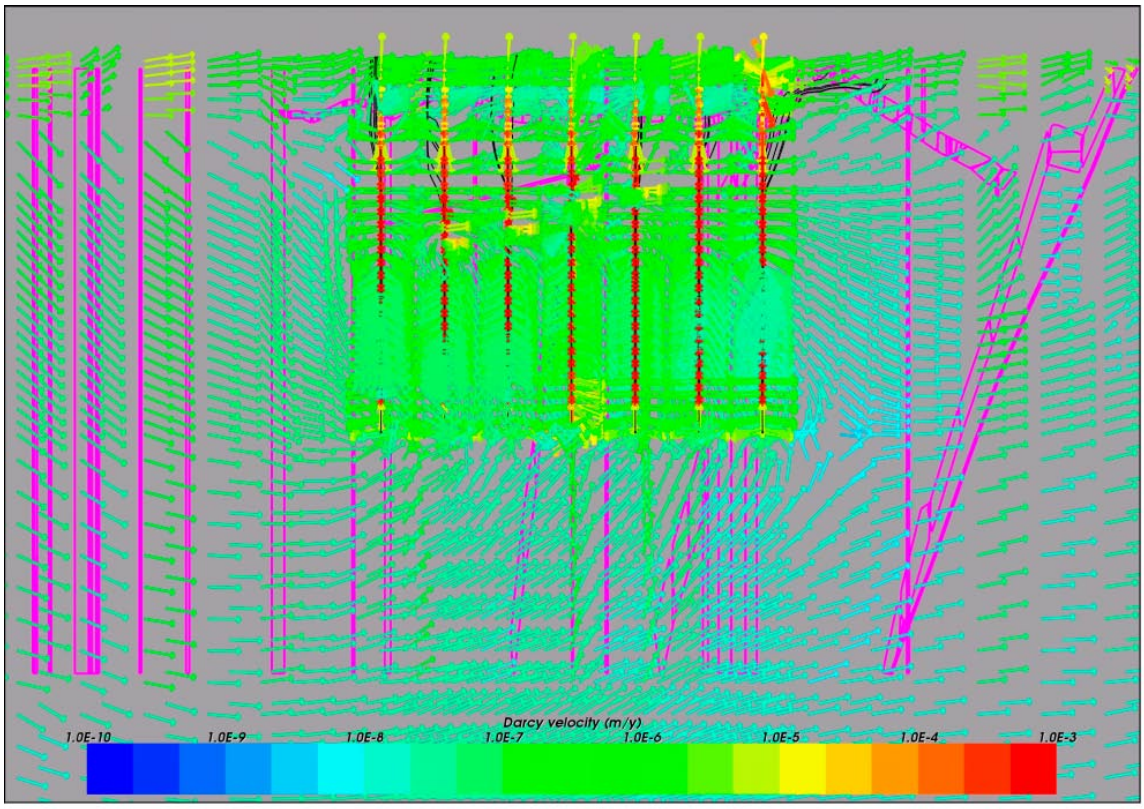

Figure 3-65. *Case 24. Close-up view of a vertical section showing Darcy velocity vectors. Flow paths are superimposed for illustration. Time = 100 years.*

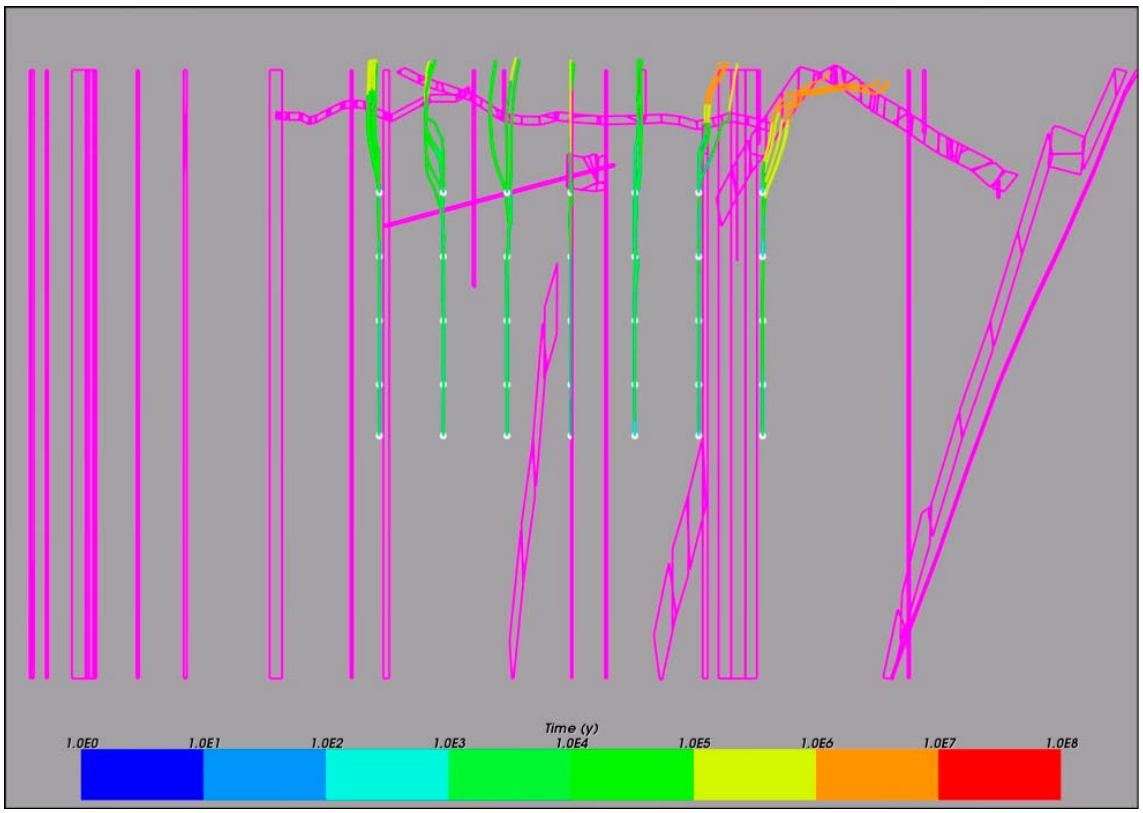

Figure 3-66. *Case 24. Vertical section showing flow paths coloured by travel time along the paths. Particle release time = 100 years.*

3.7.3 Case 25. Refined model grid

The final variant is based on Case 24 but uses a refined model grid. When generating a model grid there is usually need for compromise when it comes to choosing the grid refinement, or grid size. The reason is that the time required for solving the flow equation increases with increasing model size. The cost in solve time caused by an increased grid refinement is actually greater than what comes from the increase in number of finite element nodes due to the fact that a decrease in element size necessitates that also the size of the time step is decreased. However, the need to properly represent structures and features in the model may put certain requirements on the minimum grid refinement. In addition, an increased grid refinement increases the numerical accuracy of the results.

All models presented this far have had the same grid refinement, primarily in order to keep the solve times reasonable, but also to simplify the comparison of the results of the calculated variants. In this variant, a refined model has been used consisting of $2.5 \cdot 10^6$ nodes (compared to $5.4 \cdot 10^5$ nodes in the model used in all the previous variants). The solve time increased by a factor of 17, which is the motivation for using the smaller grid in spite of the loss in accuracy that is caused.

The main features of the model are:

- heat source in canisters,
- 1% head gradient as top boundary condition,
- increased depth dependent rock permeability,
- fracture network model modified from POM Laxemar v1.2 so that the vertical zones extend to 5,000 m depth,
- boreholes initially filled with freshwater to a radius of 2.0 m,
- increased permeabilities in backfill, buffer and DZ material of boreholes,
- shallower boreholes, canisters placed at a depth interval of Z = –1,000 to –3,000 m,
- refined model grid (and time step size); $2.5 \cdot 10^6$ nodes compared to $5.4 \cdot 10^5$ nodes for the original grid used in the other variants.

The results are presented in Figure 3-67 and Figure 3-68 and show that there are quite significant changes to the flow field compared to Case 24 even if the only difference between the models is the grid refinement. The overall Darcy velocities increase by approximately one order of magnitude. Moreover, the flow field changes direction to being more vertical above the repository area. Effects can be seen also to the west of the repository where the flow direction changes from being inward to becoming outward from the repository. At the bottom of the repository, the flow field is more upward than before. The travel times for the released particles are not affected much though, which can be explained by the flow paths still being mostly in the rock when leaving the canister section of the boreholes.

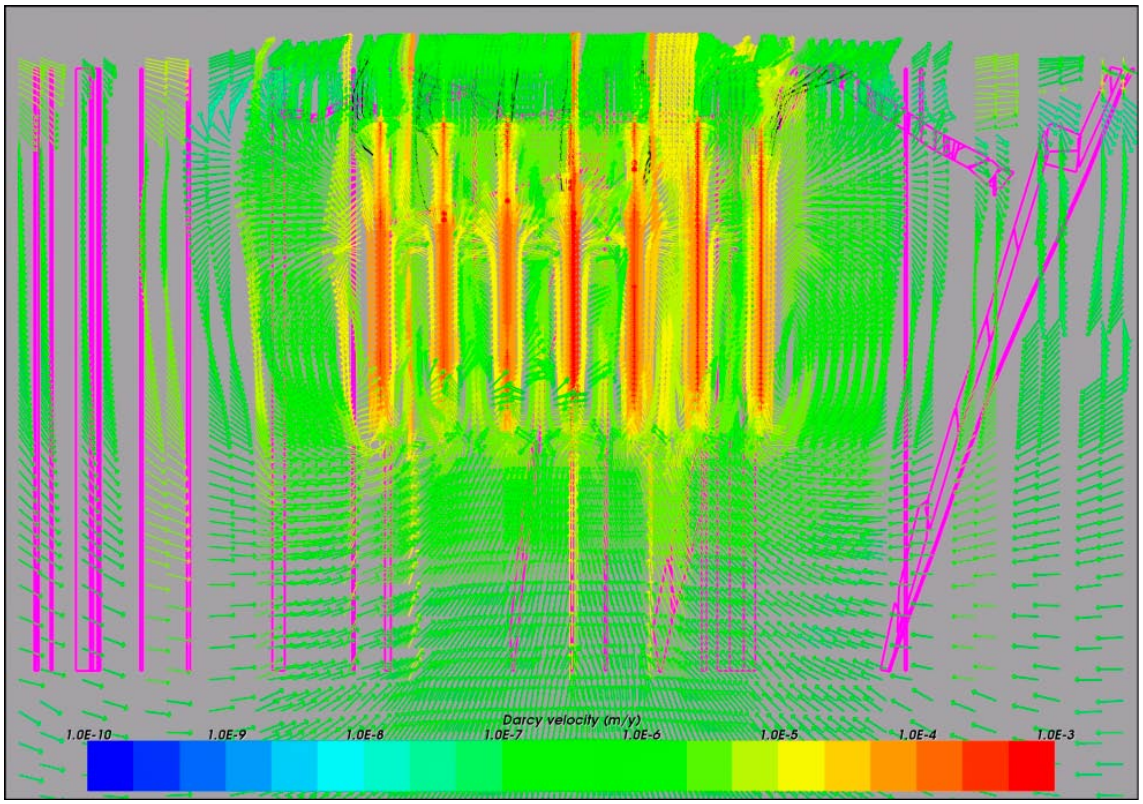

Figure 3-67. *Case 25. Close-up view of a vertical section showing Darcy velocity vectors. Flow paths are superimposed for illustration. Time = 100 years.*

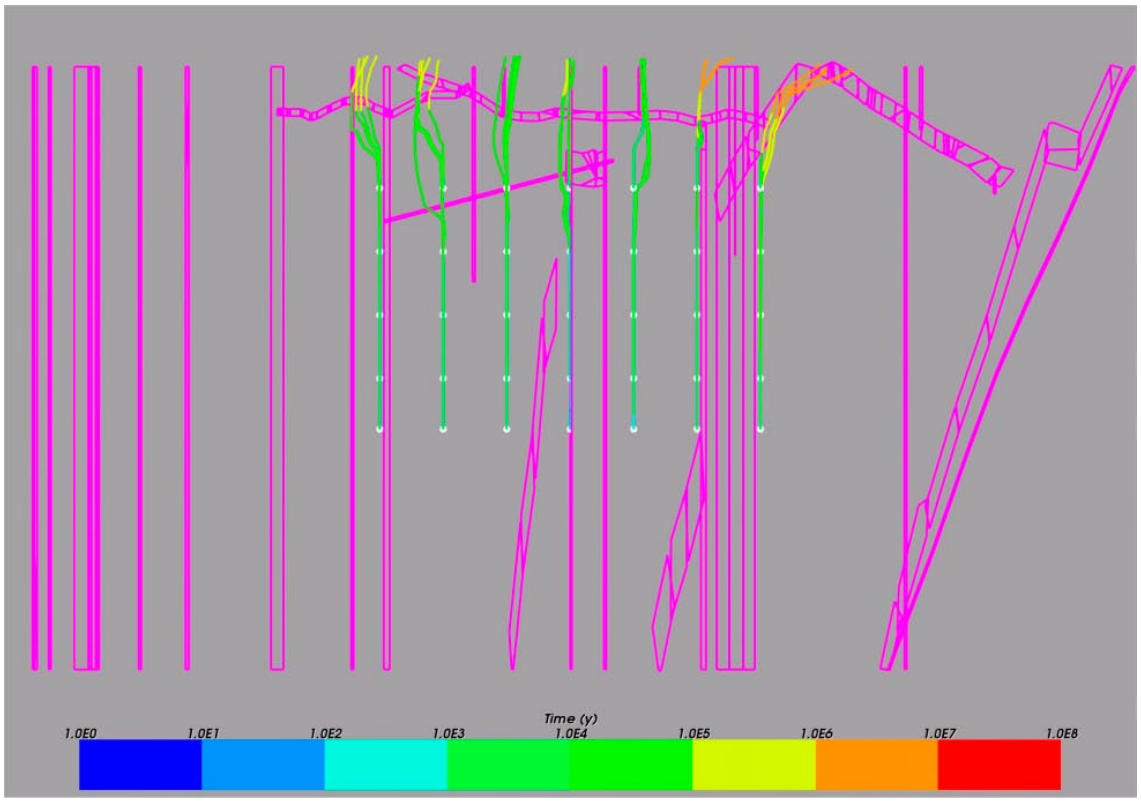

Figure 3-68. *Case 25. Vertical section showing flow paths coloured by travel time along the paths. Particle release time = 100 years.*

4 Discussion

The main objective of the present study has been to investigate if the thermal output from spent nuclear fuel disposed in deep boreholes would create sufficient buoyancy to jeopardise the stability of the groundwater system created by the salinity at depth. The short answer to this question is no. Given the assumptions used in the present model, the calculated variants all show that the thermal output from the canisters is not sufficient to destabilise the saline groundwater. Even if convection cells are formed around the repository due to the generated heat, the flow velocities induced by the heat transport are very low and do not significantly change the stability of the virtually stagnant saline groundwater at depth. A reason for this is that the power of the heat source is to low and that its duration is to short.

During the study, the effects of various conceptual models for groundwater flow coupled with transport of salt and heat have been explored. This has been carried out as a sensitivity study by computing a large number of model variants of which only the ones considered most important and interesting have been reported here.

Overall conclusions

The results presented here show that the thermal output from the canisters is not sufficient to alter the stability of the saline groundwater. The calculated hypothetical travel times for the groundwater are in all studied variants very long, orders of magnitude longer, compared to the duration of the decaying heat source. Therefore, the results in terms of performance measure should be treated more as an indication of a very slow and stabile system rather than being realistic values of the transport of released particles. Even if the performed sensitivity analysis does show effects on the Darcy velocities, flow field and calculated travel times, the differences are rather small and in a range that does not have any practical effect on the performance of the repository.

The main findings from this sensitivity study with respect to specific topics and uncertainties are presented below:

Top boundary condition

Two different boundary conditions were tested at the top surface. The first was a uniform prescribed head and the second was a 1% linearly varying head gradient. The applied head gradient imposes a horizontal flow in the upper part of the rock. The effects of the top boundary condition on the performance of the repository in terms of flow rates and calculated hypothetical travel times were not very pronounced in the present study. However, the importance of having a good representation of the surface topography in order to be able to model the flows in the rock and the fracture network properly cannot be enough stressed.

Hydraulic rock properties

The hydraulic properties of the rock are crucial for the performance of the repository and the modelling results. There is very little knowledge of the rock properties at the depths considered in the Very Deep Hole concept. Two main representations of the rock domain were used in these sensitivities. One with homogeneous rock properties and one with an increased permeability in the top 500 m of the rock. As an additional variant the effect of a depth dependent increased permeability was investigated. The properties of the rock have a direct effect on the flow velocities and flow pattern and therefore the performance measures. The magnitude of the thermal convection of groundwater is highly dependent on the properties of the rock

and the hydraulically active structures. In order to be able to present a credible conceptual model representing a repository at great depths large efforts are required to create a proper understanding of the properties of the very deep rock.

Fracture zones

A large number of variants using different fracture networks were calclated. These ranged from simple single fracture zone models to elaborated more realistic fracture networks used within the site investigations of POM Laxemar v1.2. If we believe that groundwater mainly flows along fracture zones within the more or less intact rock then it is easy to understand the importance of having a realistic representation of the fracture zones in order to be able to produce reliable results from the simulations. The calculated variants show that the effects of different fracture zone models are significant, in particular when adding structures to the deep rock.

Heat source

The thermal output from the canisters decreases rapidly. Already after 500 years the thermal output is reduced to 10% of its initial value. The potential effects on the groundwater flow are therefore expected within the first couple of hundred years. The results show that the Darcy velocities in the groundwater caused by buoyancy are overall very low and would be overshadowed by any naturally occurring flows. The dense brine increasingly filling the rock below 700 m depth is not significantly affected by the convection created by the heating. The salt interface stays virtually unchanged compared to the initial condition.

Freshwater filled boreholes

During the process of drilling the boreholes and stacking canisters in the boreholes it is likely that the boreholes will be freshwater introduced with the drilling fluid and with the deposition slurry forming the buffer. In the calculations, the initial presence of freshwater in the boreholes surrounded by dense brine proved to have a significant effect on the groundwater flow velocities. The hydrostatic pressure of the brine creates and upward gradient in the boreholes adding to the buoyancy forces.

Borehole properties

The effects of poor backfill properties in the boreholes were examined by varying the physical properties of different parts of the sealing and the buffer. The upper part of the boreholes, i.e. down to 2,000 m depth, includes various materials such as concrete, asphalt and bentonite. The deeper section of the boreholes, between 2,000 and 4,000 m depth include the buffer material. The boreholes are surrounded by a zone with an increased permeability due to fracturing following the stress redistribution caused by the drilling. The model proved to be quite insensitive to the properties of the boreholes. Only for the most extreme variants tested, effects on the Darcy velocity inside and outside the repository could be seen. A reason for this apparent insensitivity is that the particles released enter the rock surrounding the borehole when they reach the zone above the disposal zone because of the horizontal gradient applied at the surface.

Borehole depth

The effects of placing the canisters higher up in the rock were studied. In the original concept the boreholes are drilled down to 4,000 m depth and the canister are placed between Z = –2,000 and –4,000 m. By moving the canisters 1,000 m higher up in the boreholes, i.e. between Z = –1,000 and –3,000 m, the upper part of the canister section will reside in the middle of the initial transition from freshwater to brine. Thus, potentially there is a risk for faster transport from the top canisters to the surface. The results indicate travel times for the calculated particles

that are one order of magnitude shorter than for the deeper boreholes. This corresponds to the shorter paths for the shallower boreholes. There are no effects from having some of the canisters inside a less saline groundwater.

Discretisation of grid

As a final variant the effects from having a finer discretisation of the model grid was tested. The level of grid refinement is of great importance for the results, in particular when trying to represent small-scale structures as is in many of the presented variants. Ideally, one would like to use element sizes no larger than the size of the small-scale structures included in the model. However, since many of the fracture zones modelled have a thickness of about 10–50 m, the number of finite elements in the model would become high giving very long times for solving the flow equation. Therefore, in the bulk of calculations presented in this report, the grid refinement used was a compromise between numerical accuracy and computational time. This may ahve lead to fracture zones being smeared out when included using the implicit methods where the permeabilities of the zones are averaged together with the background permeability of the rock. Therefore, the expected effects of the fractures may not appear as intended. Another negative effect arising from a coarse element grid is that the numerical dispersion is introduced in the simulations. This may cause an over-estimation of the area influenced by heat transport from the canisters radially into the rock.

The results using an increased grid refinement show that there are quite significant changes to the flow field when the grid refinement is increased. The overall Darcy velocities increase and the flow field becomes more vertical above the repository area. More flow enters the repository through the bottom, which also has an impact on the flow velocities. The calculated hypothetical groundwater travel times are, however, still long compared to the duration of the decaying heat source.

5 Acknowledgement

Peter Jackson at Serco Assurance is gratefully acknowledged for the valuable help afforded in the initial work of setting up the model and debugging the numerical code Connectflow.

6 References

Agrenius L, 2006. Clab – Resteffekt i lagringsbassängerna, Appendix 1 in SKB R-06-62, Svensk Kärnbränslehantering AB.

Birgersson L, Skagius K, Wiborgh M, Widén H, 1992. – Project Alternative Systems Study – PASS. Analysis of performance and long-term safety of repository concepts. SKB TR-92-43. Svensk Kärnbränslehantering AB.

Harrison T, 2000. Very deep borehole – Deutag's opinion on boring, canister emplacement and retrievability. SKB R-00-35. Svensk Kärnbränslehantering AB.

Hartley L, Hunter F, Jackson P, McCarthy R, Gylling B, Marsic N, 2006. – Regional hydrogeological simulations using Connectflow, Preliminary site description Laxemar subarea – version 1.2. SKB R-06-23. Svensk Kärnbränslehantering AB.

Juhlin C, Sandstedt H, 1989. Storage of nuclear waste in deep boreholes – Feasibility study and assessment of economic potential. SKB TR-89-39. Svensk Kärnbränslehantering AB.

Marsic N, Hartley L, Jackson P, Poole M, Morvik A, 2001. Development of hydrogeological modelling tools based on NAMMU. SKB R-01-49. Svensk Kärnbränslehantering AB.

SKB, 1992. Project on Alternative Systems Study (PASS) – Final Report. SKB TR-93-04. Svensk Kärnbränslehantering AB.

SKB, 2000. – Förvarsalternativet djupa borrhål – Innehåll och omfattning av FUD-program som krävs för jämförelse med KBS-3 metoden. Svensk Kärnbränslehantering AB. (In Swedish)

Smellie J, 2004. Recent geoscientific information relating to deep crustal studies. SKB R-04-09. Svensk Kärnbränslehantering AB.